2012

Molecular Dynamics Modeling Of Scalable Micro/Nano Manufacturing

Ravindra Damodarrao Kaware
North Carolina Agricultural and Technical State University

MOLECULAR DYNAMICS MODELING OF SCALABLE MICRO/NANO MANUFACTURING

by

Ravindra Damodarrao Kaware

A dissertation submitted to the graduate faculty
in partial fulfillment of the requirements for the degree of
DOCTOR OF PHILOSOPHY

Department: Industrial and Systems Engineering
Major: Industrial and Systems Engineering
Major Professor: Dr. Salil Desai

North Carolina A&T State University
Greensboro, North Carolina
2012

ABSTRACT

Kaware, Ravindra Damodarrao. MOLECULAR DYNAMICS MODELING OF SCALABLE MICRO/NANO MANUFACTURING. (**Major Professor: Dr. Salil Desai**), North Carolina Agricultural and Technical State University.

In this research, 'Droplet Based Direct Write' micro/nano manufacturing is investigated using a molecular dynamics modeling and simulation approach. The aim of this investigation is characterization of the direct write inkjet printing process to promote optimization for the enhancement of scalability. The study was completed in four phases; nanodroplet evaporation modeling, substrate-nanodroplet interaction modeling, nanodroplet impingement study and nanodroplet-patterned substrate interaction modeling. For the evaporation study, the two typical solvents water and acetone were used. Under this phase, characterization of nanodroplet evaporation was accomplished including evaluation of droplet size variations at different temperatures and time scales. The results of evaporation modeling were validated using an established Goering's heat and mass transfer model. The second phase investigated water nanodroplet spreading dynamics on silicon dioxide and silicon nitride substrates at four different temperatures. The results of this study were validated using a robust molecular-kinetic theory. The third phase focused on the evaluation of silicon dioxide substrate wetting behavior by water nanodroplets under the influence of three different impingement velocities. The fourth phase of this research assessed the shift in hydrophobic behavior of the silicon dioxide substrate due to surface topology variations. This research provides basic understanding of direct write inkjet printing process at the molecular level and is expected to aid in determining appropriate process controls towards its scalability enhancement.

School of Graduate Studies
North Carolina Agricultural and Technical State University

This is to certify that the Doctoral Dissertation of

Ravindra Damodarrao Kaware

has met the dissertation requirements of
North Carolina Agricultural and Technical State University

Greensboro, North Carolina
2012

Approved by:

_____	_____
Dr. Salil Desai Major Professor	Dr. Steven Jiang Committee Member
_____	_____
Dr. Daniel Mountjoy Committee Member	Dr. Silvanus Udoka Committee Member
_____	_____
Dr. Paul Stanfield Department Chairperson	Dr. Sanjiv Sarin Associate Vice Chancellor of Research and Graduate Dean

DEDICATION

This dissertation is dedicated to my loving parents, son Sharvil and wife Arati who made enormous sacrifices to help me to achieve this milestone in my life. My parents selflessly spent most of their lives seeking to see my younger sister Smita and me happy. They inculcated the importance of humanity, uprightness, hard work and perseverance which helped me to reach my goal despite of our humble background in a small village. I had to leave behind three year old Sharvil with Arati in India during first year of my doctoral studies. Sharvil has seen many tough moments during last four years; due to his illness and my demanding schedule. Arati's support was very instrumental for sustenance, especially during difficult times due to health and financial challenges. I love you all and I express my deep gratitude to you all for your support, help and encouragement.

BIOGRAPHICAL SKETCH

Ravindra Damodarrao Kaware was born on April 8, 1974, in Amravati (MS), India. He obtained his secondary school diploma in June 1989 from Bhartiya Vidyalaya at Rajurwadi village with a merit scholarship for further education. He received his higher secondary school diploma from Vidyabharati Mahavidyalaya at Amravati in 1991. Further, he received his Bachelor of Science degree in Mechanical Engineering from Government College of Engineering at Amravati (MS) in 1997 and Master of Science in Production Technology and Management from VJTI, University of Mumbai (India) in 2004. He has an experience as a project engineer in manufacturing industry for two years and as an Assistant Professor in University of Pune (India) for eight years. Later, in May 2008, he enrolled in the doctoral program in Industrial and Systems Engineering at North Carolina Agricultural and Technical State University. He is a candidate for the PhD in Industrial and Systems Engineering in the Manufacturing and Service Enterprise Engineering track.

ACKNOWLEDGEMENTS

I thank God for the favor towards helping me to finish this thesis. His blessings and will throughout my life have shown me this beautiful moment. He has been always kind and merciful to keep me encouraged during difficult times.

I thank my altruistic parents next to god, who contributed to my life despite hardships, disasters and challenges in their own lives. Their uphill struggle in India enabled me to complete this research.

I am very much thankful to my advisor, Dr. Desai, for his support both academically and financially throughout the doctoral program. I am also grateful for his guidance, insight, conviction, specific directions and active involvement during every step of my research. He imparted me the confidence needed to overcome blocks in my research during last four years. I express my deep gratitude for his emotional support and consideration during my difficult phase of health and financial challenges. He always ensured that I overcame obstacles in my research; provide necessary resources for the same and for that I am very thankful. I also thank my committee members (Dr. Jiang, Dr. Mountjoy, and Dr. Udoka) for their contribution on my committee and active support and guidance through various stages of the doctoral program. They always encouraged and actively helped me during various research stages.

Many thanks to Dr. Park who has always been supportive as a graduate coordinator. Dr. Park also helped me during my doctoral qualifying examination for which I am so thankful.

I am thankful to all the faculty members in the department who have helped me as a teacher along the way since last four years. They also agreed to serve as references whenever I needed them. Furthermore, they provided materials, guidance and encouragement during my course work and doctoral qualifying examination. Thus I am truly appreciative for Dr. Stanfield, Dr. Ram, Dr. Ntuen, Professor Oneyear, Dr. Davis, Dr. Qu and Dr Li. My special thanks to Mr. Demetrius Martin who helped me over the years; especially for his great help in setting up and accessing new hardware and software for my research. I also thank our department secretary, Mrs. Brooks, for being always cordial and helpful. I express my gratitude for Industrial and Systems Engineering Department for supporting me in various ways.

I thank all of my colleagues for their support and aid over the years. Particularly, those in my research group Dr. Taye Esho, Mr. Jonathan Rodrigues, and Mr. Kwame Adarkwa. Dr. Taye Esho assisted me with the initial experimental phase of this research and its publication. He also shared his dissertation writing experiences and for that I am really grateful. I am very much thankful to Mr. Jonathan Rodrigues for his great help in data analysis and validation using MATLAB. I also thank Mr. Kwame Adarkwa for his assistance in data analysis and Ms. Jessica Perkins being supportive research group member. I am thankful to my out of research group colleagues Dr. Jules Chenou and Mr. Emmanuel Basie for being supportive, especially during my course work. I thank Dr. J.C Phillips and Theoretical and Computational Biophysics Group at University of Illinois Urbana-Champagne, for helping me with useful tips and updates on new developments on molecular modeling and simulation codes VMD and NAMD.

I also thank my family for their support and continual motivation. They have always been caring for me. I thank my wife Arati and son Sharvil for their patience and pains they lived with over the last four years. I also thank my sister Smita who has always been loving, supportive and helped me to continue my doctoral program especially by caring for our parents during their illness. I am also thankful to her husband Mr.Vijay for extending kind support to my parents during my studies.

I am truly thankful to everyone, who directly or indirectly helped me to reach this precious goal and I express regret if I failed to mention a name, it was not deliberate. Last but not least, I am very much grateful for the learning opportunities extended to me by North Carolina Agricultural and Technical State University.

TABLE OF CONTENTS

LIST OF FIGURES

FIGURE **PAGE**

LIST OF TABLES

TABLE **PAGE**

CHAPTER 1

INTRODUCTION

1.1 Brief Overview of Micro/Nano Manufacturing

Micromanufacturing is the process of fabricating micron level features generally required in miniaturized electronic devices such as sensors, solar cells, etc. Microfabrication technology has experienced rapid development in last few decades motivated by the market thrust for low-cost consumer products such as portable telecommunication equipments, computers, and healthcare diagnostics. Recently, microfabrication technology has been extended to the development of micro/nano-electro-mechanical system for fabricating miniature devices based on silicon and other semiconductor materials. Push for reducing device size and maximizing the functionality is ever increasing, especially in the field of information technology & telecommunications, healthcare, biotechnology, instrumentation and sensors.

Nanomanufacturing is defined as any technology associated with developing materials or structures with nanometer scale (or below 100 nanometer) features. Nanomanufacturing is also a scaled-up, dependable and economical manufacturing of nanoscale materials, structures, devices and systems. Furthermore, nanomanufacturing encompasses the research, development and amalgamation of top-down processes with intricate bottom-up or self-assembly processes. The boundaries between nanotechnology and microtechnology are thin as there is a close agreement in the approaches and equipments adopted in both regimes. However, the fields of their application are diverse.

At the nano scale, the physical and chemical properties are substantially different. Microfabrication is basically a top-down technology. However, at the nanoscale, either top-down or bottom-up approaches can be used, which may be considerably different. Most micro/nanofabrication processes are originated from the standard fabrication methods developed for the semiconductor industry. Some of these processes such as thin-film deposition and etching are common between the micro/nano and very large-scale integration (VLSI) microchip fabrication technology.

Nanomanufacturing is transforming almost every sector of industry including electronics, biotechnology, pharmaceuticals, agriculture, food production, printing, plastics, metals, and others. Examples of nanomanufacturing processes include thin film deposition, chemical synthesis, nano-imprint lithography and advanced atomic/molecular engineering.

Current advances in nanotechnology and translation of these advances to practical nanomanufacturing processes are primarily aimed at shrinking device dimensions to the smallest possible extent. Major challenges with nanopatterning are scalability, repeatability and material compatibility. These are elemental issues of significance to understand and control nanomanufacturing processes to extend its application at sub 50 nanometer regimes. Scalable nanomanufacturing processes are aimed at high throughput production of nanostructures with substantial repeatability. In order to achieve a precise control of these processes, a fundamental understanding of the underlying phenomena and their optimization is of paramount importance.

Among many nanomanufacturing methods, direct writing (DW) method possesses extensive capabilities to process wide range of materials, at low temperatures and high speeds [1]. Moreover, it has great potential to meet larger scale industrial needs [2]. Inherent scalability of DW method and its advantages in several areas can be exploited to develop fabrication methods for mass customization of high volume production.

This research studies one of the 'Droplet Based Direct Write' micro/nano manufacturing method using the molecular dynamics modeling and simulation approach. Its aim includes the basic understanding of the process and its further optimization for the enhancement of scalability.

The Molecular Dynamics modeling approach discussed in this research is aimed at modeling and characterization of a droplet based DW nanomanufacturing process. In the proposed approach droplets undergo controlled evaporation to transform their sizes at the nanoscale dimensions. Furthermore, these droplets can be laden with nanoparticles that can be deposited on substrates to form feature patterns for different applications. In the DW approach, features are built directly without the use of masks, allowing rapid prototyping and manufacturing. The fluids discussed in this article (water and acetone) serve as universal solvents for suspending nanoparticles that can be printed into desired features using the proposed DW process. This research aids in the understanding of the evaporation dynamics of the solvent droplets using an external heat source and spreading mechanism for deposition of colloidal nanodroplets on substrates.

1.1.1 Direct Write Method

DW method encompasses a diverse, versatile and multi-scale group of process technologies [3]. Direct writing is also known as direct printing and digital writing. It is the micro/nanomanufacturing process for depositing, dispensing or processing different types of materials over various surfaces along a predetermined pattern or layout [2]. It is a fabrication method using computer-controlled pattern-generating device, e.g. ink deposition nozzle or laser writing optics, to create desired features on substrates [3]. As described in Figure1.1, direct writing is a broad term covering a number of processes, using a variety of techniques for material transfer on to a surface. DW is a versatile technology as it covers a wide length scale from tens of nm to several mm in terms of feature dimensions. Based on the mechanism of materials transfer, DW methods can be grouped under 4 major titles; Droplet-based, Energy Beam, Flow and Tip. Droplet–based DW method can be further subdivided into two groups: inkjet and aerosol jet.

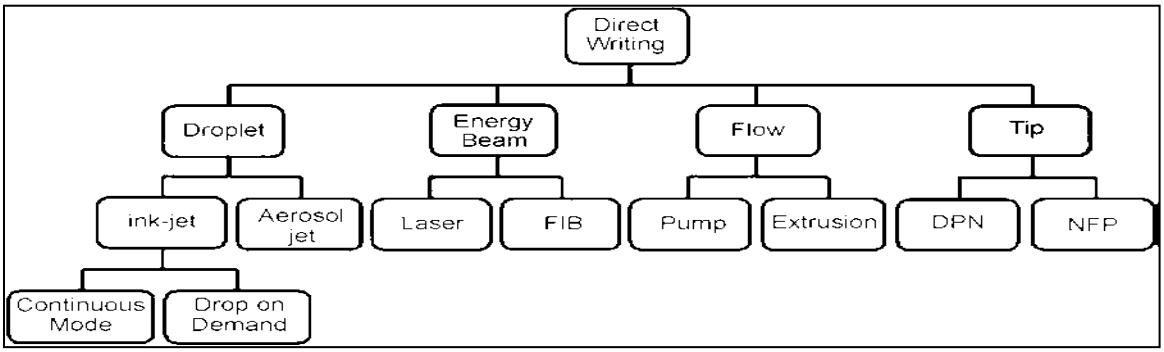

Figure 1.1. Classification of direct writing methods. (KKB Hon et.al)

Currently, thermal and piezoelectric drop-on-demand inkjet methods are the most popular. In aerosol jets, unlike inkjet systems, the driving force is based on a gas to provide the kinetic energy for the deposition of materials. Energy beam-based DW refers

to deposition of materials by laser or ion beams. A Laser-based DW deposits, transfers or consolidates a strip of material through the action of a high-energy laser beam. This can be further subdivided into four groups based on the precursors, i.e. solid, liquid, gas or cell. Several processes have been developed from laser DW as it is highly versatile. Focused ion beam (FIB) DW requires a precursor gas and its resolution is nearly two orders of magnitude better than laser although at a slower writing speed. Flow-based DW requires high precision micro-dispensing technology which could be in the form of a precision pump. Usually, the delivery of the flowable material is through a very small orifice or a needle. Unlike inkjet where the ink is discretized as individual droplets, the delivery of material for flow-based DW is continuous. Tip-based DW is a nanomanufacturing method represented by two processes. In dip-pen lithography, molecules diffuse on to a substrate in an ordered pattern through the micro-capillary action between the tip and the surface. The properties of the meniscus formed between the tip and the surface are highly significant for direct writing by this method.

Nanofountain probe (NFP) patterning is a promising direct write approach capable of delivering liquids to a surface. NFP is a cantilevered micro-fluidic device terminated in a nanofountain. The embedded microfluidics facilitates rapid and continuous delivery of molecules from the on-chip reservoirs to the fountain tip. By controlling the geometry of the meniscus through hold time and deposition speed, various inks and biomolecules could be patterned on a surface, with sub 100 nm resolutions.

In this research, the molecular dynamics (MD) methodology is applied for modeling

and simulation of a droplet based direct writing method that is an emerging nanomanufacturing method.

1.1.2 Applications of DW Methods

Significance of DW technologies is ever growing in materials processing and fabrication of miniaturized electronic circuits. The applications of DW methods are progressively widening with current advances in materials and processing technology [2]. DW techniques are used in the fabrication of passive electronic components and interconnects using a wide range of materials [3]. Currently, DW of biomaterials is being used for tissue engineering [4] and array-based biosensors [5].

As discussed in previous section, many different approaches exist to direct write or transfer patterned materials, and each technique has its own strengths and limitations. However, all DW techniques are dependent on high-quality starting materials, specially tailored chemistries and material properties (such as viscosity, density, and surface tension). The starting materials, commonly termed as inks comprised of combinations of powders, nanopowders, flakes, surface coatings, organic precursors, binders, vehicles, solvents, dispersants, and surfactants. These materials play the role of conductors, resistors, and dielectrics and are being developed specifically for low-temperature deposition (less than 300^{o}C to 400^{o}C). They are expected to fabricate passive electronic components and radio frequency devices matching or exceeding the performance of conventional thick film materials, but on low-temperature flexible substrates, such as plastics, paper, and fabrics. The desired final electronic materials deposited may be silver, gold, palladium, and copper conductor alloys or polymer thick film [1].

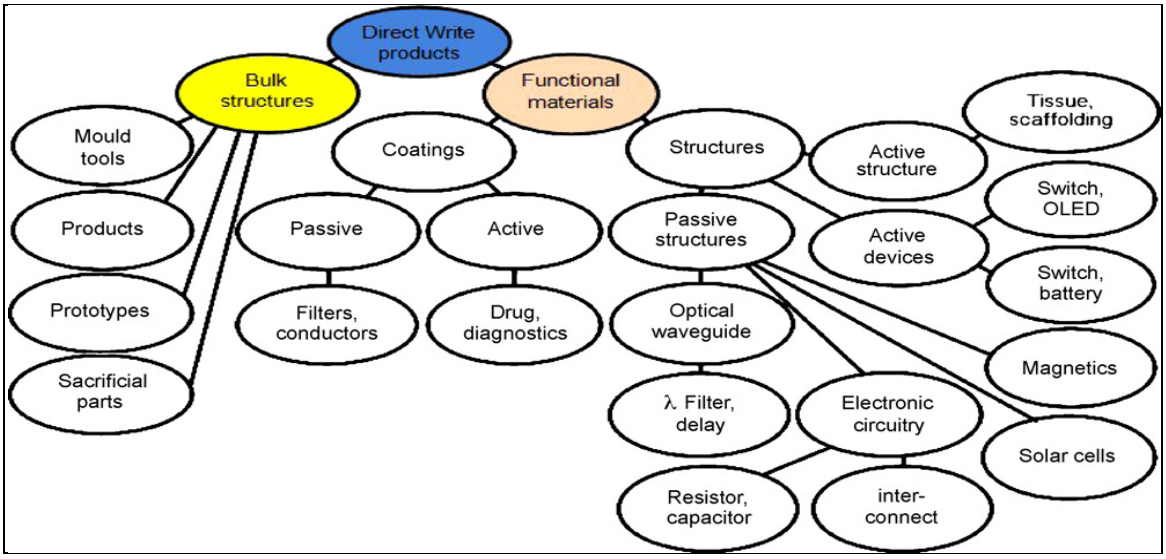

Figure 1.2. DW product overview (K.K.B. Hon et. al).

Figure 1.2 summarizes an application scope of DW method. Direct writing applications envelop very wide segments of industry including micro-electronics, Micro-Electro-Mechanical Systems (MEMS), optics, pharmaceutics and biomedical engineering because of its multi-length process capabilities. The scope of application is also improved by the diverse range of materials and process simplicity. In addition, the substrate topologies for DW method can be flat, round, flexible, inflatable, irregular and 3D.

1.1.3 Scalability and Other Challenges for DW Method

Typically, individual DW techniques have trade-offs between resolution or speed and increasing particle bonding to help the transfer process [2]. The use of electronic materials that have been already optimized for DW technologies results in deposition of finer resolution features, minimal process variation, lower prototyping and fabrication costs, higher manufacturing yields, reduced prototyping and production time, better manufacturing flexibility, and reduced capital investments. However, there are a number

of common challenges in DW technology. Most prominent aspect is the improvements in adhesion, surface finish and resolution of the deposited materials with faster deposition rates that are required to enable commercialization of some techniques which are still mainly laboratory-based. There is a strong need to enhance scalability of DW methods for high throughput production of quality features [6].This necessitates deeper understanding of the processes with development of more quantitative process parameter relationships, which will facilitate more accurate and reliable process modeling leading to process optimization.

Specifically, in the inkjet-based direct writing methods (considered in this research), there are several aspects which need further research. Accurate models for jet and drop formation, drop impingement and drying/curing would aid the understanding of process and material design. Also, there is further scope to extend the range of fluids/solvents which can be printed. To achieve substantially higher concentrations of solid particles or polymer; better understanding of the printing of non-Newtonian fluids would be beneficial. Inexpensive conductive inks, which can achieve highly stable and durable conductivity deposits, would be readily accepted. There are ample opportunities for further development of functional optical, magnetic, optoelectronic and semiconducting materials with inkjet printing. With the development of new methods of droplet generation, it is expected that the applications of inkjet printing in direct write manufacturing will become much broader.

1.1.4 General Principle of Droplet Based DW Inkjet Printing Method

Inkjet technology is a well established form of DW technology and has two modes: continuous and drop-on-demand (DOD) [1]. Inkjet-based direct writing involves the formation and deposition of a sequence of droplets of liquid material, often called an ink or fluid. After deposition this material becomes solid, by the evaporation of a solvent, chemical changes (e.g. through the cross-linking of a polymer) or through cooling (e.g. by crystallization). Subsequent processing steps, such as sintering, may be involved. There are two different methods most commonly used to generate drops in inkjet printing, termed continuous inkjet (CIJ) and drop-on-demand [DOD].As shown in Figure 1.3, in CIJ a continuous stream of ink drops is generated from a nozzle by exciting the natural tendency of a continuous liquid jet to break-up under surface tension forces. Each drop is then individually steered (deflected) to write spots on the substrate. Drops that are not selected in this way are fed into a gutter and recycled. Simple CIJ systems use single nozzles, but systems also exist with multiple nozzles. As shown in Figure 1.4, DOD system has an array containing a large number of nozzles, each of which can generate a single drop of ink on demand, by inducing a transient pressure pulse in a chamber behind the nozzle. The drops then travel in straight trajectories from the nozzle to deposit on the substrate. Other methods of drop generation are possible, including the use of an electric field to draw out a liquid from a nozzle.

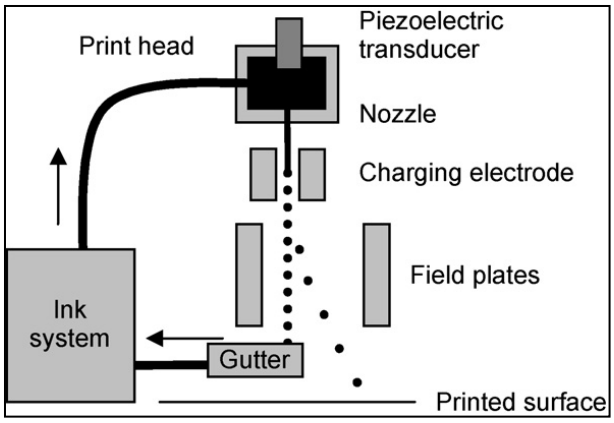

Figure 1.3. Principle of operation of a continuous inkjet system.
(K.K.B. Hon et. al).

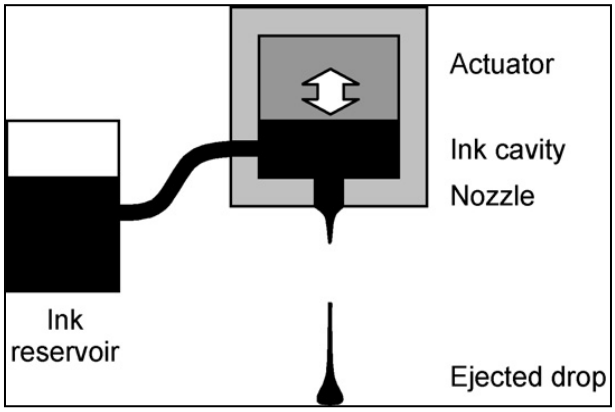

Figure 1.4. Principle of operation of drop-on-demand inkjet system.
(K.K.B. Hon et. al).

This DW approach of nanomanufacturing in this research involves controlled evaporation of the ejected microdroplets using a heat source. These microdroplets ejected from an inkjet setup undergo size reductions to the nanoscale regime before deposition onto the substrate. An understanding of the evaporation mechanism is critical for determining appropriate controls in the proposed droplet based nanomanufacturing process. This research investigated the evaporation dynamics of the liquid droplet at nanoscale for characterizing physical size variation under different ambient conditions.

MD modeling and simulation approach is used for understanding of micro-to-nano transformation phenomenon with subsequent deposition of the liquid drops on substrate.

1.2 Multiscale Modeling Methods for Micro/Nanomanufacturing Processes

Multiscale modeling in physics is intended for determination of material properties or system performance at one dimension scale using information or models from different dimension levels. On each scale, particular approaches are adopted for description of a system. The level of quantum mechanical models accounts for the information at the level of electrons. Molecular dynamics model considers interactions between individual atoms. Further, mesoscale or nano level provides information about groups of atoms and molecules. Continuum models describe interactions at macroscopic level. Each level observes physical phenomenon over a specific span of length and time. Multiscale modeling is mainly significant in study of computational materials engineering since it helps to envisage material properties or system performance based on understanding of the atomistic structure and characteristics of basic processes. Currently, various multiscale computational modeling approaches are adopted for modeling physical phenomenon at micro/nano scales (shown in Table 1.1) The main three approaches considered for modeling physical phenomenon occurring at micro/nano scales include; Continuum Mechanics, Molecular Dynamics and Quantum Mechanics. In addition to these approaches, a more refined modeling approach such as Density Functional Theory (DFT) is also employed in many material science applications [6].

Table 1.1. Current modeling approaches and their size scales (Mark T Lusk et al.)

Method	Interaction level	System size scales
Density Functional Theory (DFT)	Electron-electron , Electron-ion	10^3 atoms, $5nm^3$
Molecular Dynamics (MD)	Atom-atom	10^{11} atoms, $1\mu m^3$
Monte Carlo/Phase Field	Mesoscale continuum	$1cm^3$
Finite element Method	Macroscale Continuum	$1m^3$

Quantum Mechanics

This modeling approach pertaining to atomic scales is governed by a Quantum Hamiltonian instead of classical forces [7-8]. The quantum mechanical model is based on semi-empirical method from computational quantum chemistry termed as the "Tight Binding" method. It is based on the Born-Oppenheimer approximation. This approximation splits electron motion and nuclear motion and assumes that nuclei are basically fixed. Another approximation considers each electron as segregated from others and restricted to its own orbit. Quantum mechanics model is based on the quantum theory and yield more accurate results than statistical models based on classical theory. However, quantum mechanics modeling methods are orders of magnitude more computationally demanding than molecular dynamics modeling method, which is used to model molecular level phenomenon [8-9]. Also, this modeling method can model at most two hundred and fifty atoms at a time and modeling becomes increasingly difficult for higher number of atoms [9-10].

Density Function Theory

Density functional theory is a modeling method based on quantum mechanical approach and employed in physics and chemistry to study the electronic structure at ground state of multi-body systems comprised of atoms, molecules, and the condensed phases. With this theory, the characteristics of a many-electron system can be determined by using functional (functions of another function; in this case the spatially dependent electron density). DFT is a popular and versatile approach employed in condensed-matter physics, computational chemistry and computational physics [7].

DFT was initially popular for calculations in solid state physics and was not considered accurate enough for calculations in quantum chemistry until the 1990s. Later, the approximations in the theory were significantly refined for better reflection of correlation interactions in the model. In numerous studies, the outcomes of DFT application for solid state systems were found in close agreement with experimental data. Moreover, computational costs are comparatively lower than for traditional methods.

Despite current enhancements, there is still complexity involved in using DFT to accurately depict intermolecular interactions such as forces, charge transfer excitations, transition states, global potential energy surfaces and some other strongly correlated systems.

Continuum Mechanics (Linear Elastic Theory)

Continuum mechanics approach is used to model the large scale phenomenon and is based on linear elastic theory, which relates, stress (a measure of force applied per area with strain (a measure of corresponding deformation) from equilibrium at a point [8].

Linear elastic theory, supplemented with a set of experimentally determined parameters for the specific material under observation, facilitates estimation of the potential energy stored in a solid as a function of its local deformations. Linear elastic theory is basically a continuous theory. Thus, for using linear elastic theory in a computational model, it has to be discretized. This is accomplished using a "finite element" method. This technique involves a "mesh" fabricated of points that effectively covers the entire modeling region with standard shape elements such as tetrahedra. Each mesh point is linked with a certain amount of displacement. At each time step, the total energy of the system is determined by integration over each element. The gradient of this energy function is used to determine the acceleration of each grid point, which is then used to calculate its projected position for the next time step [9].

Computational Fluid Dynamics (CFD) is the tool based on continuum model that uses the finite element method. It is used to simulate fluid behavior based on Navier-Stokes classical theory for the solution of the basic flow dynamics equations for mass, momentum and energy conservation. These equations are solved for grid of discrete points (nodes) of the computational domain. The nodal values of physical variables are used to interpolate the variable fields in each point of the domain.

CFD modeling shows its limitation near the wall surface, where the phenomena occurring at molecular distances cannot be taken into account by the continuum approach. Generally, the near-wall flow behavior is simulated in CFD by pre-defined functions. These functions interpolate the flow velocity from the boundary condition set at the wall to the first internal computational node. Such approach is not capable of

accounting the effects induced by a functionalized interface at a distance from the wall. To overcome these limitations of CFD, specifically developed User-Defined Subroutines (UDS) are included with the standard modules of the CFD software. The solver uses the results of the finer scale models facilitated by UDS to establish required relationship among continuum and discrete variables.

Thus, continuum approach (Finite element method) is better modeling approach to describe the macroscale phenomenon up to system size scales of $1m^3$ [7].

Molecular Dynamics

Molecular simulations are carried out for understanding the structural properties of molecular assembly and the microscopic interactions between them. This simulation method serves as a complimentary approach for laboratory experiments. The two main types of molecular simulation technique are molecular dynamics (MD) and Monte Carlo (MC). The MD technique is preferred over MC as it enables determination of dynamical properties of the system such as time-dependent responses to perturbations and rheological properties. MD simulation acts as an interface between microscopic and macroscopic views and provides an estimate for the molecular interactions to obtain exact predictions of bulk properties. The predictions can be made accurate based on the availability of computational power. Simulations act as a link between theory and experiment. Theoretical principles can be tested by conducting a simulation using an equivalent model. The MD models can be tested by comparing with experimental results. Computer simulations are also carried out to simulate ambient conditions otherwise difficult to attain in the laboratory such as extremes of temperature or pressure. A good

model of molecular interactions is necessary to make direct comparisons with experimental measurements made on specific materials. The Ab initio molecular dynamic model is preferred to reduce the amount of fitting and guesswork. On the other hand, a realistic molecular model that incorporates the essential physics may be appropriate to study the phenomena of a rather generic nature and to distinguish between good and bad theories.

Molecular dynamics (MD) is a type of computer simulation in which atoms and molecules are allowed to interact over a period of time by approximations of known physics principle. Molecular dynamics allows studying motion of individual atoms with predefined initial and ending conditions and obtaining the results which are not possible to realize in laboratory experiments. A molecular dynamics simulation requires the definition of a potential function, or a description of the terms by which the particles in the simulation will interact. In chemistry and biology this function is usually referred to as a force field. MD generates atomic and molecular trajectories, by the numerical integration of Newton's laws of motion. This process requires specification of initial conditions and knowledge of the forces acting on all constituents, which can be obtained either algebraically or numerically from a previously calculated potential energy functions. MD has important application in a variety of chemical disciplines, but is especially useful in biochemistry in the study of protein-folding. Molecular dynamics is a specialized discipline of molecular modeling and computer simulation based on mechanics. The main justification of the MD method is that statistical ensemble averages are equal to time averages of the system. Benefits of MD include:

1. Simple energy functions and therefore faster computations
2. Ability to cope up with large molecules
3. Capability to reproduce the force field (interpolative) for more accurate models and
4. Reasonably accurate estimation of van der Waals interactions at non-bonded distances for larger molecules

Governing laws of physics, assumptions and properties for study of material transformations are widely different at nanoscale compared to that for the bulk of material. Therefore, bulk or microscale phenomenon are studied using a continuum approach whereas nanoscale phenomenon is studied using molecular dynamics (MD) approach. The aggregation process under consideration involves transformations at both the scales, micro and nano. Therefore, both approaches can be adopted for modeling nanoscale to microscale transformation. For example, nanodroplet movement during aggregation can be modeled using the MD approach and post-aggregation transformation involving micron scale features can be modeled using continuum approach.

As study of nanoscale droplet evaporation and substrate deposition is mainly focused in this research; results are obtained using molecular dynamics approach for liquid nanodroplet. However, the continuum approach may be used in future to model and simulate some initial micro-to-nano and post deposition nano–to-micro transitions in the direct write inkjet printing micro/nano manufacturing process.

1.3 Physical Phenomenon under Consideration

Figure 1.5 shows microscale to nanoscale droplet transformation mechanism under consideration. In this approach, micron size droplets will be reduced to nanoscale through evaporation phenomenon [11]. A controlled heat source is intended to evaporate the microdroplet after its ejection from nozzle and before deposition on substrate. The droplet transformation is observed with high speed camera, usually a charge-coupled device (CCD) camera.

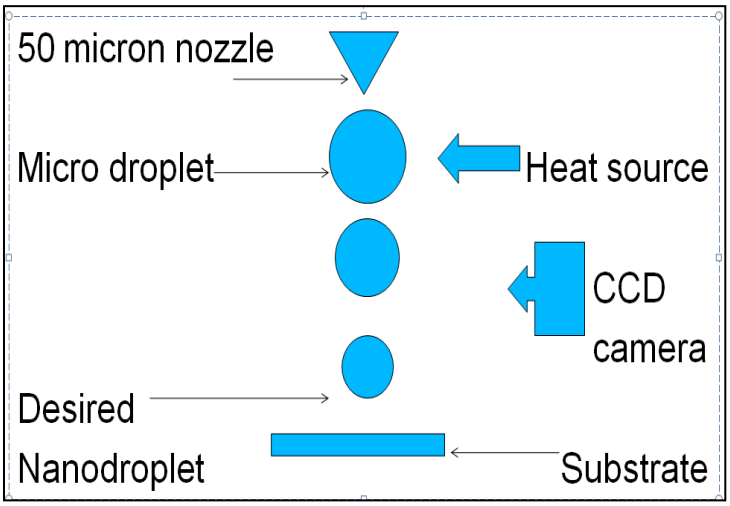

Figure 1.5. Micro-to-nano transformation scheme under consideration.

1.4 Research Objectives / Hypotheses

The main focus of this research is the understanding of micro-to-nano transformation of liquid droplet through evaporation and mechanism of its subsequent deposition on substrate. The specific objectives of this research include the modeling and simulation of:

1. Micro-to-nano transformation of liquid droplet through evaporation.
2. Impingement and deposition of nanodroplet on substrate, and

3. The spreading of nanodroplet on substrate (substrate wetting behavior) with different substrate topologies.

The following questions are addressed in this research;

1. What is the effect of temperature, evaporation time and fluid type on the size reduction rate of droplet?
2. Which factors are significant in impingement and deposition of nanodroplet on the substrate?
3. Which factors have significant role in spreading of nanodroplet on the substrate with different surface topologies?

1.5 Research Outline

Molecular dynamics modeling of droplet based inkjet printing method is addressed in four phases. The first phase involved the droplet evaporation modeling and focused on size variation of droplet after application of controlled heat flux. This study investigated post ejection and pre-deposition transformation of droplet at different temperatures. The second phase included study of substrate-droplet interaction at different ambient conditions without imparting impingement velocity to the droplet. This study was specifically intended to understand the basic droplet spreading dynamics and obtain the basis for comparison of results of further investigations. The third phase studied the effect of impingement velocity imparted to droplet on its spreading mechanism on substrate. The fourth phase examined the role of substrate topology in predicting the substrate-droplet interaction. Finally, conclusions of all these four phases encompassing the study of entire process mechanism are discussed.

CHAPTER 2

LITERATURE REVIEW

2.1 Early Developments of MD Approach

The history of molecular dynamics goes back to 1953 when a modified Monte-Carlo Integration method was used to study two dimensional rigid sphere systems of molecules [12]. In this work, two molecular systems comprising 56 and 224 particle, respectively were considered and scope for further studying Lennard-Jones type interactions applied to three dimensional rigid spheres was mentioned. Later, in 1964, a system of 864 particles interacting with a Lennard-Jones potential and conforming to classical equations of motion was studied on a computer to simulate molecular dynamics in liquid argon [13]. Periodic boundary conditions were imposed for these simulations to ensure constant density and motion of argon atoms. This was the first systematic approach employed to molecular dynamics simulation to study the effect of temperature and time on the velocity of atoms. Using this work as a starting point, an algorithm to integrate equations of motions of about one thousand particles for thermodynamic study of fluids was introduced [14]. The main focus of computation was to study equilibrium quantities such as thermodynamic functions, temperature, pressure, specific heat along with time dependent correlation functions. The results obtained in this research were in overall agreement with real thermodynamic properties of the argon. In another molecular-dynamics study of liquid carbon monoxide, angular momentum functions were examined in addition to velocity [15]. Further, detailed molecular dynamics studies of liquid water particle system based on Lennard-Jones interaction was published in 1971 [16]. This

work reported comprehensive molecular dynamics study of the system of 216 water molecules and explored the role of the hydrogen bond network, temperature variation and the diffusion mechanism. This research put forward the basic dynamic model that can be used to simulate simple solutes and highlighted the need for extension of this study to include testing of the model at different densities, temperatures and solvation interfaces. However, a limited range of densities and temperatures with focus on thermodynamic aspects were considered in these early works; without much attention to solvation interfaces. Moreover, systems unrepresentative of evaporation phenomenon with a few hundred particles were studied.

2.2 Later MD Applications and Interpretation Methods

Later, various methods for interpretation of MD simulation results were developed. A method for identification of particle clusters by measurement of the proximity of particles was introduced [17]. This method used the critical radius to define the particle cluster and shown that tailored computer codes can be developed for the cluster identification under different simulation conditions. As a further simplification of this work, Fortran code for identification of clusters; customized for MD simulation with periodic boundary conditions was developed [18]. Soon after, basic theoretical concepts and corresponding practical programming instruction with sample FORTRAN codes for Monte-Carlo and MD were introduced. In addition, methodological application of MD fundamentals relating to hard spheres and Lennard-Jones atomic interactions were reported [19-20]. These compilations systematically explained the basic concepts of MD to develop MD codes and to interpret simulations.

2.3 MD Applications to Solvent Based Systems

In a step ahead towards MD application to solvent based systems, research on aliphatic hydrocarbons in the liquid state as solvent and modeled with the molecular mechanical potential parameters was published [21]. In this work, the role of solvent interfaces in modeling of organic and biochemical systems was addressed and studied in detail with focus on the thermodynamic behavior of aliphatic hydrocarbons (methane to hexane) acting as solvents. More relevant to research under consideration, a comprehensive study on the application of MD modeling for computing evaporation rates for three-dimensional submicron argon droplets (with 2048 atoms) under subcritical conditions was published [22]. In this study, the interactions between vapor and liquid phase of argon droplets were studied to estimate the evaporation rates and compared with theoretical values. This was the first detailed study of MD application to investigate submicron droplet evaporation rates where results were in close agreement with theoretical models for macroscopic evaporation rates. However, the study was focused on argon fluid with limited number of atoms in the simulation system. Similarly, investigation of transport phenomena at liquid-vapor interfaces of argon using molecular dynamics was reported [23]. This work accomplished evaporation-condensation dynamics studies of argon and water in a wide range of temperatures. Molecular exchange and surface migration were subsequently observed. However, the main focus of study was on gas absorption dynamics of the pure liquid and mixtures.

Another study on application of MD for liquid evaporation simulation emphasizes the binding energy level requirement for liquid atoms to participate in the evaporation

process[24]. In this work, the role of binding energy of atoms in the surface layer was shown to be instrumental in the progress of evaporation. This work also investigated the transition between liquid and gaseous phases and velocity distribution function of the atoms for evaporation into a vacuum. Further, MD simulation methods were applied to the system of biological molecule surrounded with solvent clusters of water [25]. MD simulation was used to describe a method to model water drop evaporation and dynamical behavior of the liquid-vapor molecular system [26]. However, the numbers of molecules included in the system were few (2,037) due to the lack of computing resources. For more accurate results, a system more than 5,000 molecules was recommended. Molecular dynamics simulations were also used to study the sub-critical evaporation of a nanometer-size droplet at 300K and 3MPa and heat conduction problems in submicron scales were addressed [27]. Further, the evaporation of a thin liquid argon layer into a vacuum was investigated employing molecular dynamics simulation method based on the Lennard-Jones potential [28]. Similar research investigated the evaporation of a thin water layer into vacuum using molecular dynamics simulations based on TIP4P model intermolecular potential [29]. The results of these simulations described micro scale physical phenomena at the liquid–vapor interface such as evaporation, condensation, recoil after evaporation or condensation, and molecular exchanges. This research highlighted the significant role of the hydrogen bond on the molecular behavior at the interface and its effect on the evaporation coefficient. An MD approach was adopted to simulate an equilibrium situation for liquid evaporation and condensation for analyzing temperature profile, density profile, pressure profile and enthalpy for validation

of experimental results [30]. Vaporization phenomenon of 2 nm thin layer of liquid argon on a platinum surface was successfully simulated at different temperatures [31]. The significance of this work is that, in contrast to earlier studies focused on evaporation at liquid-vacuum or liquid-gas interface, the molecular dynamics approach was used to model evaporation of liquid at liquid-solid interface. A new molecular dynamics simulation methodology was reported to study the evaporation of submicron xenon droplets in nitrogen surrounding under subcritical and supercritical conditions [32]. In this research, MD results were used to evaluate the effects of ambient and droplet properties on the evaporation characteristics of submicron droplets. Further, a new method was reported for investigating surface tension, as one of the parameters for studying droplet size variation at high temperature, using molecular dynamics simulations [33]. This method used the inter-particle forces to characterize the surface region of liquid. The average particle energy in this region was then used to evaluate the surface tension of droplet and thereby its effect on droplet size. This work provided a new characterization method for droplet size variation. The only fluids considered in all these studies were argon, xenon, and water, until evaporation results were obtained using MD simulation of acetone and butyramide for different available force fields suggesting the use of multiple force fields for better prediction of experimental values [34].

2.4 Computational Advances in MD

Simultaneously, with numerous studies on MD modeling and simulation of basic liquid evaporation phenomenon, efforts were being focused on the development of efficient parallel molecular dynamics codes for simulating large systems at comparatively

low computational cost. A research work in this direction reported development and application of parallel molecular dynamics code Nanoscale Molecular Dynamics (NAMD) designed for high-performance MD simulation of large bimolecular systems [35]. NAMD was reported to have good compatibility with AMBER (Assisted Model Building with Energy Refinement) and CHARMM (Chemistry at Harvard Macromolecular Mechanics) potential functions, parameters, and file formats.

2.5 MD Applications to Substrate-Droplet Interaction Modeling

Most recent research was published on the application of a molecular dynamic approach to deviation of static and dynamic contact angle of a water droplet on a solid surface [36]. This research provides appropriate methodology for the validation scheme for characterization of substrate-droplet interaction. Similar research has also studied substrate-droplet interaction in detail for 1.4mm diameter water droplet [37]. The results obtained in this research were then used in another study of interaction between substrate and water nanodroplet for validation.

The wetting behavior of water is appropriately investigated on the macroscopic scale [38-40]. However, many nanoscale wetting phenomena have demonstrated entirely different mechanism compared to ones on macroscopic scale.

Fan-Gang Tseng studied the effect of surface tension and contact angles between a protein solution and substrate made from silicon compounds at the molecular level [41]. Research on nanoscale liquid interaction with different solid surfaces such as graphite [42], polymers [43], metals [44] and self-assembled monolayers [45] is already reported. Moreover, Sedighi et al. [46] and Park et al. [47] studied the effect of change of the

interaction energy of the solid surface with respect to the liquid and observed that the wetting ability can be extensively improved by elevating the interaction energy.

Seung Do Hong investigated the variation of static contact angle of a water droplet in equilibrium with a solid surface using an MD approach [36]. However, the research was not specific to certain substrate material. Instead, contact angles were studied for a range of characteristics solid surface energies mimicking different solid surfaces. B. Ohler and W. Langel reported MD modeling and contact angle measurement for TiO2-water interaction [48]. Cheng-Da Wu used MD simulation to investigate the effects of temperature, nanodroplet size, and surface roughness on the wetting properties of water with gold substrate [49]. Taura and Matsumoto studied water microdroplet shape variation under high impingement velocity [50]. However, the research was focused on microdroplet without considering specific substrate materials. Instead, the new wall model with Leonard–Jones potential was proposed to act as a friction surface.

2.6 Significance of Current Research

Although ample research is conducted to simulate liquid evaporation, either with vacuum/gaseous ambience or with liquid-solid interface, the study of volumetric shrinkage and molecular dispersion within nanodroplets warrants further investigation. Earlier MD models for droplet evaporation have been reported for water, argon and xenon fluids. Acetone, a commonly used solvent for nanoparticulate colloids lacks attention in terms of its nanoscale evaporation behavior. Also, though water molecule has been extensively studied at the nanoscale, the focus has been from a thermodynamic and kinetic energy transition perspective. Substrate-droplet interactions are studied in context

with water and limited substrate materials. This research investigates the evaporation behavior of two solvents (water and acetone) with a focus on the volumetric variation of the droplet. The change in the droplet density during evaporation at different temperatures is used to characterize its volume change. The effect of widely varying volatilities of water and acetone solvents on the corresponding nanodroplet evaporation timescales on the order of several magnitudes is studied. Further, root mean square deviation (RMSD) values are used to characterize the mobility of molecules and thereby evaporation rates at different time periods and temperatures. The standard density value for a liquid under given ambient conditions was used to validate the volume variation results obtained in MD simulations. Furthermore, phenomenon of nanodroplet impingement and spreading of water on different substrate materials was modeled, characterized and validated using relevant parameters. This research is a preceding step towards studying nanodroplet impingement and deposition dynamics on the diverse substrate materials.

CHAPTER 3

NANODROPLET EVAPORATION MODELING

In order to aid precise control of the nanodroplet deposition on substrates, it is important to first study its evaporation dynamics. This chapter focuses on the evaporation mechanism of nanodroplets at different temperatures and time scales. Water and acetone are used as candidate fluids for the simulation based on the differences in their densities and volatilities. The MD simulations were performed to describe the effects of ambient conditions and fluid properties on the vaporization of the nanodroplets [51]. Physical drop size reductions, volume slices at the cross section, and root mean square deviations are evaluated for different time scales and temperature ranges. The MD results show different evaporation rates and varied molecular dispersion patterns outside the droplet core region. These results are validated using standard molecular density values and a theoretical evaporation model for the respective fluids at given ambient conditions. This research provides a systematic understanding of droplet evaporation for predicting size variations in the nanoscale regime. These results are applicable to a direct write droplet-based approach for depositing different nanopatterns on substrates.

3.1 Methodology

The nanodroplet evaporation phenomenon was modeled using the MD Nanoscale Molecular Dynamics (NAMD) source code. Visual Molecular Dynamics (VMD) graphics software was used as a pre and postprocessor for molecular model development and visualization. NAMD and VMD were developed by the Theoretical and Computational Biophysics Group in the Beckman Institute for Advanced Science and

Technology at the University of Illinois at Urbana–Champaign [52-53]. NAMD was preferred over other MD codes available for the task because of its computational robustness [35] and its compatibility with a wide range of force fields from the most commonly used CHARMM [54] and AMBER [55] family. Water and acetone were the two liquids considered in the simulations based on differences in specific heat properties and evaporation dynamics.

3.1.1 Modeling of Water Nanodroplet

The modified TIP3P model was implemented within the CHARMM force field to simulate the water nanodroplet. This water model places Lennard–Jones parameters on the hydrogen atoms in addition to the oxygen atoms. However, similar atomic charges are maintained.

3.1.2 Control Volume for Water Nanodroplet

The size of the water droplet was chosen to be 40 Å (4 nm). The origin of the coordinate system was located at the centre of the droplet. To facilitate the use of periodic boundary conditions and to provide a rarified liquid vapor surrounding for simulating droplet evaporation, the control volume for the water droplet was enclosed in a liquid cube of size 70 Å × 70 Å × 70 Å. The entire water system (water droplet with 3,171 atoms and vapor ambience) consisted of 30,081 atoms. Figure 3.1(a) and Fig. 3.1(b) show the water nanodroplet model and the water droplet system with rarified vapor respectively. Normalized coordinates, optimized geometry, atomic charges, and potentials were assigned to the entire water system that included the droplet and vapor ambience using CHARMM 27 parameters [54].

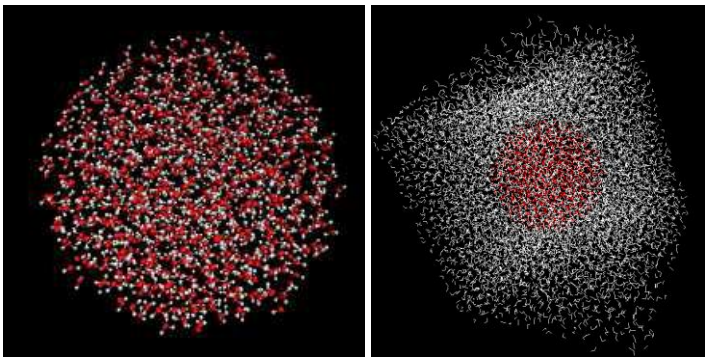

Figure 3.1. Molecular models of (a) the water nanodroplet; (b) the water droplet system with rarified vapor.

3.2 Modeling of Acetone Nanodroplet

The acetone nanodroplet system was modeled similar to the water nanodroplet system that included 40 Å acetone nanodroplet and its control volume.

3.2.1 Molecular Model of Acetone

The acetone ((CH3)2CO) molecular model with the CH3 methyl groups represented by one strong (in plane) and two weak (out-of-plane) C-H bonds was employed. This difference in C-H bond types is indicated by varying thicknesses as shown in Figure 3.2.

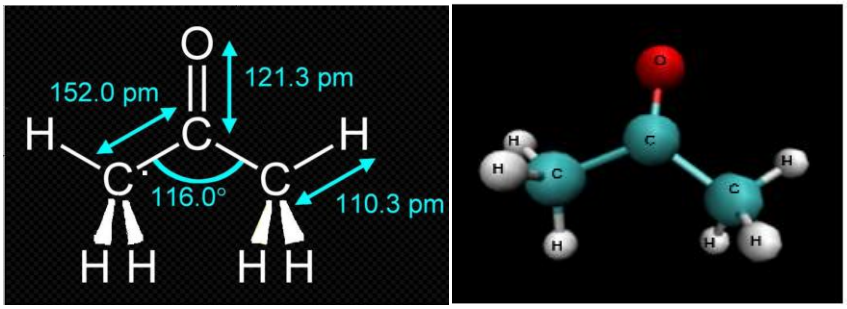

Figure 3.2. Atomic configuration of acetone molecule.

Bond lengths are mentioned in picometers. For the acetone model, the CHARMM27 common parameter database lacks some essential bond parameters that are

required to run the MD simulation. Therefore, a separate parameter database was compiled for acetone, by drawing data from CHARMM27 force fields and other relevant (Wonpil Im et al. 1994 and Marcus G. Martin et.al 2005) sources. Using this database, the VMD parameterization tool was used for assigning charges, potential and bond parameters to generate coordinate and structure files required for the acetone model.

3.2.2 Control Volume for Acetone Nanodroplet

Based on the standard intermolecular distances and molecular overlap values for acetone, the acetone droplet (40 Å) was modeled using 3,071 atoms. Due to volatile nature of acetone, the size of a periodic cell was modeled as (50 Å × 50 Å × 50 Å) liquid cube to mimic a denser acetone vapor surrounding for the droplet evaporation. The complete acetone system (droplet with 3,071 atoms and vapor ambience) was comprised of 10,000 atoms. Figure 3.3 shows the (a) acetone nanodroplet model and (b) acetone droplet system with rarified vapor.

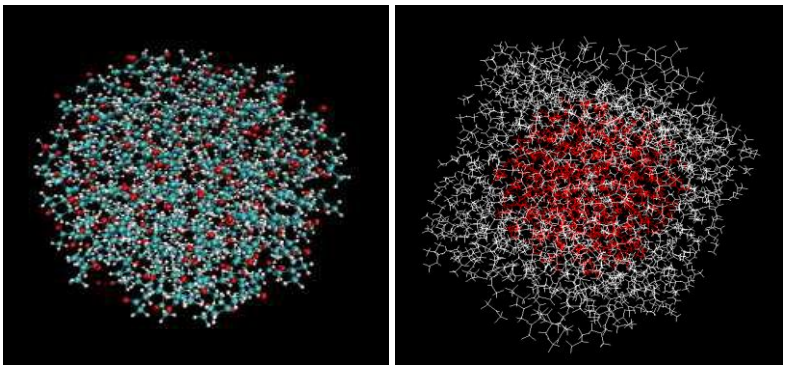

Figure 3.3. Molecular model of (a) the acetone nanodroplet; (b) the acetone droplet system with rarified vapor.

3.2.3 Integration Scheme and Solver Method

A numerical integration scheme that employs statistical mechanics was used to solve the Newtonian equations for the MD simulations. The Particle Mesh Ewald (PME) method was used to envisage temperature, pressure, and electrostatic forces. The smooth PME method was used for full electrostatic computations. The potential energy function used for the MD simulations can be simplified as:

$$U_{Total} = U_{Bond} + U_{Angle} + U_{Dihedral} + U_{vdW} + U_{Coulomb} \quad (3.1)$$

where U_{Bond}, U_{Angle}, and $U_{Dihedral}$ express the stretching, bending and torsional bonding interactions, respectively. U_{vdW} and $U_{Coulomb}$ accounts for interactions between nonbonded atom pairs that correspond to the van der Waal's forces; predicted by a Lennard-Jones 6-12 potential and the electrostatic interactions, respectively. This potential function considers interactions between all the atoms within the system or simulation volume with an assumption that every atom experiences a force determined by a model force field for interacting materials.

The selection of a suitable potential function results in optimization of computational efficiency and expected accuracy of the results. Validated force field parameters from CHARMM were used to determine the extent of the bonding interactions. The inter-molecular interaction among water molecules is described by pair wise additive Lennard-Jones potential. It is written as:

$$E_{LJ} = 4\mathcal{E}\left[\left(\frac{\sigma}{r_{ij}}\right)^{12} - \left(\frac{\sigma}{r_{ij}}\right)^{6}\right] \quad (3.2)$$

where E_{LJ} is the intermolecular potential between the two atoms or molecules, ε is a measure of attraction between two particles, and σ is the distance at which the intermolecular potential between the two particles becomes zero and gives possible closeness of two nonbonding particles (also known as van der Waals radius). Lastly, r is the center-to center distance between both particles.

To avoid surface effects at the boundary of the simulated system, a periodic boundary condition was used where the particles confined in a simulation cell were mimicked in the space through periodic translations of particles. This scheme ensures that there is always a vapor environment that envelopes spreading droplet. An NPT ensemble (constant temperature, pressure, number of particles and variable volume) was used for all simulations.

Langevin dynamics was employed to held temperature constant with a smaller coupling constant of 1 ps^{-1}. Similarly the pressure was maintained (NPT ensemble simulations) by Nosé-Hoover-Langevin piston at 1 bar. Lennard-Jones switching function of 10 Å was used for both water and acetone nanodroplet evaporation. PME grid size of 125 x 125 x 125 and 81x 81 x 81 was adopted for all water and nanodroplet simulations respectively. Based on difference in volatility, a 2 femtosecond time step was used for water whereas a 0.05 femtosecond time step was preferred for acetone nanodroplet. Multiple time step integration was achieved using impulse-based Verlet-I /r-RESPA method. The lists of neighboring atoms are considered at the frequency of 10 time steps with a cut-off radius (local interaction distance common to both electrostatic and van der Waals calculations) of 11 Å for water and 16 Å for acetone nanodroplet.

3.3 Results and Discussion for Nanodroplet Evaporation Simulation

Water and acetone nanodroplets were simulated at different temperatures namely; 293 K, 323 K, 373 K and 473 K. The water model was simulated for a period of 50 picoseconds (ps) while the acetone model was simulated for a period of 50 femtoseconds (fs), respectively. The choice of the timescale for the two fluids was based on the differences in their specific heats, volatility and the resulting evaporation dynamics. Variations in the molecular evaporation profiles and volume slices (atomic density) were studied at different temperatures and time periods. Root mean square deviations (RMSD) between individual atoms were calculated to evaluate the molecular evaporation profiles.

3.3.1 Physical Droplet Size Variations

Figures 3.4 to 3.7 show the progressive evaporation of water nanodroplets at different temperatures for an initial period of 50 ps. As can be seen from the images, the core region of the water droplet gradually decreases over the 50 ps, especially at higher temperatures. There is a marked difference in the molecular spacing between the rarified peripheral volume and that of the denser inner core, which indicates the presence of a vapor phase.

Acetone nanodroplet evaporation was observed for an initial period of 50 fs. A shorter time period was observed for the acetone nanodroplet as its molecules tend to rapidly disperse (completely evaporate) at comparable time periods to the water nanodroplet (50 ps).

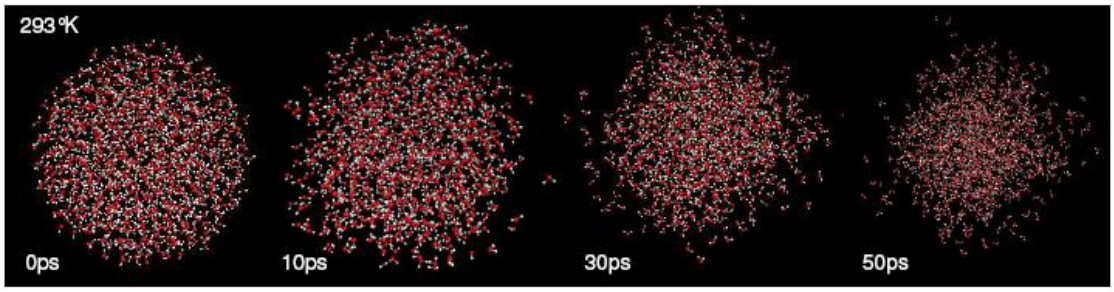

Figure 3.4. Water nanodroplet evaporation at 293 K.

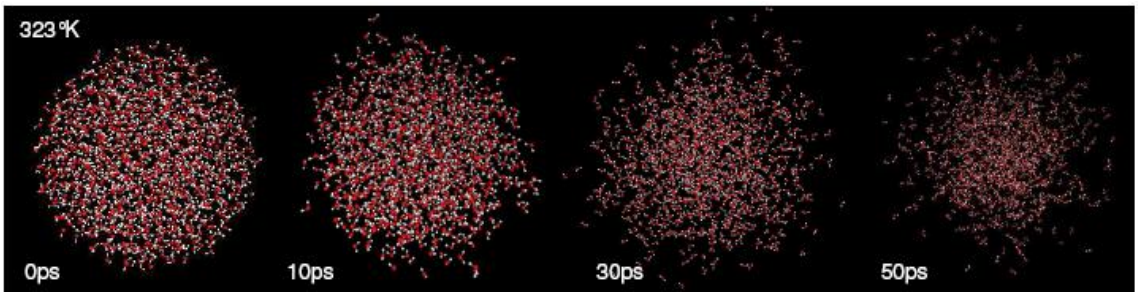

Figure 3.5. Water nanodroplet evaporation at 323 K.

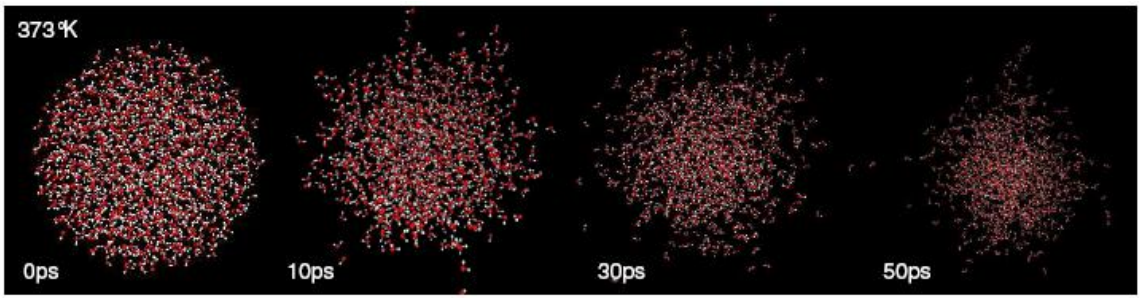

Figure 3.6. Water nanodroplet evaporation at 373 K.

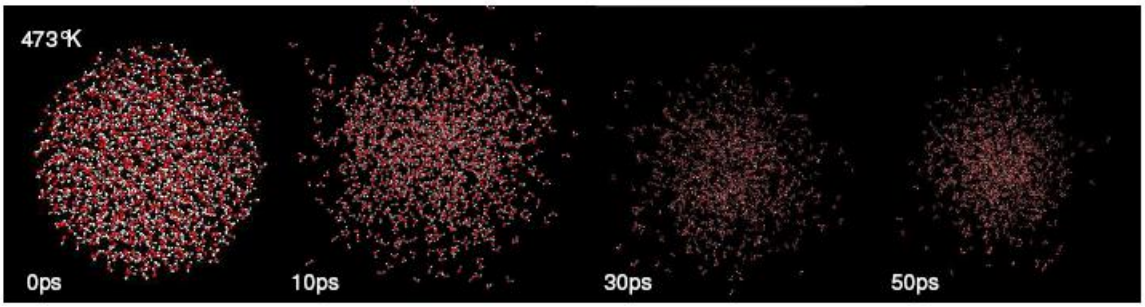

Figure 3.7. Water nanodroplet evaporation at 473 K.

Figures 3.8 to 3.11 show the progressive evaporation of an acetone nanodroplet at different temperatures. The acetone droplet shows molecular dispersion and rarification throughout the droplet volume, compared to a decrease in the central core region for the water nanodroplet. There is a pronounced phenomenon for acetone at higher temperatures to form molecular clusters within the nanodroplet volume, which can be attributed to the lower specific heat and higher vapor pressure of acetone compared to that of water.

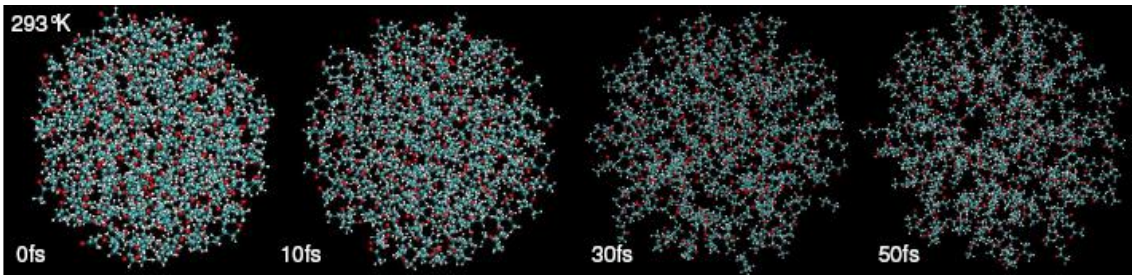

Figure 3.8. Acetone nanodroplet evaporation at 293 K.

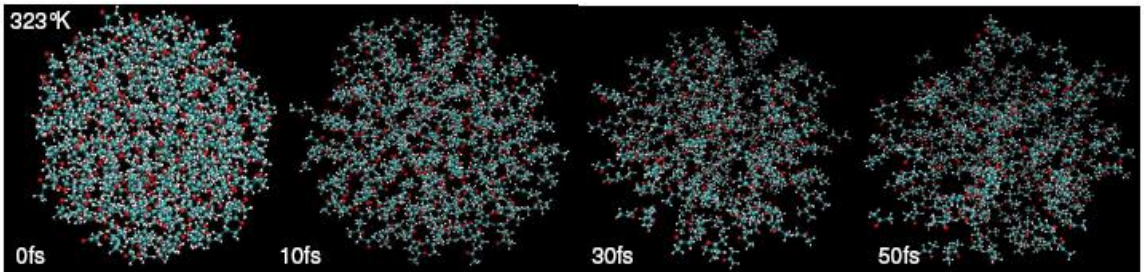

Figure 3.9. Acetone nanodroplet evaporation at 323 K.

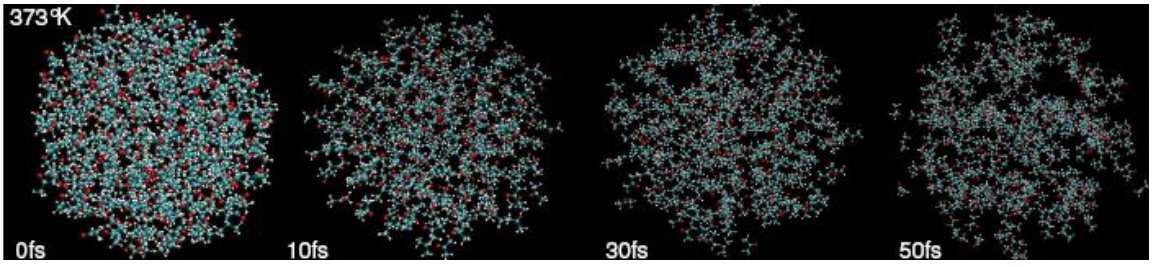

Figure 3.10. Acetone nanodroplet evaporation at 373 K.

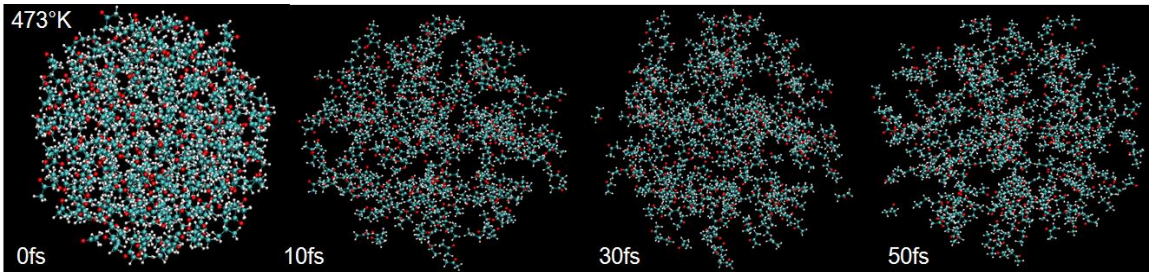

Figure 3.11. Acetone nanodroplet evaporation at 473 K.

3.3.2 Volume Slice Variations

Volume slices represent the projection map of nanodroplet atoms on the central cross-section plane. This plot indicates the occupancy profile of the droplet volume based on the atomic density. Figures 3.12 and 3.13 show the nanodroplet volume slices at different time periods and temperatures for water (30 ps) and acetone (30 fs), respectively.

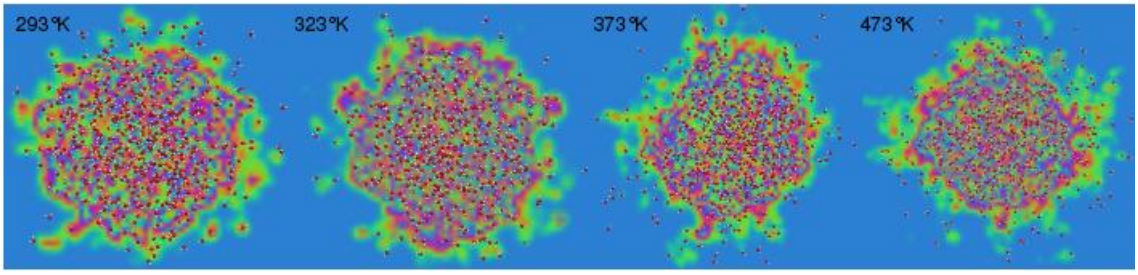

Figure 3.12. Volume slices of water nanodroplet at 30 ps.

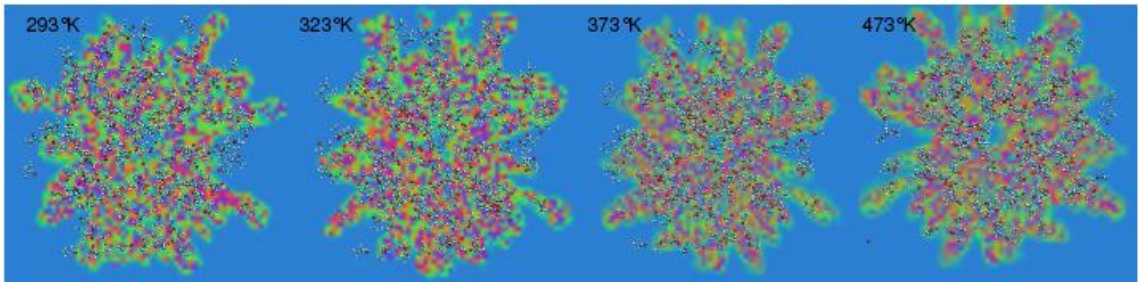

Figure 3.13. Volume slices of acetone nanodroplet at 30 ps.

The water nanodroplet shows a reduction in the atomic density on the volume slice with an increase in temperature. These results correlate with the RMSD and physical drop size measurements, indicating a reduction (evaporation) in the droplet core radius at higher temperatures. In the case of acetone, the volume slice at lower temperatures shows a uniform atom distribution. However, at higher temperatures (473 K) the volume slice shows a clustered patterned for the atoms. These results correlate with the physical drop size reduction and evaporation profiles described for acetone.

3.3.3 RMSD Variations

The RMSD is a numerical measure of the difference between two structures. It is the measure of the average distance between the atoms over a period of time at a given temperature. RMSD values between individual atoms were calculated to evaluate the molecular evaporation profiles. Here, these values are used to observe the evaporation trend at given temperature. The average RMSD values were determined using an algorithm in VMD for every temperature and at a specific interval for a given simulation. These values were then used to characterize evaporation dynamics of the droplet. It should be noted that higher RMSD values signify higher evaporation rates. RMSD for the water nanodroplets consistently increases with temperature (see Figure 3.14). These trends imply proportionate evaporation rates for water nanodroplets right from the beginning phase of the evaporation. However, while maintaining a similar trend as that of water, the RMSD values for acetone nanodroplets show significant growth at 473 K compared to that of lower temperatures (see Figure 3.15). This is mainly because of a rapid rise in the vapor pressure of acetone at elevated temperatures.

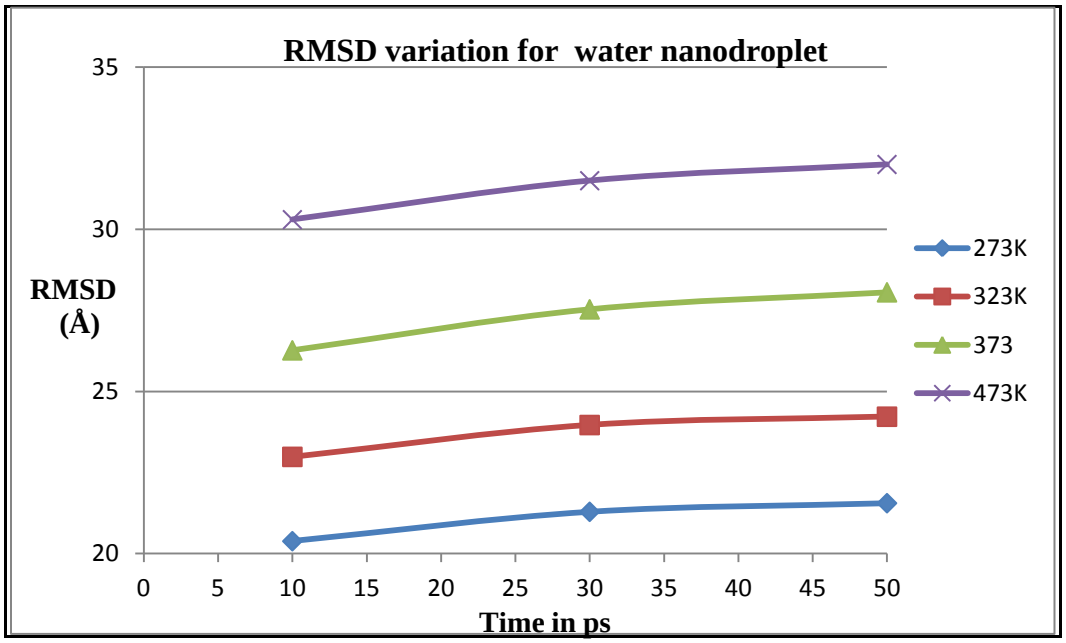

Figure 3.14. RMSD variation for 40 Å nanodroplet at different temperatures (water).

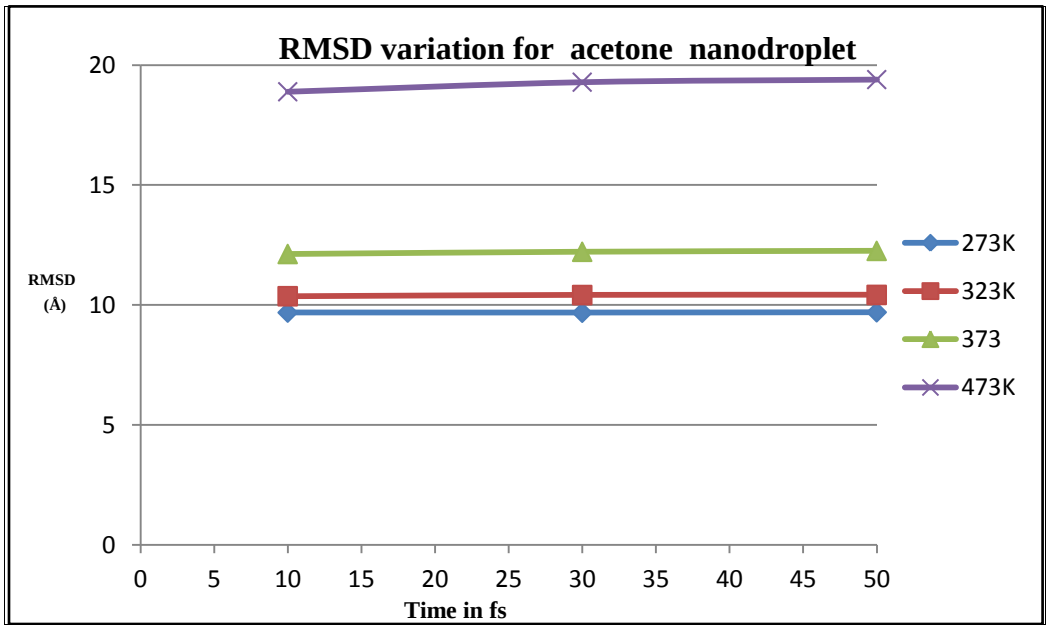

Figure 3.15. RMSD variation for 40 Å nanodroplet at different temperatures (acetone).

Moreover, as evaporation of acetone nanodroplets starts from within the body of the droplet (unlike the water nanodroplet), the RMSD variation rate is lower compared to that of the water nanodroplet where differential evaporation phenomena occur at the surface and core of the nanodroplet. In the case of acetone nanodroplets, the acetone molecules disperse as clusters during evaporation, thereby reducing the average interatomic distances, resulting in lower RMSD values compared to water. However, the increase in RMSD values for an acetone nanodroplet is consistent at different temperatures.

3.4 Validation Scheme for Nanodroplet Evaporation Models

The results of the MD simulations were validated by two methods. In the first method, the theoretical atomic density values for water and acetone were compared with their respective MD results. The second method involved tracking the evaporation profiles for a droplet with an equivalent heat and mass transfer model (Goering et al., 1972).

3.4.1 Theoretical Atomic Density

The atomic density for the simulated nanodroplet (core radius) was measured in VMD. Furthermore, the standard (theoretical) liquid atomic density was calculated using the molecular packing density for both fluids. Both the simulated and theoretical atomic densities were compared at ambient conditions.

3.4.1.1 Atomic Density Calculations for Water

The calculations for theoretical atomic density of water are shown. The nanodroplet simulation condition was as follows:

T =373 K and P =1 atm. (1.013 bar). Water has 18.02 g per mole. Thus, 1 g of water has 1/18.02 moles. Based on Avogadro's constant (6.02 × 1023), 1 g of water contains (1/18.02) × 6.02 × 1023 molecules.

Number of molecules in 1 g of water = (1/18.02) × 6.02 × 1023.

Density of liquid water at 373 K and 1 atm. = 958 kg/m^3 = 9.58 × 10^{-25} g/$Å^3$.

That is, there are 9.58 × 10^{-25} g of liquid water in a 1 $Å^3$ volume.

Number of molecules at 373 K in 9.58 × 10^{-25} g of water in 1 $Å^3$ = (1/18.02) × 6.02 × 1023× 9.58 × 10^{-25}

= 0.032 molecules/$Å^3$

= 3 × 0.032 (water molecule has three atoms)

= 0.096 atoms/$Å^3$.

Therefore, the theoretical density of a 10 Å radius liquid water core at 373 K and 1 atm. pressure was 0.096 atoms/$Å^3$.

The observed density for a 10 Å radius liquid water core at 373 K and 1 atm pressure after MD simulation (calculated in VMD) was 0.0978 atoms/$Å^3$ (close to standard density of 0.096 atoms/$Å^3$).

3.4.1.2 Atomic Density Calculations for Acetone

Similarly, the acetone nanodroplet was simulated at T = 293 K, P =1 atm (1.013 bar). Acetone has 58.08 g per mole. Thus, 1 g of acetone has 1/58.08 mole. One mole of

acetone also has 6.02 × 1023 molecules (Avogadro's number). Therefore, 1 g of acetone has (1/58.02) × 6.02 × 1023 molecules.

Number of molecules in 1 g of acetone = (1/58.02) × 6.02× 1023

Density of liquid acetone at 293 K and 1 atm. = 790 kg/m3 = 7.9×10^{-25} g/Å^3.

That is, there are 7.9×10^{-25} g of liquid acetone in a 1 Å^3 volume.

Number of molecules at 293 K in 7.9 ×10−25g in 1 Å^3

$$= (1/58.08) \times 6.02 \times 1023 \times 7.9 \times 10^{-25}$$

$$= 0.0082 \text{ molecules/Å}^3$$

$$= 10 \times 0.0082 \text{ (acetone molecule has 10 atoms)}$$

$$= 0.082 \text{ atoms/Å}^3.$$

Therefore, the theoretical density of a 10 Å radius liquid acetone core at 293 K and 1 atm. pressure is 0.082 atoms/Å^3. The observed density for a 10 Å radius liquid acetone core at 293 K and 1 atm. pressure after MD simulation (calculated in VMD) was 0.0826 atoms/Å^3 (close to standard density of 0.082 atoms/Å^3). Thus, both water and acetone MD models displayed close conformance with their respective theoretical atomic densities.

3.4.2 Theoretical Model for Evaporation Profile

The evaporation phenomenon for nanodroplets was validated by an equivalent heat and mass transfer model proposed by Goering et al. [56]. This model was used by Kincaid and Langley [57] to predict the rate of diameter change for an evaporating droplet, based on Equation (3.3). The diffusivity K, as stated in Equation (3.4), is a function of both air temperature and pressure [58]. The empirical relation for the mass transfer number developed by Froessling [59] is stated in Equation (3.5).

$$\frac{dD}{dt} = -2(M_v/M_m)(K/D)(\rho_a/\rho_d)(\Delta P/P\ f)\ Nu' \quad (3.3)$$

$$K = \left(\frac{101.3}{P_a}\right) \text{x } 8.8 \text{ x } 10^{-10} \text{ x } Tk^{1.81} \quad (3.4)$$

$$Nu' = 2 + 0.60 S_c \text{ x } \frac{1}{3} \text{ x } R_e^{1/2} \quad (3.5)$$

Where, the following nomenclature applies,

D Initial droplet diameter (m)

t time for evaporation (s)

M_v molecular weight of the diffusing liquid vapor

M_m mean molecular weight of the gas mixture (air and liquid vapor)

K diffusivity (function of air temperature and pressure) in m^2/s

P_a atmospheric pressure in kPa

T_K liquid temperature in K

ρ_a density of air (Kg/m^3)

ρ_d density of liquid in drop (Kg/m^3)

Pf partial pressure of air, kPa

Δp Pressure difference between air and liquid vapor (kpa)

Nu' mass transfer number

Re Reynolds's Number = DV/ν

V velocity of droplet relative to air, m/s (assumed 1m/s)

ν Kinematic viscosity of air, m^2/s

Sc Schmidt Number = ν /K

3.4.3 Evaporation Profiles for Water and Acetone

Water and acetone MD models were simulated for a period of 500 ps and 300 fs, respectively. These time scales were chosen based on the time period it takes to completely evaporate the two liquids based on the *dD/dt* model.

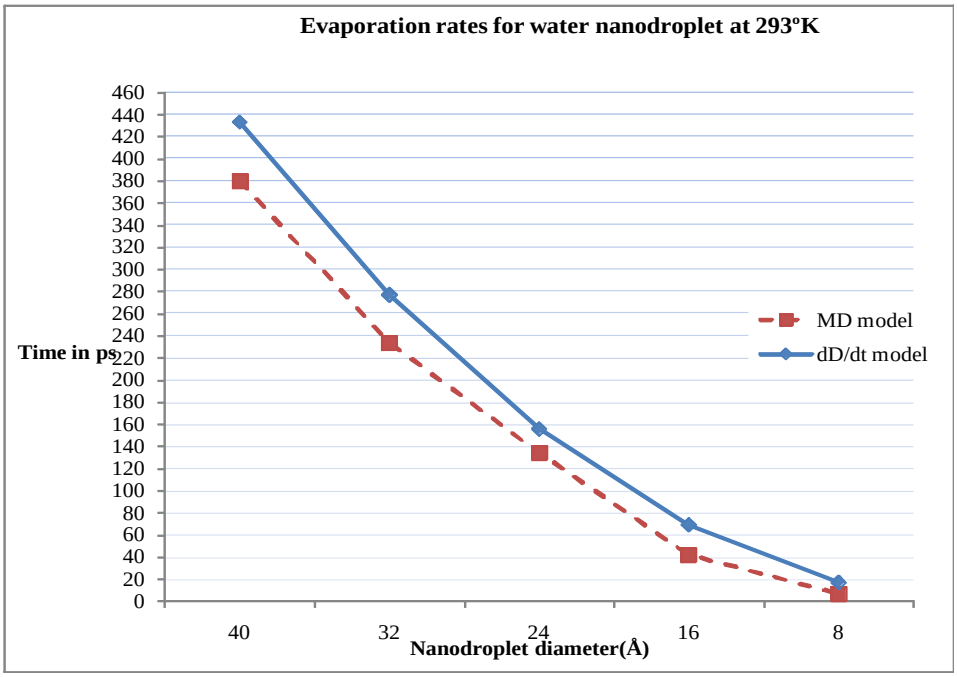

Figure 3.16. Evaporation rates for water nanodroplet at 293 K.

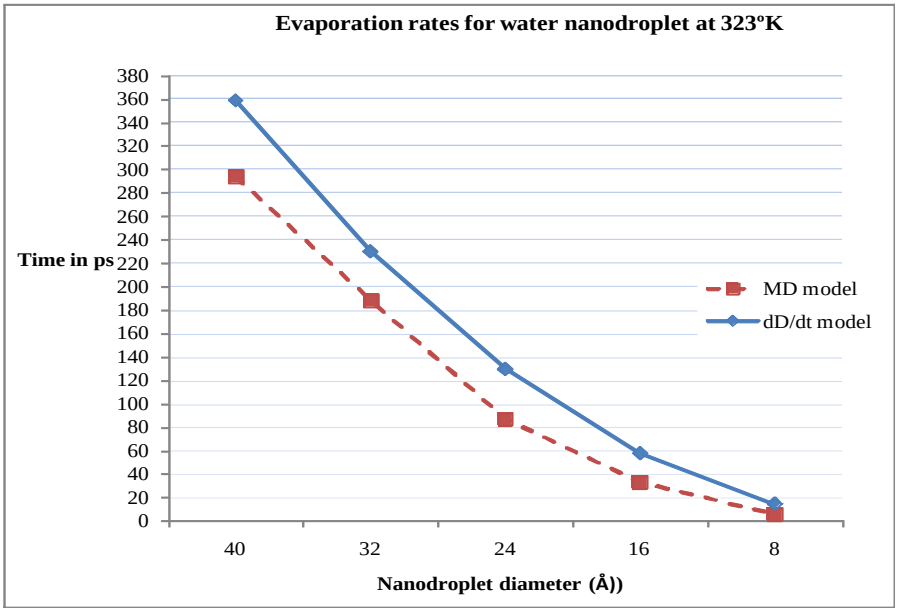

Figure 3.17. Evaporation rates for water nanodroplet at 323 K.

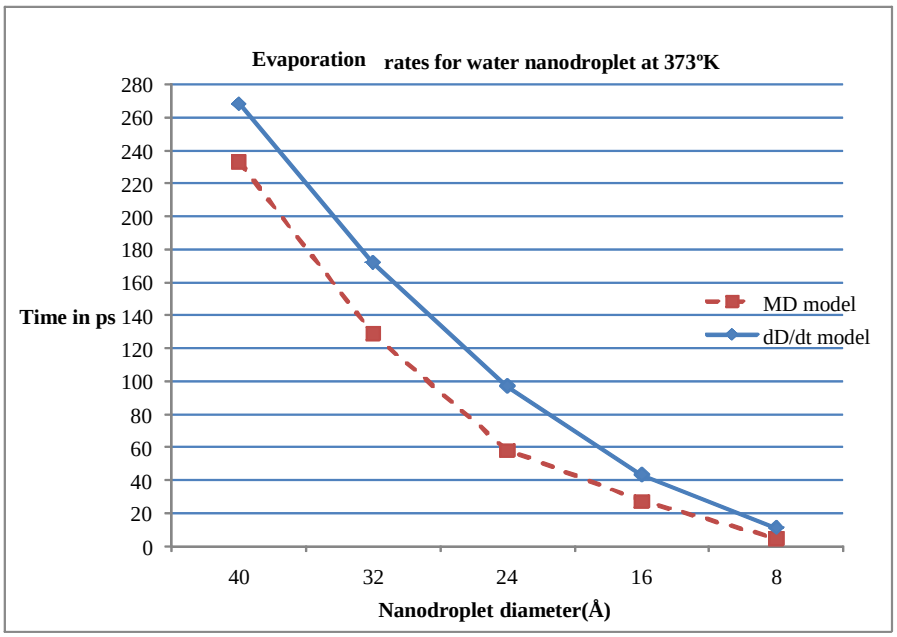

Figure 3.18. Evaporation rates for water nanodroplet at 373 K.

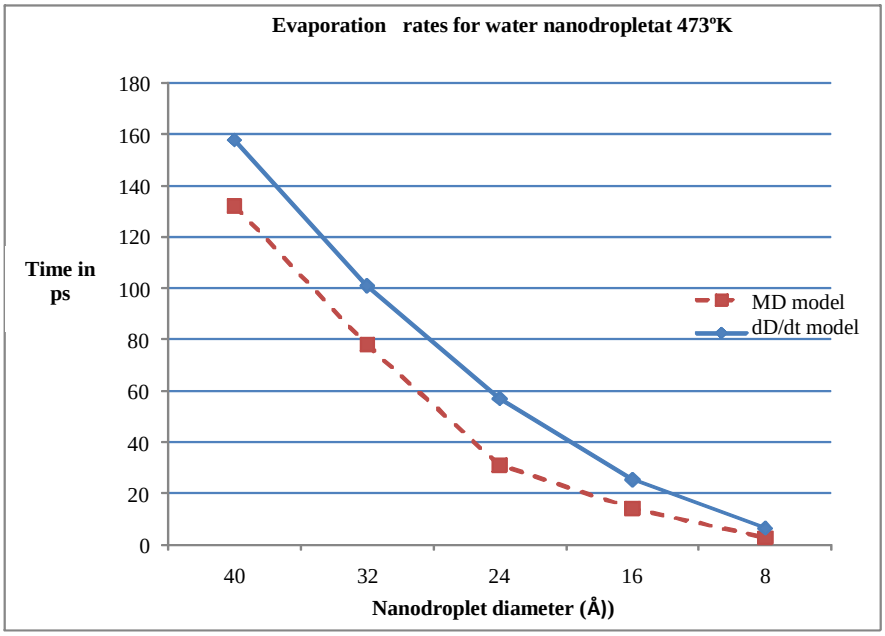

Figure 3.19. Evaporation rates for water nanodroplet at 473 K.

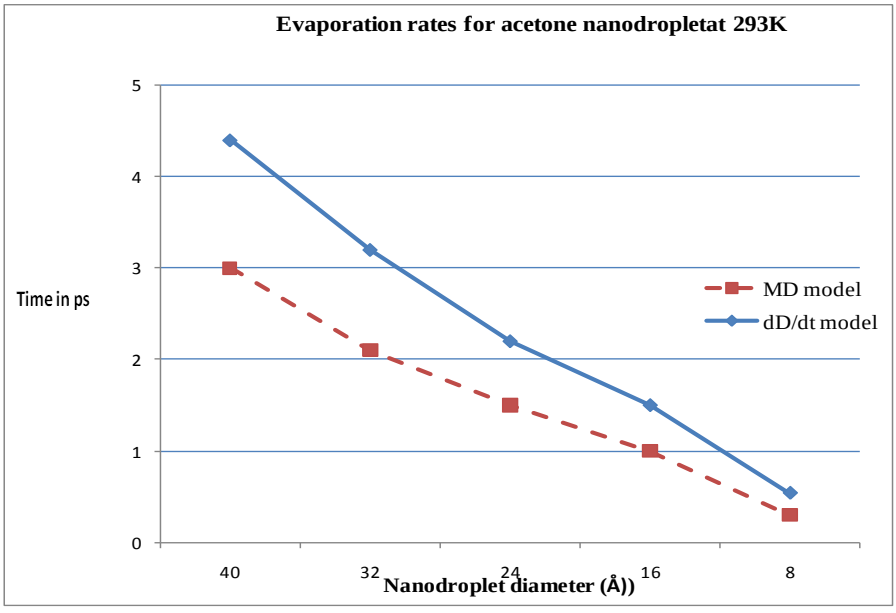

Figure 3.20. Evaporation rates for acetone nanodroplet at 293 K.

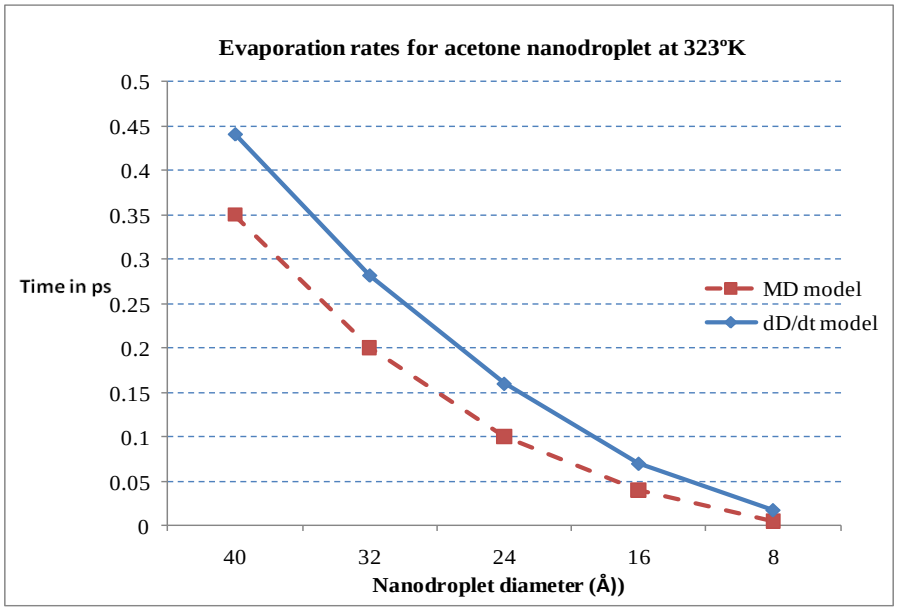

Figure 3.21. Evaporation rates for acetone nanodroplet at 323 K.

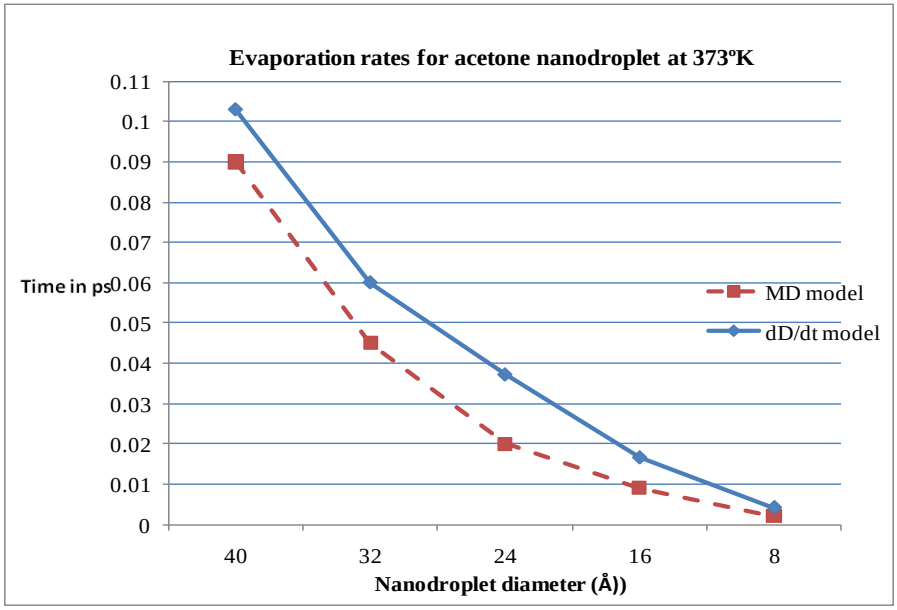

Figure 3.22. Evaporation rates for acetone nanodroplet at 373 K.

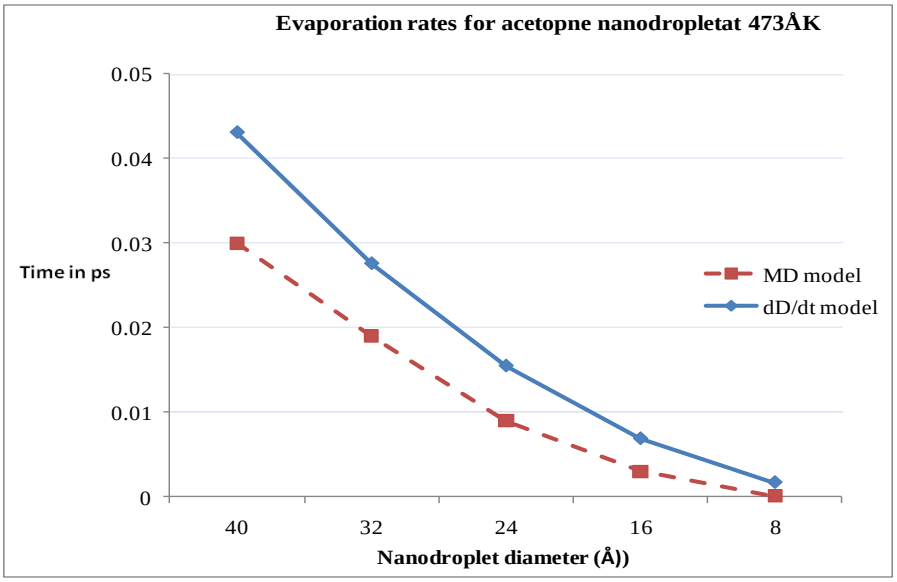

Figure. 3.23. Evaporation rates for acetone nanodroplet at 473 K.

Figures 3.16 to 3.23 show the comparison of evaporation rates for MD and the *dD/dt* model for water and acetone liquids. For both water and acetone, the MD models indicate faster rates of evaporation compared to that given by the *dD/dt* model. The variations in the evaporation profiles with respect to temperature indicate a differential evaporation phenomenon. The water and acetone nanodroplets at lower temperatures (293 K) take longer times to evaporate compared to higher temperatures (473 K). Although most of the MD evaporation profiles conform closely to the *dD/dt* model, the error between the two evaporation rates is evident at the start of the evaporation of the acetone nanodroplet at 293 K and 473 K, respectively. This can be attributed to the fact that the MD approach applies a more realistic energy minimization/distribution algorithm at lower and higher temperatures for volatile liquids, unlike the *dD/dt* model, which assumes an equal energy level at all temperatures at the beginning of the evaporation. Thus, the MD models are reliable predictors of the evaporation phenomenon of water and

acetone droplets at nanoscale dimensions. Understanding this evaporation mechanism is essential for the determination of appropriate controls in the proposed droplet based nanomanufacturing process.

3.5 Conclusion of Nanodroplet Evaporation Study

This study was focused on the evaporation mechanism of nanodroplets at different temperatures and time scales. The physical drop size reductions, RMSD values, and volume slice variations for water and acetone nanodroplets are evaluated. In the case of the water nanodroplet, there exists a distinct difference in molecular spacing between the rarified peripheral volume and the denser inner core, which indicates the presence of a vapor phase. Also, at higher temperatures, the droplet core region decreases at a rapid rate compared to the lower temperatures, suggesting a differential evaporation phenomenon. In contrast to water, the acetone droplet shows molecular dispersion and rarification throughout the droplet volume. The formation of dispersed molecule clusters within the nanodroplet volume at femtosecond time scales can be attributed to the lower specific heat and higher vapor pressure of acetone compared to that of water. These molecular models provide a better understanding of the heat flux, time scales, and vapor phase evolution during nanodroplet evaporation. Theoretical validation models have shown close conformance with the MD results for evaporation profiles of water and acetone nanodroplets. The results of this research are critical in determining process parameters for scalable (micro to nano) droplet-based manufacturing. In addition, the MD models developed served as a basis for simulating nanodroplet impingement on substrates.

CHAPTER 4

NANODROPLET-SUBSTRATE INTERACTION MODELING

SiO2 and Si_3N_4 are the two substrate materials considered in this research; especially because of their wide range applications in micro/nano/bio manufacturing industry for developing nano-biodevices. In photovoltaic cell fabrication, the nanoparticles are formed directly on top of these two most common dielectrics materials [60]. Thin films of electrical insulators are indispensable in fabrication of electronic devices. Most widely used electrical insulators are SiO_2 and Si_3N_4. SiO_2 is extensively used as critical material in integrated circuits as insulating layers, diffusion masks, ion implantation masks for the diffusion of doped oxides, passivation against abrasion, scratches and penetration of impurities and moisture [61]. Thus, SiO_2 and its modified forms have numerous applications in integrated circuits and being considered as promising material for future microelectronics and nanoelectronics. Si_3N_4 is very hard and scratch resistant electrical insulator and mostly used as an insulator and chemical barrier in manufacturing integrated circuits. Si_3N_4 is also used as a passivation layer for microchips. Moreover, unlike SiO2, it possesses an exceptional diffusion barrier that wards off corrosion and instability in microelectronics. Si_3N_4 is also used as a dielectric between polysilicon layers in capacitors in analog chips [61].

The basic parameters controlling inkjet-printed liquids are the viscosity and surface energy [62]. The pattern formed when an ejected drop of liquid strikes the substrate depends mostly on the ink–surface interaction. The wetting contact angle determines the

spread of a liquid droplet on the substrate and depends on the relative surface energy of the solid–liquid, solid–vapor, and liquid–vapor boundaries. High-energy surfaces produce small wetting angle and greater spread, while a low surface energy results in a smaller trace. The surface energy and contact angle also relate to the hydrophilic or hydrophobic behavior of the liquid to the substrate. Strong adhesion is linked with good wetting (hydrophilic) and low adhesion with high contact angles (hydrophobic). Most circumstances need a high contact angle to limit the spread of the printed liquid to allow further processing [63].

To inkjet print fine features on a flat surface is a challenging task because of the complexity in controlling the spread of a liquid on a free surface. The printed feature size will not only determine adhesion of material to the substrate, but will also play an important role on the design of devices.

Molecular interactions between the liquid and the solid surface essentially determine nanoscale surface wetting behavior. Therefore, detailed information regarding their chemical composition, surface structure, geometry, ambient condition and the dynamics of the liquid/solid interface is needed for estimation of wetting capability for a particular liquid/solid combination. Atomistic simulation of materials is expected to provide most realistic information in this regard. Therefore, in this research MD simulation of a SiO_2 and Si_3N_4 substrates and a liquid interface is used for exploring the nature of substrate wetting. The MD modeling approach adopted in this paper is intended to model and characterize droplet based direct write (DW) inkjet nanomanufacturing

process. More specifically, the MD approach is applied to model the molecular level nanodroplet-substrate interactions.

This research aids in the understanding the spreading mechanism of the solvent droplets for deposition of colloidal nanodroplets on different substrates. Furthermore, this research investigates the spreading phenomenon of the water nanodroplet in order to understand its substrate wetting behavior at different ambient conditions.

4.1 Methodology

For modeling the substrate-nanodroplet interaction, the water nanodroplet model was integrated with SiO_2 and Si_3N_4 substrate models. Initially, a water nanodroplet was enclosed in the simulation box and then centrally located on substrates.

4.1.1 Molecular Model of Substrates With Water Box

An identical modified TIP3P water molecular model (discussed in section 3.1.1) that is adopted within the CHARMM force field system was used to build the water nanodroplet. The 4 nm diameter nanodroplet model was built using 3,171 water atoms (1,057 molecules). The water nanodroplet was enclosed in cubical water box of size 4.6484 nm X 4.632 nm X 5.984 nm for providing flexible simulation volume for spreading droplet. Water box was created using 5,361 water atoms (1,787 molecules). The simulation volume is provided to facilitate application of periodic boundary conditions. The simulation volume (water box) was made flexible and stretched as required to accommodate spreading droplet during entire simulation. Figure 4.1 shows the (a) water nanodroplet model and (b) water nanodroplet and simulation box.

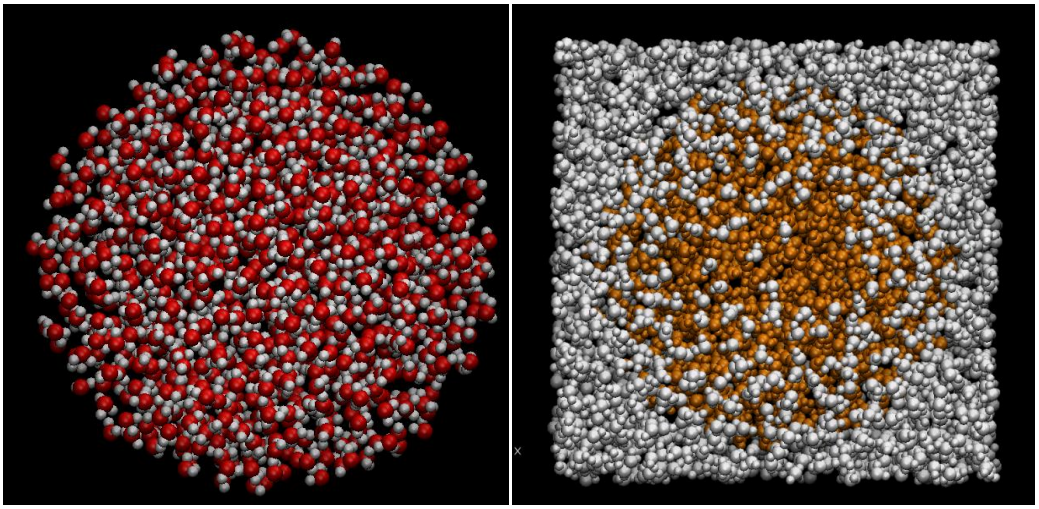

(a) **(b)**

Figure 4.1. Model of (a) water nanodroplet; (b) nanodroplet and simulation box.

SiO_2 substrate model with dimensions 20.8 nm X 20.8 nm X 3.37 nm was built using 42,336 SiO_2 atoms (14112 molecules). Similarly, Si_3N_4 substrate model with dimensions 32.032 nm X 26.205 nm X 2.422 nm was built using 11,718 Si_3N_4 atoms (3,906 molecules). An identical water nanodroplet with its simulation box was placed at the center of SiO_2 and Si_3N_4 substrates, as shown in Figure 4.2 and Figure 4.3 respectively. Thus, SiO_2-water system and Si_3N_4-water system was built using total 50,169 atoms and 20,250 atoms respectively.

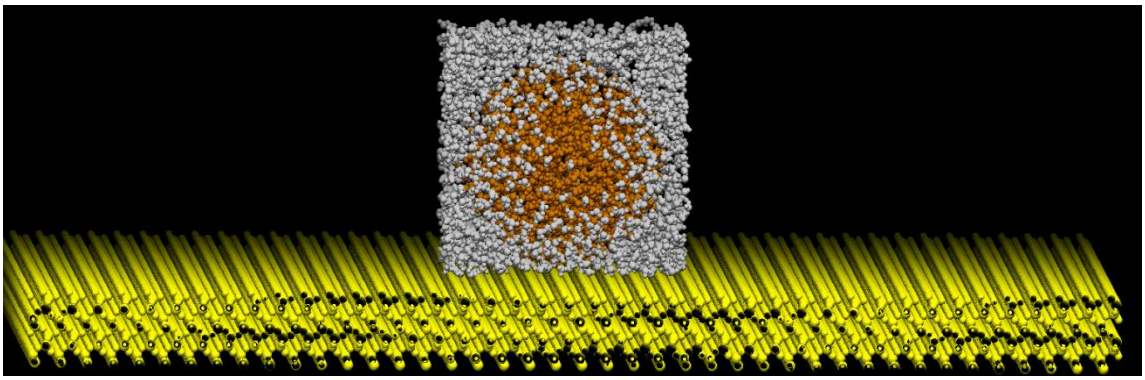

Figure 4.2. Water nanodroplet with simulation box at the center of SiO_2 substrate.

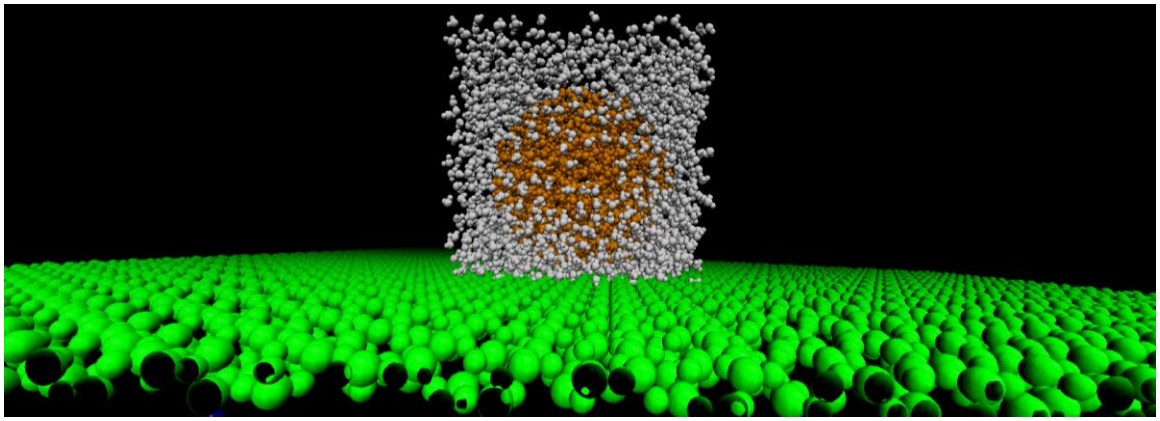

Figure 4.3. Water nanodroplet with simulation box at the center of Si_3N_4 substrate.

4.1.2 Integration Scheme and Solver Method

A numerical integration scheme and solver method discussed in section 3.1.3 was employed for simulating SiO2-water and Si_3N_4-water systems. Both the systems were simulated at 293 K, 323 K, 373 K and 473 K with 0.5 femtosecond time step. The temperature was held constant by Langevin dynamics with a smaller coupling constant of 1 ps^{-1}. Similarly the pressure was maintained (NPT ensemble simulations) by Nosé-Hoover-Langevin piston at 1 bar. Lennard-Jones switching function of 12 Å and PME grid size of 1 was adopted for all simulations. Multiple time step integration is accomplished using impulse-based Verlet-I/r-RESPA method. The lists of neighboring atoms are accounted at the frequency of 10 time steps with a cut-off radius (local interaction distance common to both electrostatic and van der Waals calculations) of 11 Å.

4.2 Results and Discussion for Nanodroplet and Plane Substrate Interaction

With the configuration discussed in section 3.2.2, plane SiO_2-water system and plane Si_3N_4-water system were simulated for 100 picoseconds and 1 nanosecond, respectively; each at the following temperatures 293 K, 323 K, 373 K and 473 K. SiO_2-water system was simulated for shorter period due to hydrophilic nature of SiO_2 substrate which expedites spreading phenomenon and equilibrium contact angle can be observed well within 100 picoseconds timeframe. However, Si_3N_4-water system was simulated up to 1 nansecond because of hydrophobic behavior of Si_3N_4 substrate that causes delay in reaching equilibrium. The dynamic contact angles were measured using Image-J software. Simulation snapshots at certain time interval were analyzed in Image-J software and average contact angles for both the systems were determined at given instants as shown in Figure 4.4.

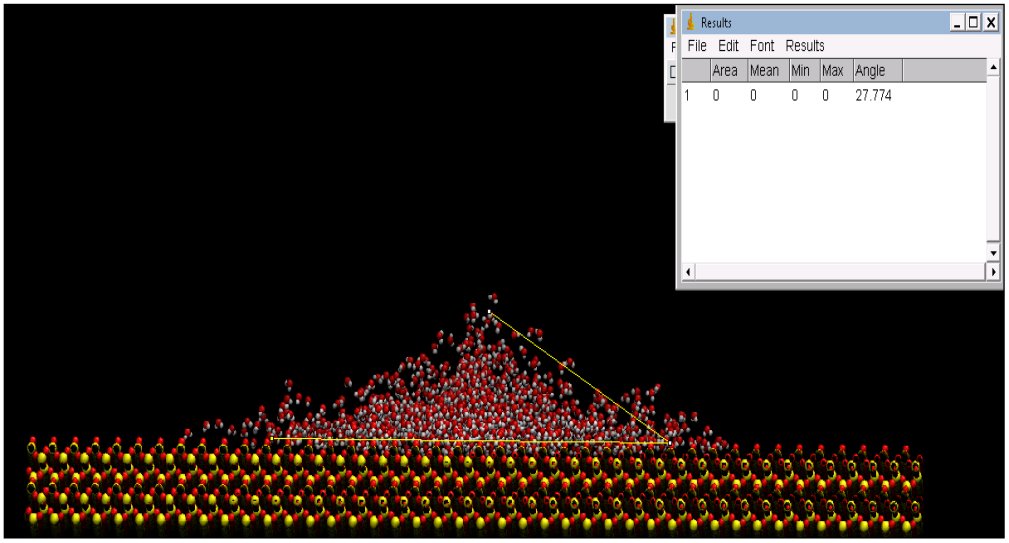

Figure 4.4. Dynamic contact angle measurement in Image-J.

4.3 Validation Scheme for Nanodroplet and Plane Substrate Interaction

Dynamic contact angle values obtained from molecular dynamic simulation were validated using molecular-kinetic theory [64]. According to this theory, the macroscopic activities of the wetting line are determined by the overall statistics of the individual molecular displacements which occur within the three-phase contact region where the liquid and gaseous phase meets the solid surface. The velocity of the wetting line is described by the frequency of molecular displacements (K) and average length of these displacements (λ). For simplicity, λ can be assumed space between two adjacent adsorption sites on the solid surface. If $K+$ is the frequency of molecular displacements in the direction of wetting and $K-$ is that in the opposite direction, then the net frequency is (K_{net}) is given by

$$K_{net} = (K+) - (K-). \quad (4.1)$$

The velocity advancement of the wetting line is therefore can be expressed as

$$v = \lambda K_{net} . \quad (4.2)$$

At equilibrium, K_{net} is zero and $(K+) = (K-) = K^0$.

Blake and Haynes assumed that unbalanced surface tension force $\gamma_{LV}\left(\cos(\theta^0) - \cos\theta\right)$ is the main driving force for advancement of wetting line where γ_{LV} is the surface tension of the liquid in contact with air [64]. Using Eyring's activated-rate theory for transport in liquids [65-66] ; Blake et. al developed the final relationship between θ and v as,

$$v = 2K^0\lambda \sinh\left[\left(\frac{\gamma_{LV}\left(cos(\theta^0) - cos(\theta)\right)}{2nK_B T}\right)\right] , \quad (4.3)$$

where

K^0 = frequency of molecular displacements at equilibrium,

λ= average length of molecular displacements,

γ_{LV} = the surface tension of the liquid in contact with air at given temperature,

θ^0 = equilibrium contact angle,

θ = instantaneous contact angle,

n = number of adsorption sites per unit area on solid surface,

K_B = Boltzmann's constant, and

T = temperature (K).

This molecular theory discussed is independent of geometry of the spreading shape. It has been normally applied for study of capillary displacement but may also be applied to spreading droplet analysis. When applied to nanodroplet spreading phenomenon, gravity force can be neglected and the shape of the spreading droplet can be assumed as a spherical cap. The geometry of a spherical cap is described by the following expression:

$$r = \left[\frac{3V}{\pi}\frac{sin^3(\theta)}{2 - 3\cos(\theta) + \cos^3(\theta)}\right]^{\frac{1}{3}} \quad (4.4)$$

Where r is the contact radius with solid surface, V is the droplet volume, and θ is the instantaneous contact angle. Assuming the constant volume of spreading droplet and partially differentiating, Blake et al. obtained following equation for instantaneous contact velocity.

$$\frac{\partial r}{\partial t} = -\frac{\partial \theta}{\partial t} \frac{\left(1-\cos(\theta)\right)^2}{\left(2-3\cos(\theta)+\cos^3(\theta)\right)^{\frac{4}{3}}} \tag{4.5}$$

Equations (4.3) and (4.5) are a linked set of partial differential equations that can be first solved for wetting line velocity (v) and eventually for dynamic contact angle θ.

This set of equations was used to validate the nanodroplet spreading phenomenon in this research. The equations (4.3) and (4.5) were solved using partial differential equations (PDE solver) in MATLAB to obtain the solutions for the v over the period required to reach equilibrium. For example, SiO_2-Water system at 293 K needed 70 picoseconds to reach equilibrium contact angle of 27^o. Therefore, the solutions to equations were obtained over a period of 70 picoseconds. After getting solution in terms of instantaneous wetting line velocity (v), the values of instantaneous contact angle (θ) were determined in MATLAB corresponding to each value of v; at certain intervals over a period needed reach equilibrium contact angle. These values of dynamic contact angle were then plotted against simulation time to theoretically describe spreading mechanism of the nanodroplet on SiO_2 and Si_3N_4 substrates at different temperatures.

The frequency of molecular displacements quantifies vertical molecular displacements which determine the velocity of wetting. A net flux into the molecular layer adjacent to solid surface makes the wetting line to progress and a net flux out of the layer results in wetting line to retreat. Frequency of molecular displacements at equilibrium(K^0) was obtained by fitting the validation curve with simulation curve. Alternatively, K^0 was also obtained from the simulation data directly by counting the number of molecular displacements at equilibrium per unit time, vertically into or out of

the 3-4 angstroms thick layer of liquid molecule adjacent to the solid surface. For this, difference in number of molecules just before and at equilibrium within 3-4 angstroms thick layer of liquid molecule was calculated using Visual Molecular Dynamics atomcount algorithm. The close agreement was observed between the corresponding K^0 values obtained by curve fitting and atomcount algorithm in VMD.

Only displacements of length greater than $0.8\,\lambda$ were considered in order to avoid possibility of misinterpreting harmonic oscillations of atoms about its initial position as definite molecular displacements. For this reason, only the molecular activities within 3-4 angstroms thick layer adjacent to the solid surface were accounted.

Average length of molecular displacements (λ) was assumed as lattice spacing (lattice constant) of substrate material. The surface tension values of the water in contact with air (γ_{LV}) at given simulation temperature T were used from the standard water properties data. The unique values of equilibrium contact angle (θ^0) for SiO_2-water and Si_3N_4-water systems were observed from MD simulations. Number of adsorption sites per unit area on solid surface (n) was determined using lattice structure and molecular pattern of substrate material surface.

Figure 4.5 (a) shows an interface that was developed in MATLAB for facilitating inputting of variables in the solver such as $\gamma_{LV,}\,\lambda, K^0, n$ and T. Figure 4.5 (b) is an example of dynamic contact angle trial solution generated in MATLAB with abovementioned inputs. The first column in the table corresponds to different time intervals over the simulation period. The next three columns include values of dynamic contact angles obtained at 293 K, 323 K, 373 K and 473 K, respectively. The dynamic

contact angles thus obtained in MATLAB were compared with those directly measured from the results of corresponding MD simulations; using Image-J software (as depicted in Figure 4.4).

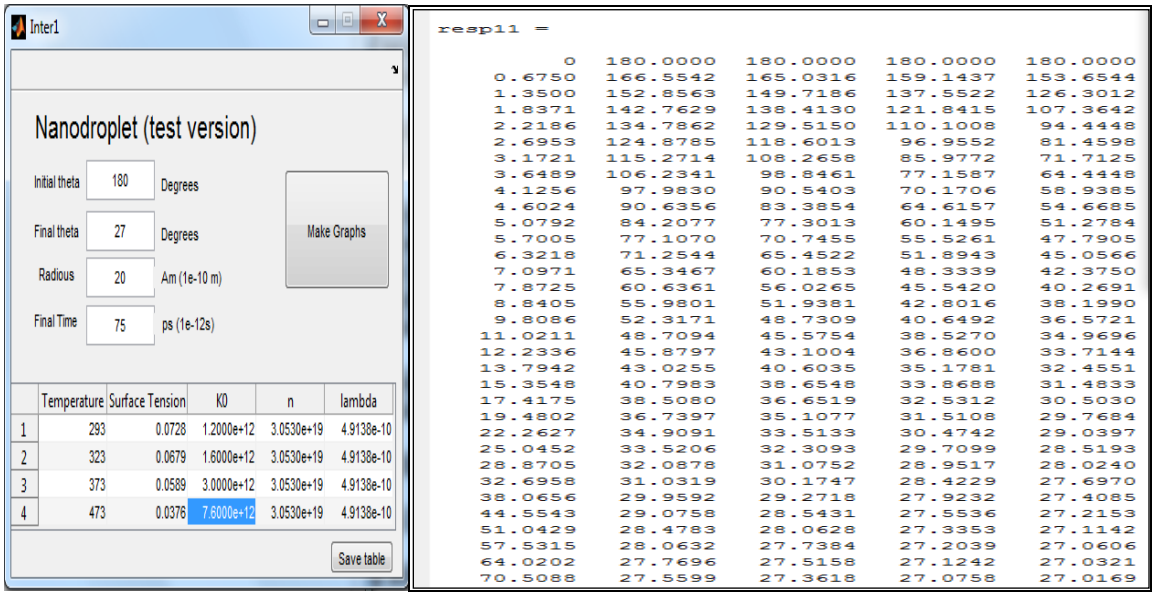

(a) **(b)**

Figure 4.5. (a) MATLAB interface; (b) Dynamic contact angle trial solution.

4.3.1 Dynamic Contact Angle Results for Nanodroplet and Plane Substrates

The Figure 4.6 through Figure 4.9 compare variation of SiO_2-water system between theoretical (those obtained in MATLAB) and MD simulation values of the dynamic contact angle with simulation time at temperature 293 K, 323 K, 373 K and 473 K respectively. For all the four temperatures, the simulation angles are observed to be slightly smaller than theoretical angles for most of the simulation time. This can be attributed to the assumption of spherical cap shape for spreading droplet while determining theoretical contact angle values. Practically, during most of the simulation period, the spreading droplet is progressively deviating from the spherical cap giving

smaller simulation angles than corresponding theoretical values. It is evident that the simulation contact angles follow the theoretical values for all temperatures, with higher rate of spreading for elevated temperatures. This can be attributed to the transfer of more molecular flux in the three phase wetting line region due to rise in kinetic energy and drop in liquid surface tension at higher temperatures.

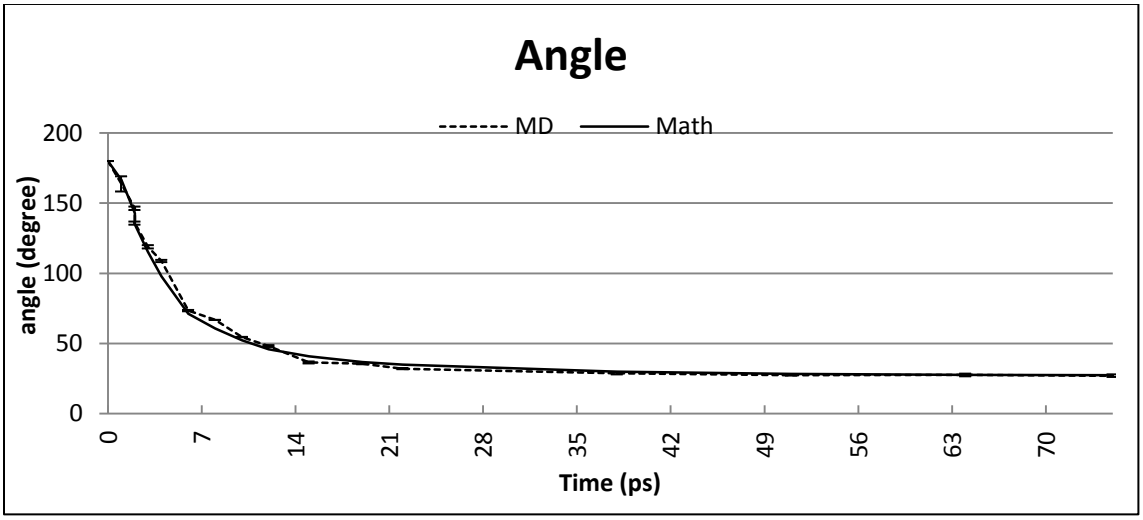

Figure 4.6. Dynamic contact angle vs simulation time for SiO_2-water at T=293 K.

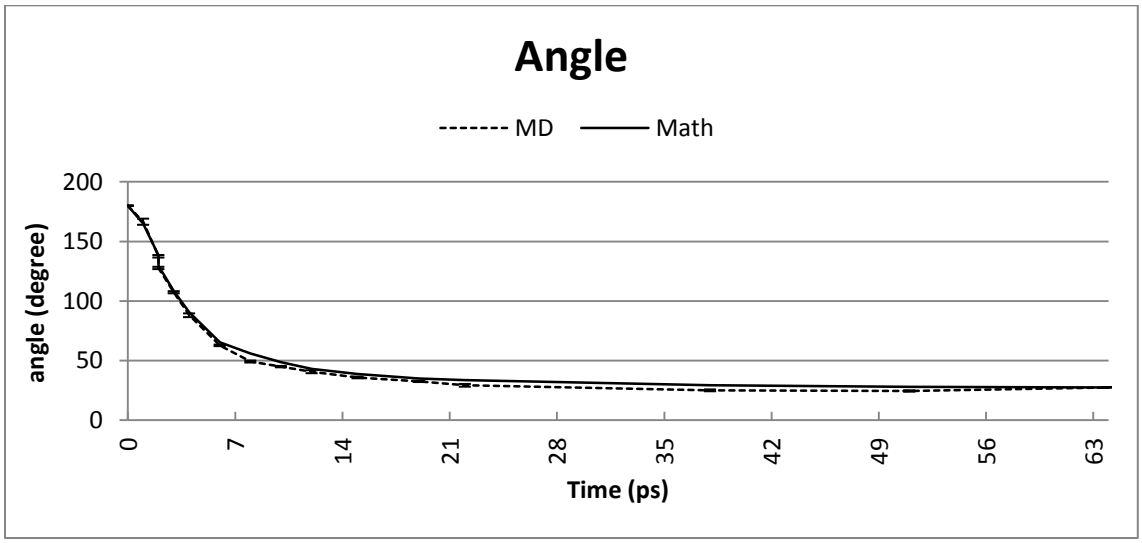

Figure 4.7. Dynamic contact angle vs simulation time for SiO_2-water at T= 323 K.

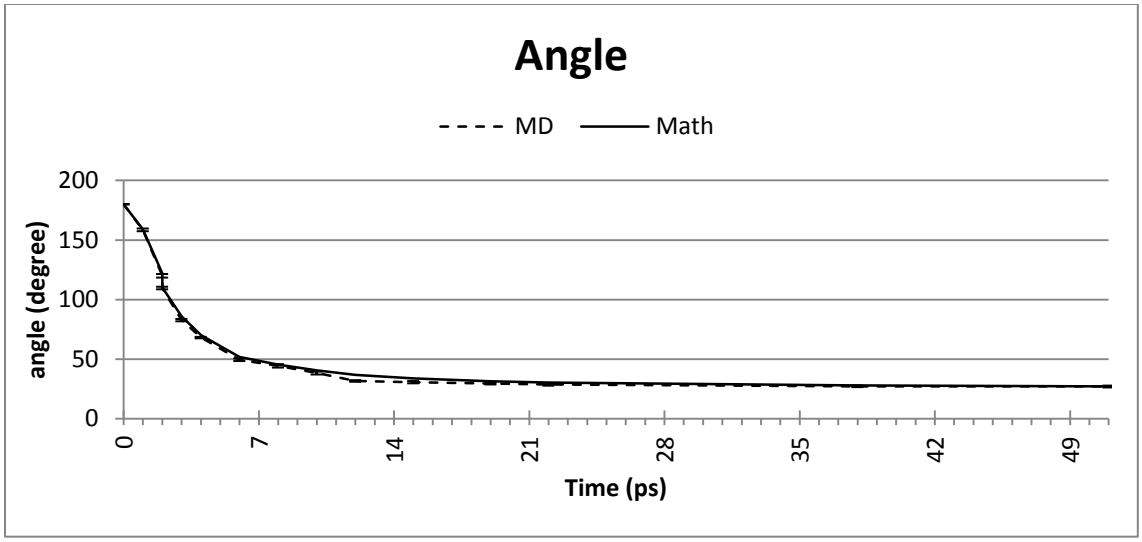

Figure 4.8. Dynamic contact angle vs simulation time for SiO_2-water at T= 373 K.

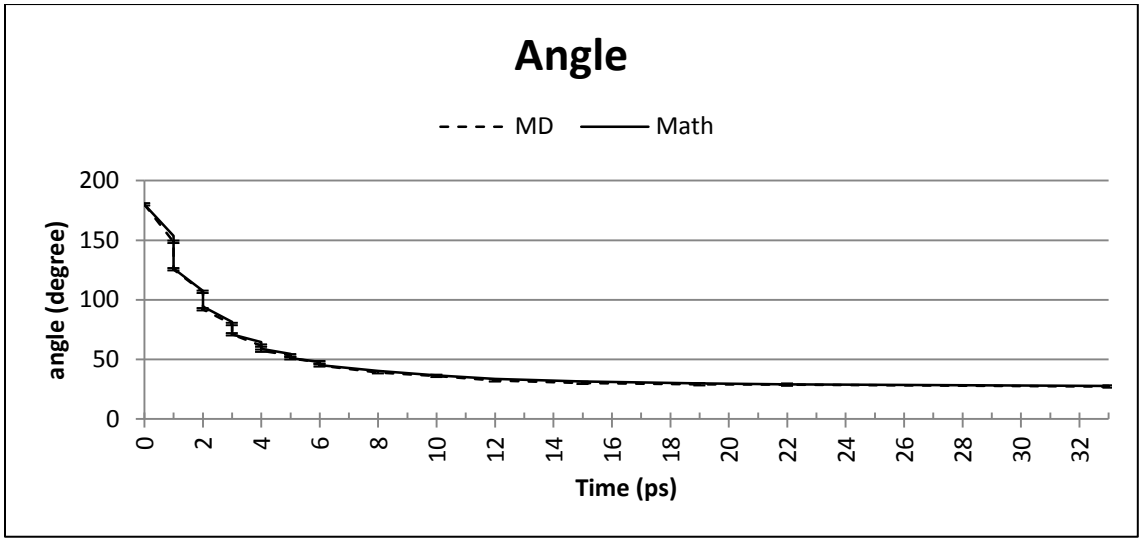

Figure 4.9. Dynamic contact angle vs simulation time for SiO_2-water at T= 473 K.

For SiO_2-water system, equilibrium contact angle (approximately 27.5^o) was observed to be reached earlier at higher temperatures. For example, equilibrium contact angle for 293 K was reached at around 70 picoseconds whereas for 473 K, equilibrium contact angle was observed approximately at 35 picoseconds. An equilibrium contact angle of 27.5^o confirms strong hydrophilic behavior of SiO_2 substrate while interacting

with water nanodroplet and closely follows macroscale SiO_2-water wetting characteristics. Figure 4.10 shows contact angle variations at different temperatures over the simulation period for SiO_2-water system

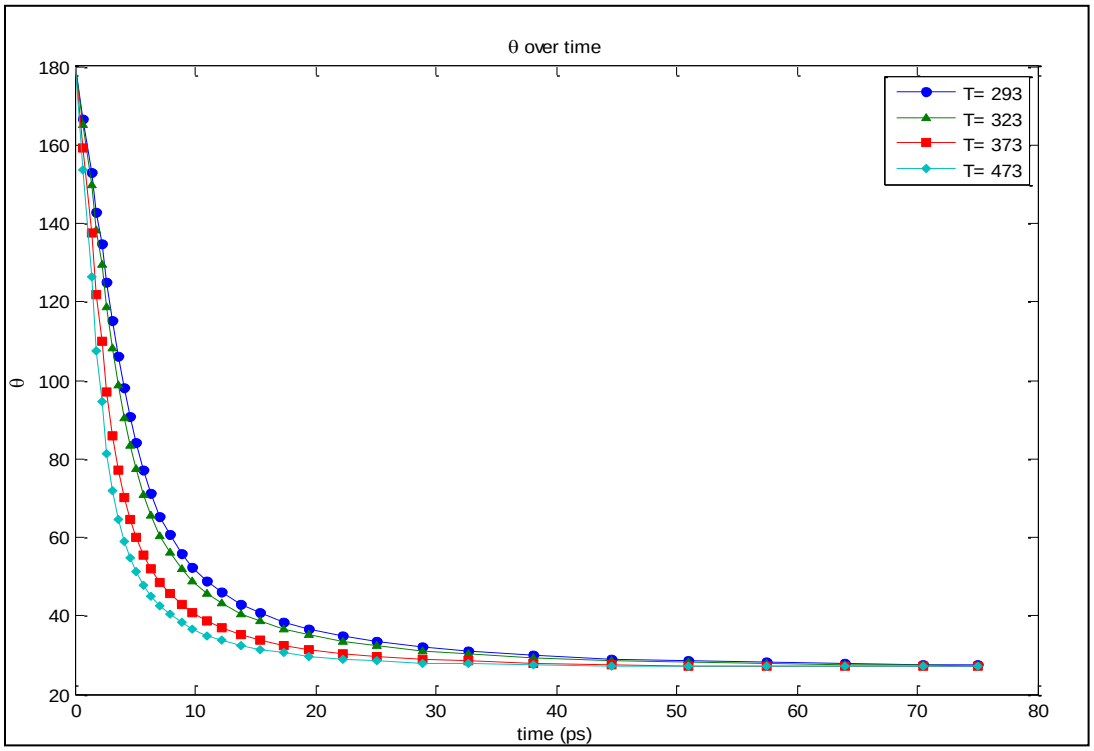

Figure 4.10. Contact angle variation at different temperatures vs simulation period for SiO_2-water system.

D/D_0 ratio (ratio of instantaneous contact diameter to the original diameter of nanodroplet) is the measure of substrate wetting phenomenon at given temperature. Figure 4.11 depicts the method of measurement of instantaneous contact diameter using Inage-J software. Figure 4.12 shows variation of *D/D_0* ratio over simulation period for plane SiO_2 substrate and water nanodroplet at different temperatures.

Figure 4.11. Scheme of measurement of instantaneous contact diameter D.

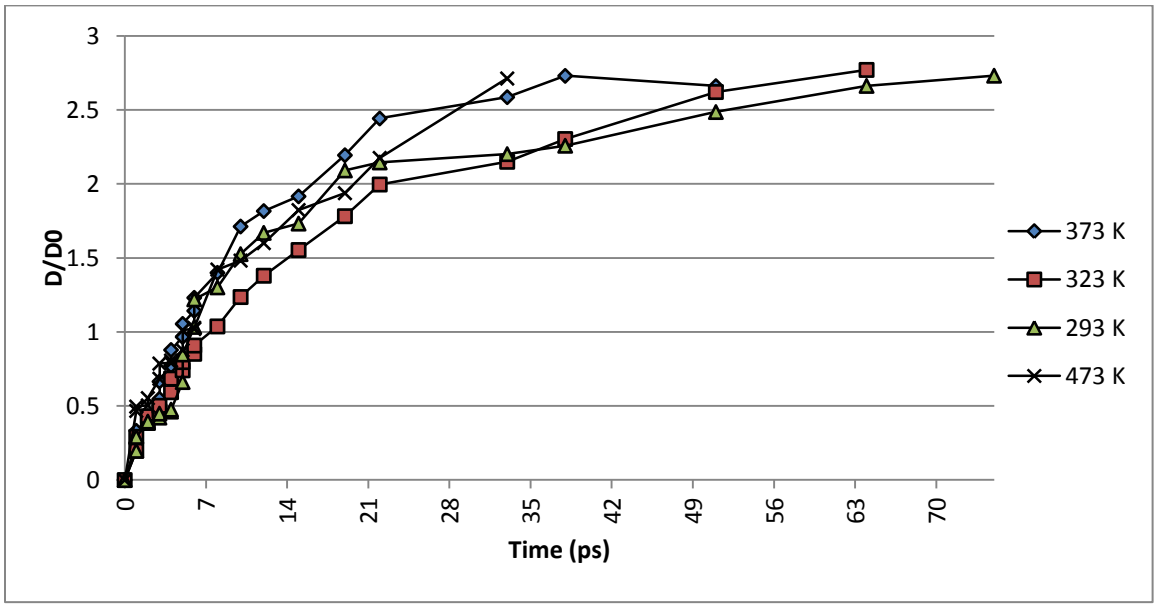

Figure 4.12. Variation of D/D_0 ratio with simulation period for SiO_2-water system.

The rate of D/Do variation is observed to be higher at elevated temperatures which indicates that at any given instant, the rate of substrate wetting is more at higher temperatures compared to that for lower temperatures.

The results of Si_3N_4-water system are shown in Figure 4.13 through 4.16.

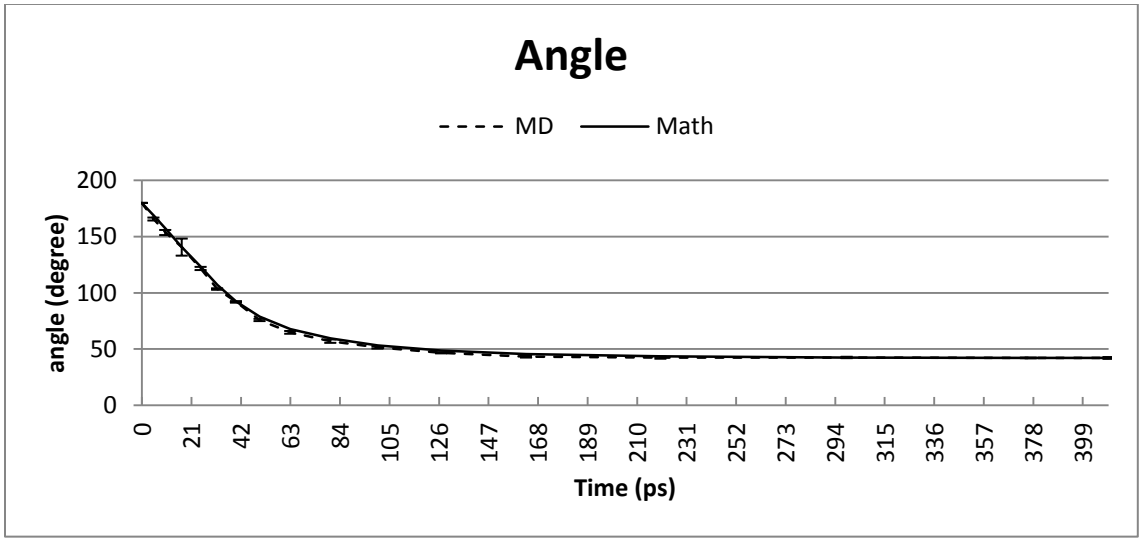

Figure 4.13. Dynamic contact angle vs simulation time for Si_3N_4-water at T= 293 K.

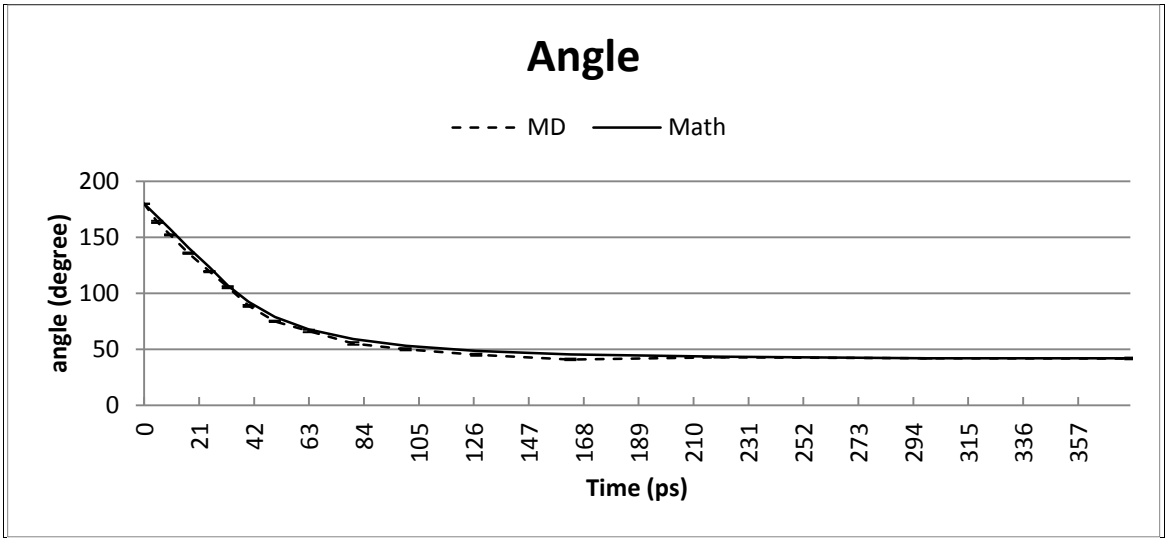

Figure 4.14. Dynamic contact angle vs simulation time for Si_3N_4-water at T= 323 K.

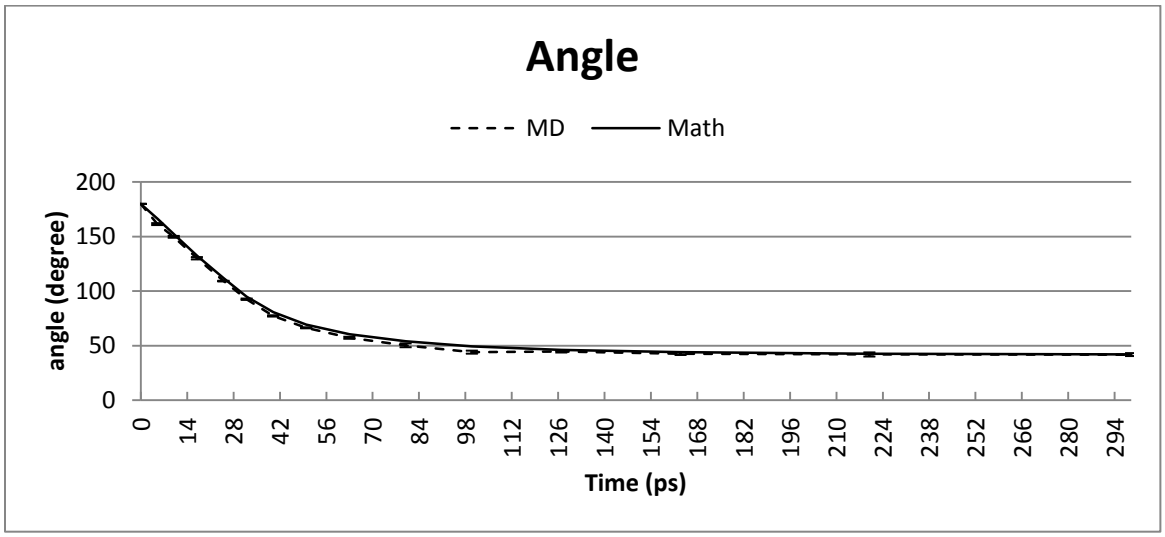

Figure 4.15. Dynamic contact angle vs simulation time for Si_3N_4-water at T= 373 K.

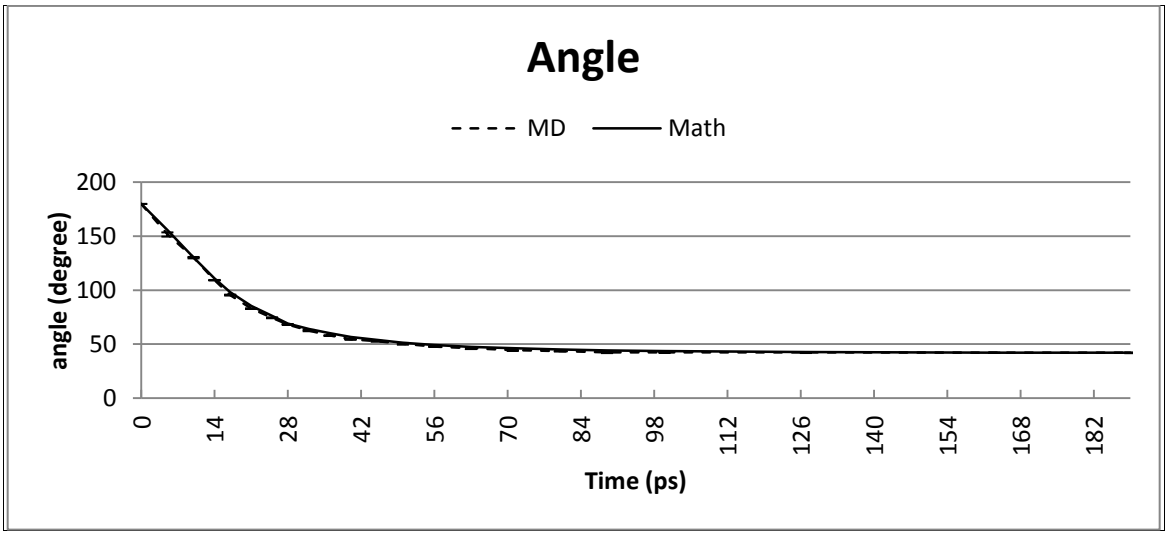

Figure 4.16. Dynamic contact angle vs simulation time for Si_3N_4-water at T= 473 K.

For Si_3N_4-water system, equilibrium contact angle was observed as approximately 42.08 degrees which was in close agreement with macroscale Si_3N_4-water equilibrium contact angle. However, the spreading time was substantially higher at all temperatures compared to that in SiO_2-water system at corresponding temperatures.

For example, equilibrium contact angle for SiO_2-water system at 293 K was observed at around 70 picoseconds whereas for Si_3N_4-water system, it was recorded approximately at 410 picoseconds. This delayed wetting pattern indicates hydrophobic behavior of Si_3N_4-water system unlike a hydrophilic SiO_2-water system. Furthermore, this difference in spreading mechanism between Si_3N_4-water system and SiO_2-water system was consistently evident at all temperatures. Moreover, similar to SiO_2-water system, the dynamic contact angle variation rate for Si_3N_4-water system was observed to be higher at elevated temperatures.

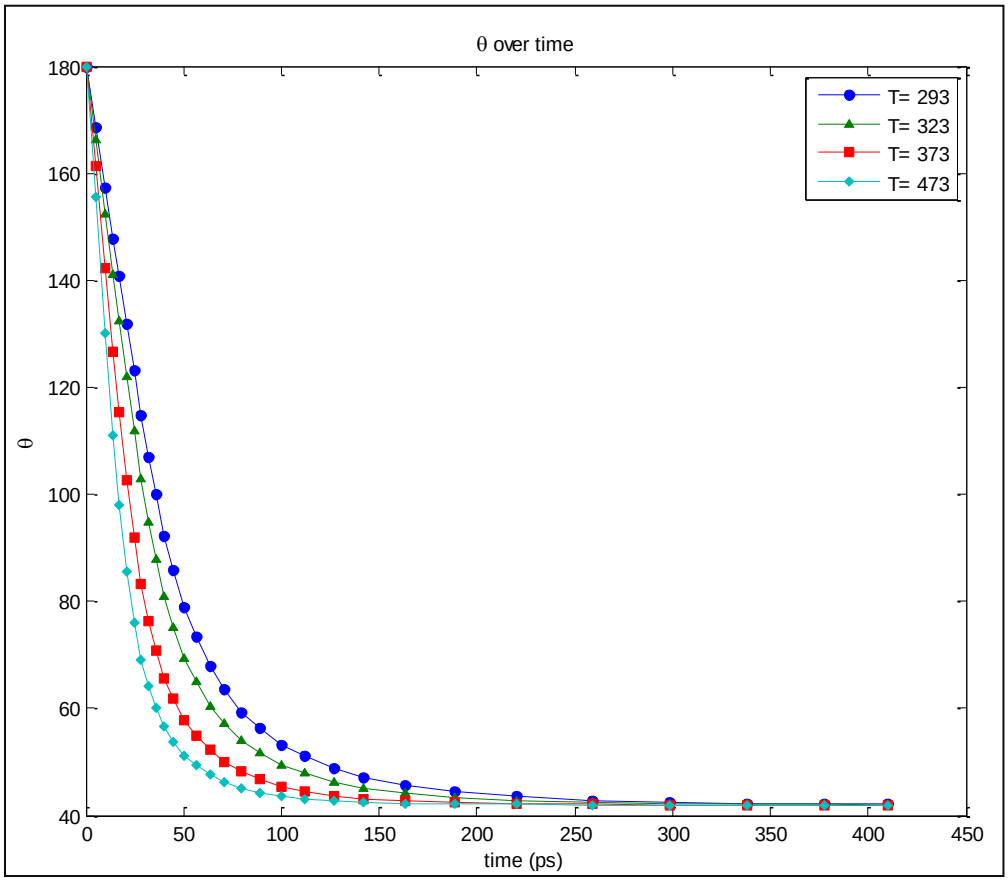

Figure 4.17. Contact angle variation at different temperatures vs simulation period for Si_3N_4-water system.

Figure 4.17 shows contact angle variations at different temperatures over the simulation period for Si_3N_4-water system

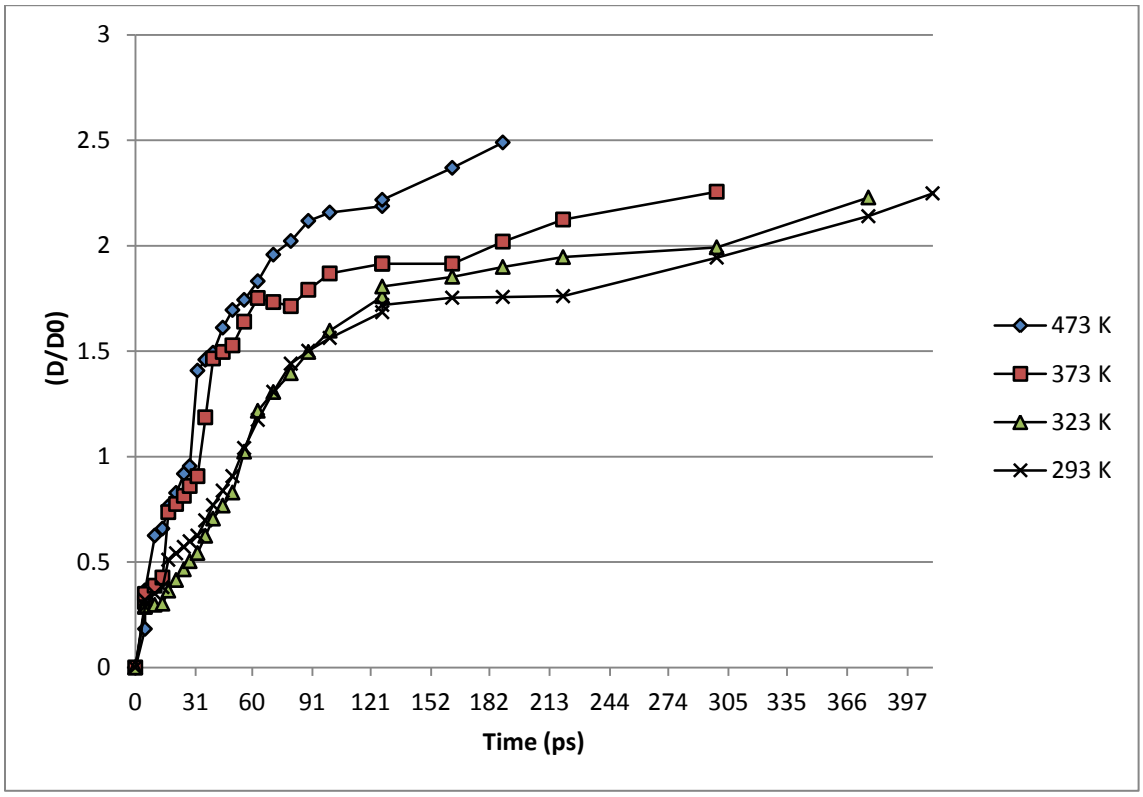

Figure 4.18. Variation of D/D_0 with simulation period for Si_3N_4-water system.

The Figure 4.18 explains the variation of D/D_0 over simulation the period for Si_3N_4-water system at different temperatures. Similar to SiO_2-water system, the rate of increase of D/Do for Si_3N_4-water system was observed to be higher at elevated temperature. Consequently, rate of increase of droplet spread area was more at any given instant for higher temperatures compared to that for lower temperatures.

4.3.2 Effect of Temperature on Equilibrium Contact Angle

In order to study effect of temperature on equilibrium contact angle, a multilevel factorial design was employed with substrate and temperature as two factors. Table-4.1 shows the factorial design details.

Table 4.1. Multilevel factorial design for temperature and equilibrium angle.

Factors	Level	Values
Temperature (K)	4	293, 323, 373, 473
Substrate	2	SiO_2, Si_3N_4

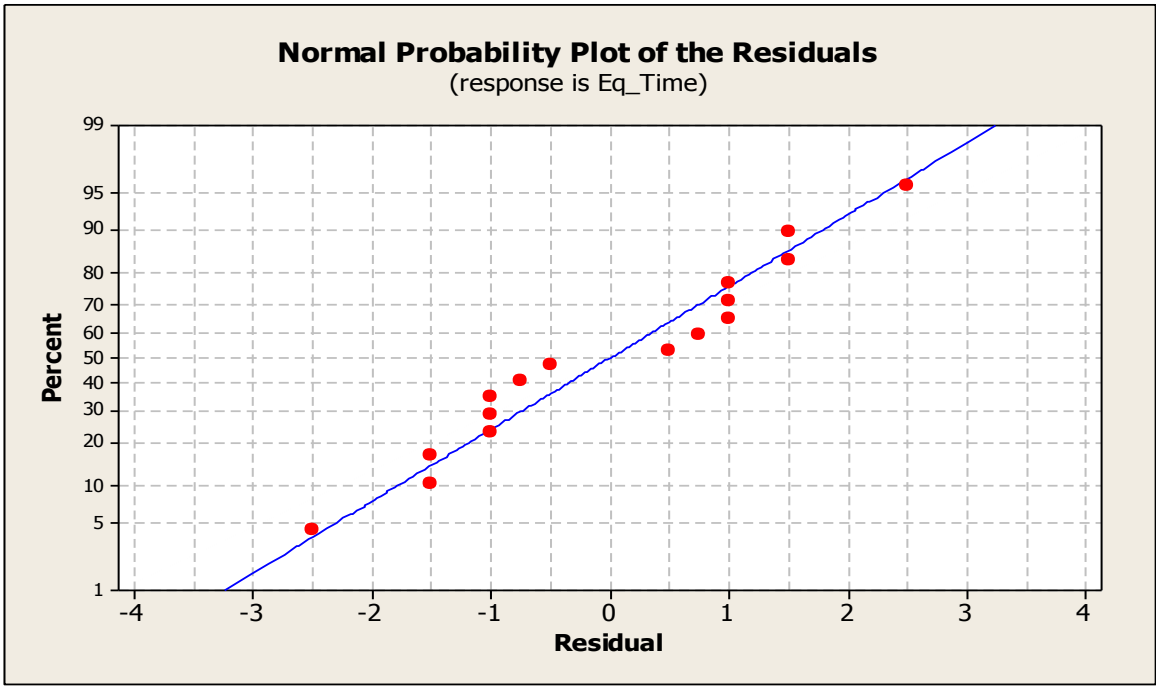

Figure 4.19. Normal probability plot for substrate-temperature analysis.

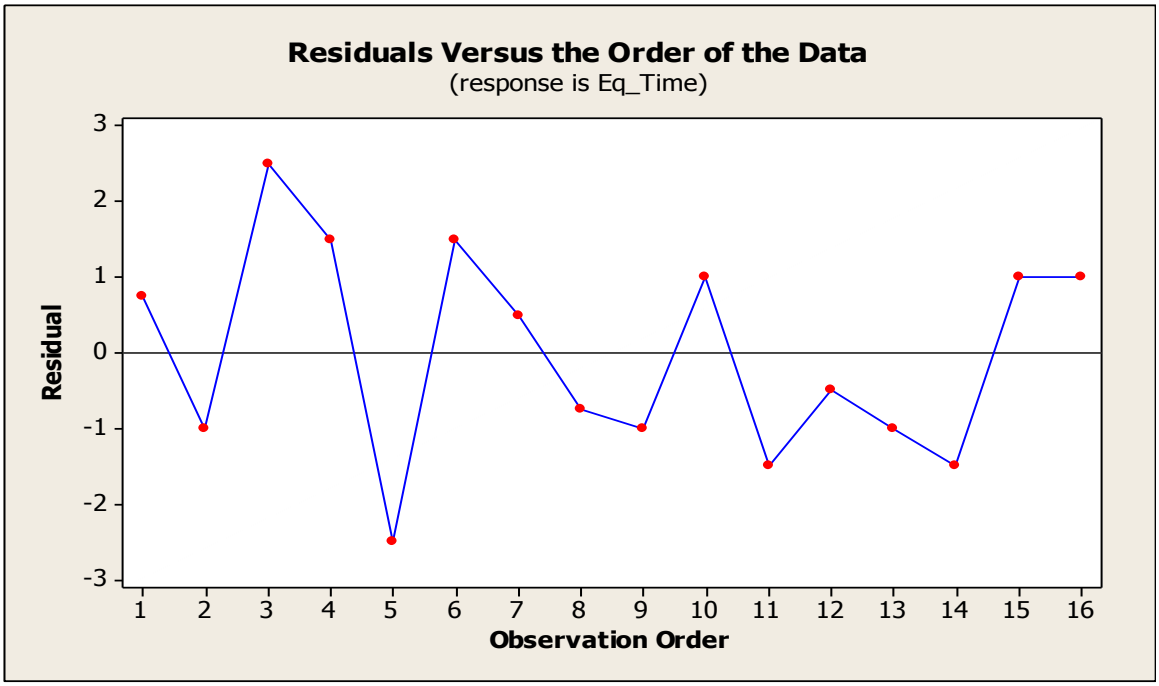

Figure 4.20. Residuals versus order of the data.

Figure 4.19 shows the normal probability plot which indicates normality of equilibrium time data. Figure 4.20 shows the residuals vs. order of data plot with the data collection order on the *x* axis and residuals on the *y* axis. Residuals are observed to be randomly distributed around the residual = 0 line indicating normal random noise. This suggests that there is no serial correlation present. Further in Table 4.2, it was observed that the type of substrate, temperature and combination of both factors are statistically significant in affecting equilibrium time as each had p-value of 0.000 that was less than the desired α level. Moreover, a regression fit for the model yielded a coefficient of determination (R-Square value) of 0.9999. Hence, it confirmed the goodness of fit of the data indicating that approximately 99.99% of the variation in the equilibrium time) was attributed to the substrate type, temperature and combination of both the factors.

Table 4.2. Output of multilevel factorial design.

```
Factors:      2     Replicates:     2
Base runs:    8     Total runs:    16
Base blocks:  1     Total blocks:   1

Number of levels: 4, 2

Design Table (randomized)

Run  Blk  A  B
  1    1  1  1
  2    1  2  2
  3    1  1  2
  4    1  3  2
  5    1  1  2
  6    1  4  2
  7    1  2  1
  8    1  1  1
  9    1  3  1
 10    1  3  1
 11    1  3  2
 12    1  2  1
 13    1  4  1
 14    1  4  2
 15    1  4  1
 16    1  2  2
```

General Linear Model: Eq_Time versus Temperature, Substrate

```
Factor       Type   Levels  Values
Temperature  fixed       4  293, 323, 373, 473
Substrate    fixed       2  SiO2, Si3N4

Analysis of Variance for Eq_Time, using Adjusted SS for Tests

Source                 DF  Seq SS  Adj SS  Adj MS         F      P
Temperature             3   40831   40831   13610   3738.48  0.000
Substrate               1  240958  240958  240958  66185.96  0.000
Temperature*Substrate   3   20874   20874    6958   1911.21  0.000
Error                   8      29      29       4
Total                  15  302693

S = 1.90804   R-Sq = 99.99%   R-Sq(adj) = 99.98%

Term                       Coef  SE Coef        T      P
Constant                178.406    0.477   374.01  0.000
Temperature
293                      62.4687   0.8262    75.61  0.000
323                      32.8437   0.8262    39.75  0.000
373                     -29.1563   0.8262   -35.29  0.000
Substrate
SiO2                    -122.719    0.477  -257.27  0.000
Temperature*Substrate
293         SiO2        -43.9062   0.8262   -53.14  0.000
323         SiO2        -25.0312   0.8262   -30.30  0.000
373         SiO2         22.4687   0.8262    27.20  0.000
```

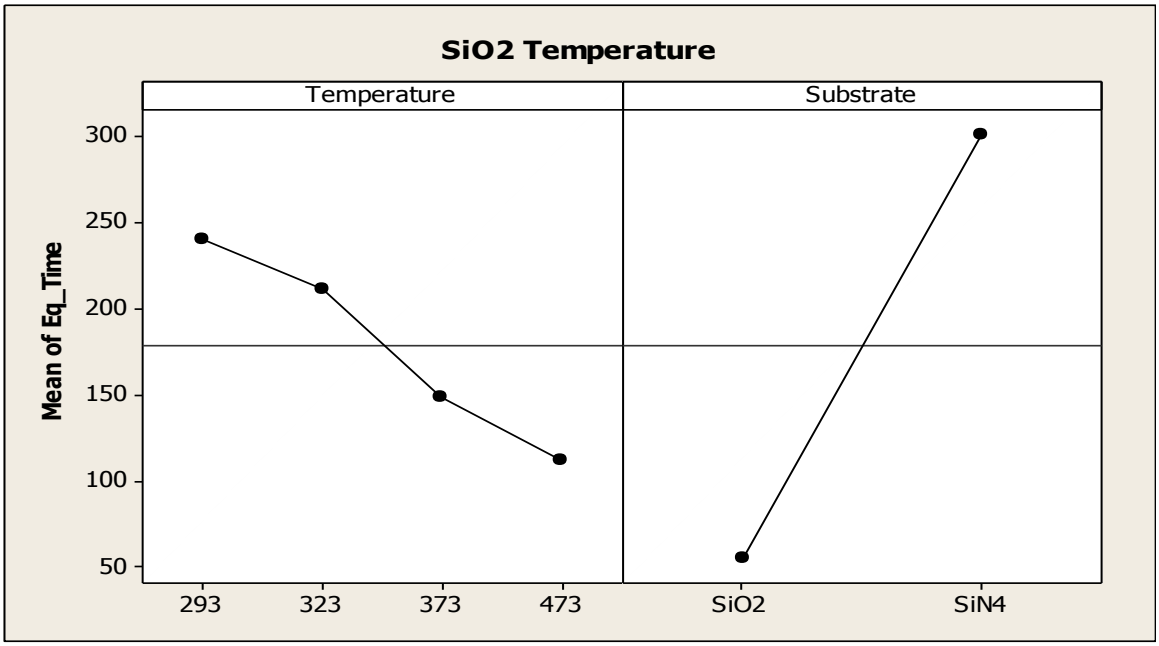

Figure 4.21. Individual effects of temperature and substrate.

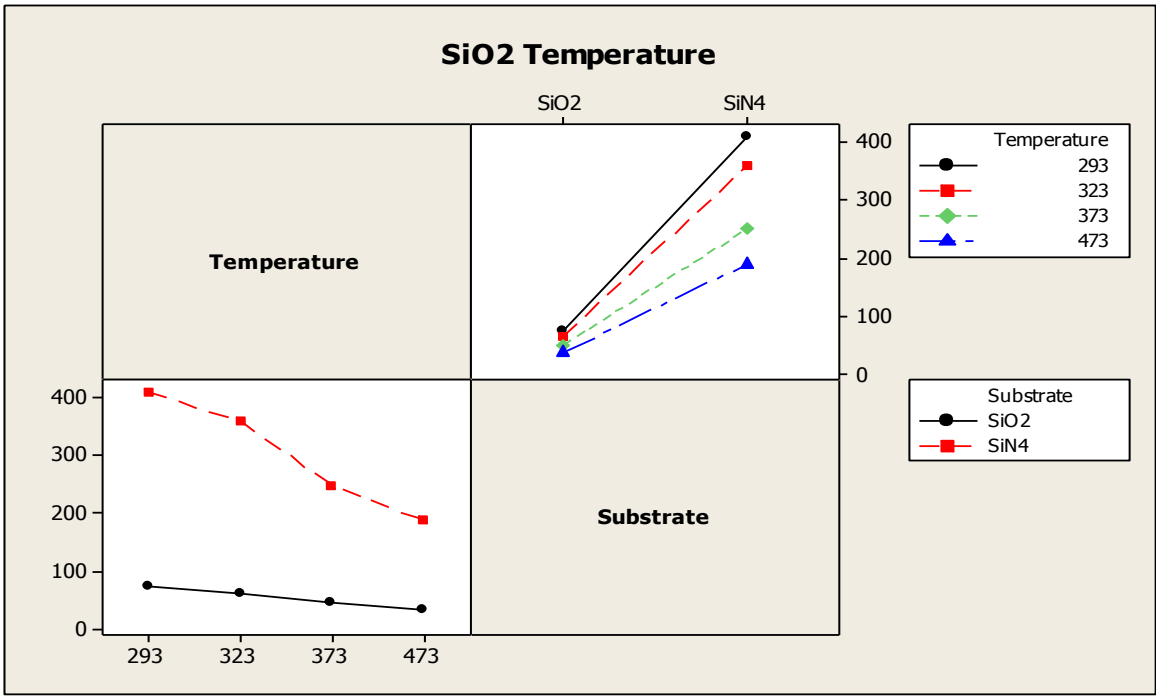

Figure 4.22. Interaction effects of temperature and substrate.

Figure 4.21 shows individual contributions of temperature and substrate type (i.e. main effects) which are significant in determining the equilibrium time. A description of the interaction effects is provided in Figure 4.22 which indicates the combination of temperature and substrate type had a significant effect on equilibrium time.

Further, the interaction effect of temperature and substrate type was investigated by comparing the contribution separately for each temperature level and substrate type. For this, the interaction was sliced by temperatures and substrate type. The results of slicing procedure performed using SAS is shown in Table 4.3 and Table 4.4.

Table 4.3. Results of temperature and substrate interaction sliced by temperature.

The SAS System

The GLM Procedure

Least Squares Means

temp*substrate Effect Sliced by temp for time

temp	DF	Sum of Squares	Mean Square	F Value	Pr > F
293	1	111056	111056	30504.5	<.0001
323	1	87320	87320	23985.0	<.0001
373	1	40200	40200	11042.1	<.0001
473	1	23256	23256	6387.98	<.0001

Table 4.4. Results of temperature and substrate interaction sliced by substrate.

The SAS System

The GLM Procedure
Least Squares Means

temp*substrate Effect Sliced by substrate for time

substrate	DF	Sum of Squares	Mean Square	F Value	Pr > F
Si3N4	3	60029	20010	5496.25	<.0001
SiO2	3	1675.843750	558.614583	153.44	<.0001

In Both the Table-4.2 and Table-4.3, Pr > F column have p-value less than 0.001 which is much smaller than the desired Type-I error level of 0.05. This confirms that interaction of temperature and substrate also indicated statistical significance in affecting equilibrium time; when observed independently for each temperature level and substrate type.

4.4 Conclusion of Nanodroplet and Flat Substrate Interaction Study

The results of water nanodroplet- SiO_2 substrate interaction simulation confirmed the hydrophilic behavior of SiO_2 substrate with equilibrium contact angle of 27.5^o. The hydrophilic behavior of SiO_2 substrate was consistent also at higher temperatures. Higher nanodroplet spreading rates were observed for elevated temperatures mainly due to reduction in surface tension of water and higher kinetic energy of molecules in the

vicinity of wetting line. Consequently, enhanced wetting rates quantified by D/D_0 curves were recorded at higher temperatures.

The results of water nanodroplet- Si_3N_4 substrate interaction simulation indicated hydrophobic behavior at nanoscale similar to one at macroscale at all temperatures. Equilibrium contact angle was 42.08^o and time to reach equilibrium was considerably higher; approximately six times of corresponding equilibrium time for SiO_2-water system at room temperature. The hydrophobic behavior of Si_3N_4-water system at nanoscale was maintained even at higher temperatures. However, the spreading rates increased with temperatures due to drop in surface tension and rise in kinetic energy. Higher values of *D/Do* ratio for elevated temperatures indicated accelerated wetting rates with temperature.

Results of multilevel factorial design employed for investigating the contribution of temperature and substrate indicated their significant role; both individually and collectively in determining the final equilibrium time for spreading nanodroplet. This indicates that there is a significant temperature effect regardless of various types of substrate and there is a significant substrate effect regardless of various levels of temperature

CHAPTER 5

NANODROPLET IMPINGEMENT ON SUBSTRATE

In the inkjet-based direct writing method considered in this research, characterization of droplet impingement phenomenon is expected to aid the understanding of process and material design. In order to envision possible spread dynamics and predict substrate wetting behavior of droplet, role of initial impact velocity imparted to droplet while ejection from inkjet nozzle needs to be thoroughly investigated. The study of droplet impingement mechanism is expected to throw more light on possible micro/nano features that can be fabricated using diverse range of solvents feasible within inkjet-based direct writing method.

This study focuses on investigation of behavioral patterns of droplet impingement onto solid plane hydrophilic substrate. As discussed in section 1.1.4, the droplet is ejected from the nozzle with certain initial velocity to facilitate its deposition on substrate. In fact, this initial velocity plays very important role in the stability of ejected microdroplet jet and ultimately in accurate and precise deposition of microdroplet. Under the proposed hybrid approach using inkjet-based direct writing method, ejected microdroplets are exposed to controlled heat flux before deposition on substrate for subsequent micro-to-nano transition. Therefore, the microdroplet is expected to enter in nano-regime while spreading on the substrate. Hence it is imperative to study the impingement phenomenon at molecular level with focus on characterization of nanodroplet spreading under the influence of different initial impact velocities. This chapter explains the relationship between nanodroplet impingement velocities and dynamic contact angle relaxation after

deposition. The water nanodroplet spreading mechanism on SiO_2 plane substrate was studied under the influence of different initial impact velocities imparted to nanodroplet. This study is expected to provide the basis for application of realistic and optimal initial velocities to ejected microdroplets. Also, there is further scope to extend the results of this study to the combinations of range of fluids/solvents and substrate materials, under diverse ambient conditions.

5.1 Methodology

For comparison of droplet spreading (without application of impingement velocity) results, an identical 4 nm water nanodroplet model and plane SiO_2 substrate model with dimensions 20.8 nm x 20.8 nm x 3.37 nm that is used in previous studies was considered for understanding impingement mechanism. Water nanodroplet model and SiO_2 substrate model were built using 3,171 atoms (1,057 molecules) and 42,336 atoms (14,112 molecules) respectively. Figure 5.1 shows the SiO_2-Water nanodroplet model used for impingement study.

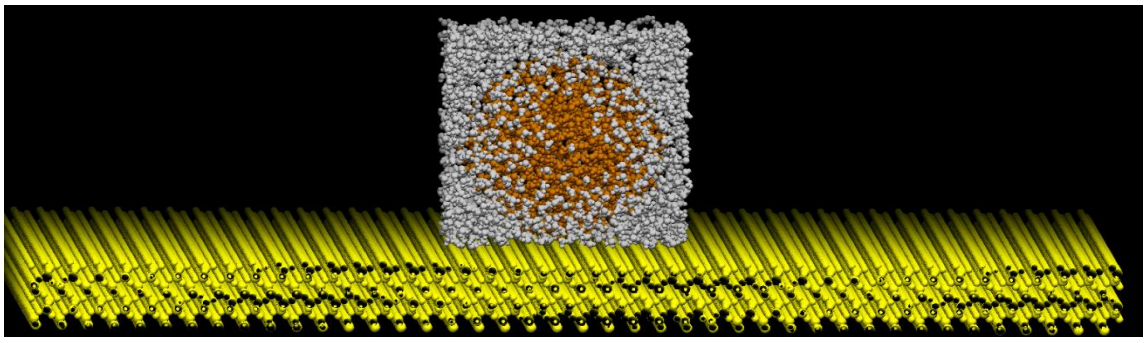

Figure 5.1. SiO_2-water nanodroplet model for impingement study.

The water nanodroplet was enclosed in cubical water box of size 4.6484 nm X 4.632 nm X 5.984 nm for providing stretchable simulation cell for spreading droplet. Water box

was created using 5,360 water atoms (2,680 molecules). Entire system (SiO_2 substrate and water box) was comprised of 50,169 atoms. The SiO2 substrate atoms were kept fixed for entire simulation. For application of velocity on nanodroplet, the Steered Molecular Dynamics approach within NAMD was used. Initially, the velocity was applied to the droplet until it touches the substrate. Once the droplet touched substrate, the velocity was removed. This allowed the droplet to spread with initially imparted momentum but without a prolonged force in the vertically downward direction.

5.2 Integration Scheme and Solver Method

A numerical integration scheme and solver method discussed in section 3.2.2 was employed for simulating SiO_2-water systems. The systems were simulated at 293 K (room temperature) with 0.5femtosecond time step. The temperature was maintained constant at 293 K by Langevin dynamics with a coupling constant of 1 ps^{-1}. All the simulation was performed using NPT ensemble and therefore the pressure was maintained constant by Nosé-Hoover-Langevin piston at 1 bar. PME grid size of 1 and Lennard-Jones switching function of 10 Å was adopted for all simulations. Multiple time step integration was arranged using impulse-based Verlet-I/r-RESPA method. The lists of neighboring atoms are accounted at the frequency of 10 time steps with a cut-off radius (local interaction distance common to both electrostatic and van der Waals calculations) of 11 Å.

The simulations were performed in two phases for total 100 picoseconds. Simulation time scale of total 100 picoseconds was preferred based on the availability of comparable results from previous study of SiO_2-water system (without consideration of

initial velocity) over the same simulation period. In the first phase, the nanodroplet approaching to the substrate with certain imparted velocity was simulated for 3 picoseconds. In the second phase, the simulation was restarted from previous check point; without application of velocity and allowed to run further for 97 picoseconds.

5.3 Results and Discussion

Dynamic contact angle variation was observed for SiO_2-water system under the influence of three different velocities; 0.01 m/s, 0.1 m/s and 1 m/s. Values of the velocity were selected based on a range of droplet impingement velocities practically used in inkjet printing method. Contact angles were plotted over a simulation period that is needed for reaching equilibrium contact angle for corresponding velocities. Appropriate value of frequency of molecular displacements at equilibrium(K^0) was used for the curve fitting with MD simulation curve. For obtaining the curve fitting to MD simulation data, equations (4.3) and (4.5) in section 4.3 were solved again using MATLAB for wetting line velocity (v) and ultimately for dynamic contact angle θ.The solution was obtained over a period equal to the simulation time needed to reach SiO_2-water system equilibrium contact angle of 27.5^o. Alternatively, K^0 was also determined from the simulation data directly by counting the number of molecular displacements per unit time adjacent to substrate at equilibrium. Visual Molecular Dynamics atom count algorithm was used for this purpose. The close agreement was observed between K^0 values for the corresponding velocities obtained by curve fitting and atom count algorithm in VMD. The K^0 values such obtained after imparting velocity were higher than the K^0 value determined (in

section 4.2) for spreading nanodroplet on SiO_2 substrate at room temperature without imparting any velocity.

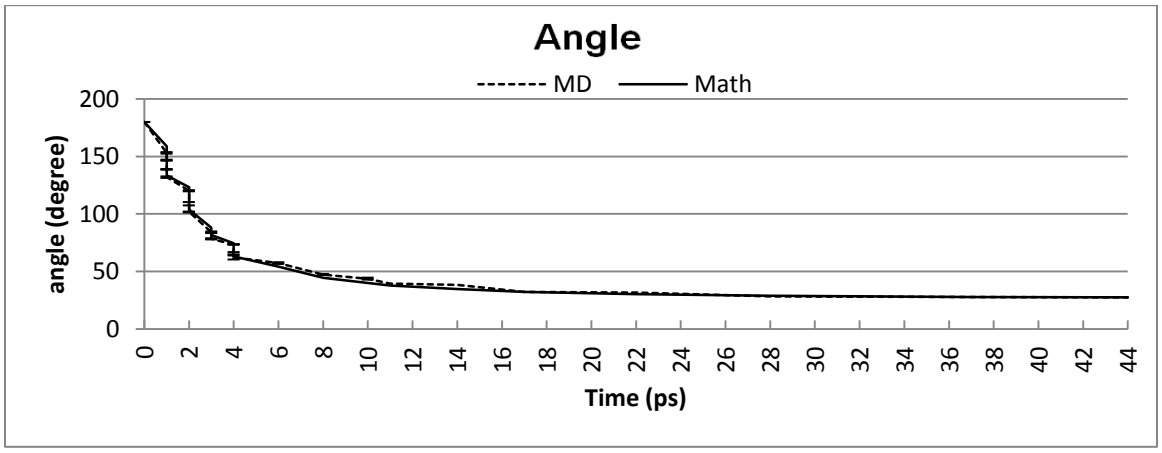

Figure 5.2. Contact angle variation with time at velocity 0.01 m/s.

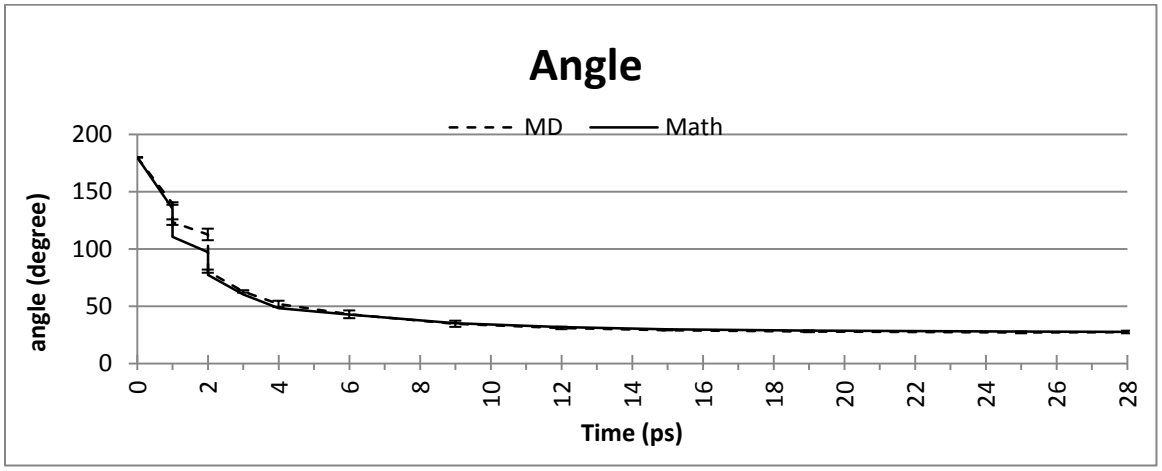

Figure 5.3. Contact angle variation with time at velocity 0.1 m/s.

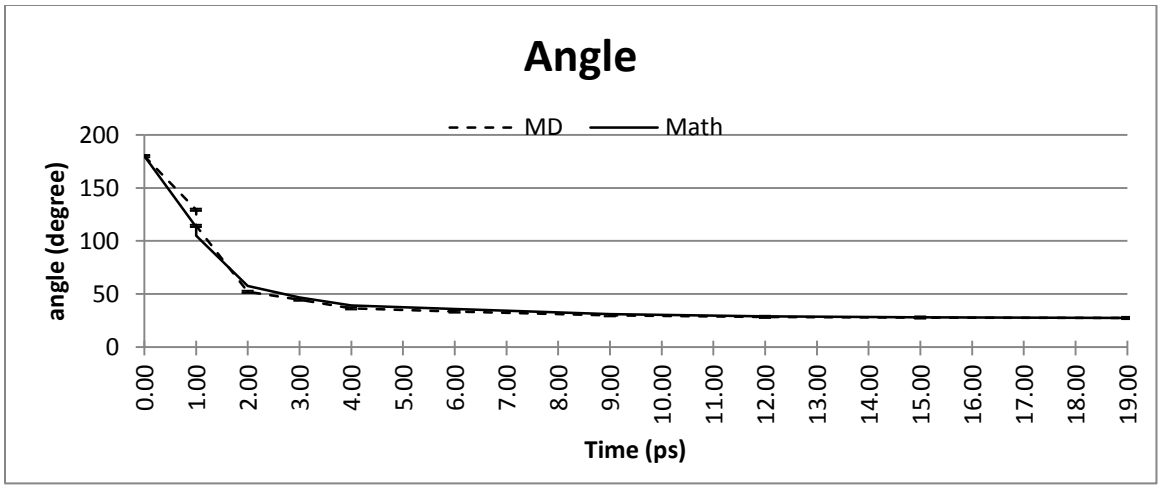

Figure 5.4. Contact angle variation with time at velocity 1 m/s.

Figures 5.2 through 5.4 show the variation of dynamic contact angles with simulation time for different impingement velocity values. For the 0.01 m/s velocity, the equilibrium contact angle of 27.5^{o} was observed at 43.65 picoseconds against 70 picoseconds of time needed for spreading nanodroplet at room temperature without imparting any velocity (Ref Figure 4.6). For 0.1 m/s velocity, the equilibrium was reached at 28.34 picoseconds. Finally, the minimum time of 19.43 picoseconds to reach equilibrium contact angle was observed for highest (1 m/s) velocity. Thus, the higher spreading rates were observed with successively increasing the nanodroplet velocity.

5.3.1 ANOVA Results for Impingement Study

Figure 5.5 suggests the normality of equilibrium time data collected for impingement study. Therefore, the one-way ANOVA was performed to find out whether equilibrium time data from different velocity groups (0 m/s, 0.01 m/s, 0.1m/s and 1 m/s) have a common mean or these groups are in fact different in the measured characteristic.

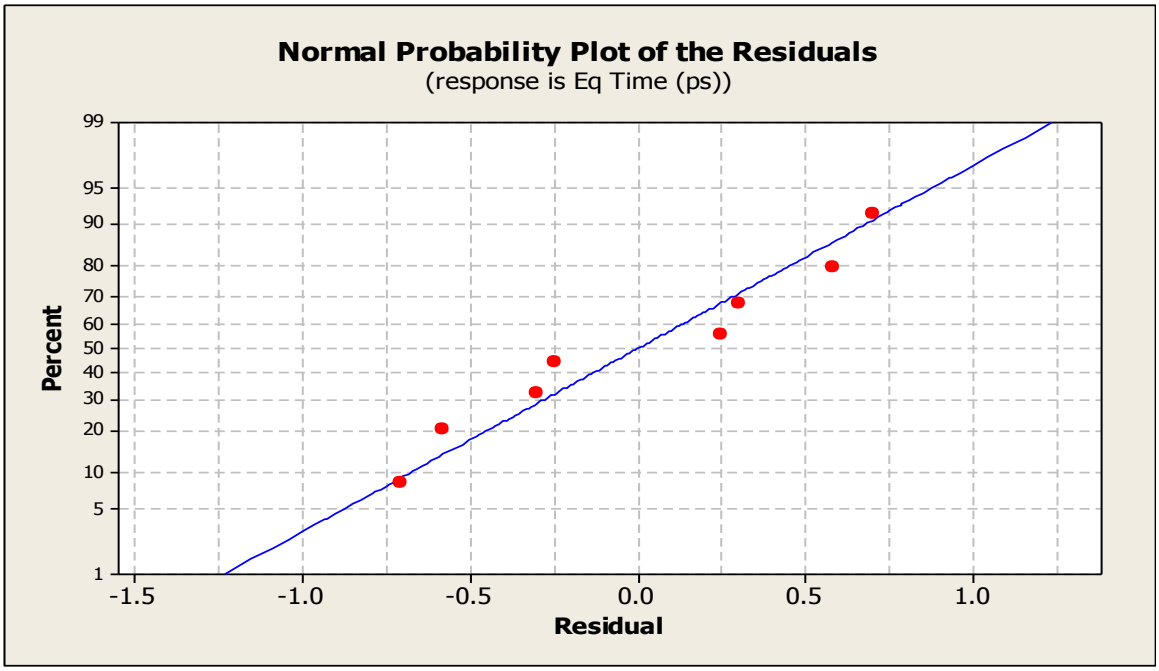

Figure 5.5. Normal probability plot for impingement analysis.

Table 5.1. Results of one-way ANOVA: equilibrium time (ps) versus velocity (m/s).

```
Source           DF        SS        MS         F      P
Velocity (m/s)    3  2992.024   997.341  2023.16  0.000
Error             4     1.972     0.493
Total             7  2993.996

S = 0.7021   R-Sq = 99.93%   R-Sq(adj) = 99.88%


                        Individual 95% CIs For Mean Based on
                        Pooled StDev
Level  N    Mean  StDev  --------+---------+---------+---------+-
0.00   2  70.750  0.354                                    (*)
0.01   2  43.080  0.820                  (*)
0.10   2  29.045  0.997        (*)
1.00   2  19.450  0.424  (*)
                        --------+---------+---------+---------+-
                               30        45        60        75

Pooled StDev = 0.702
```

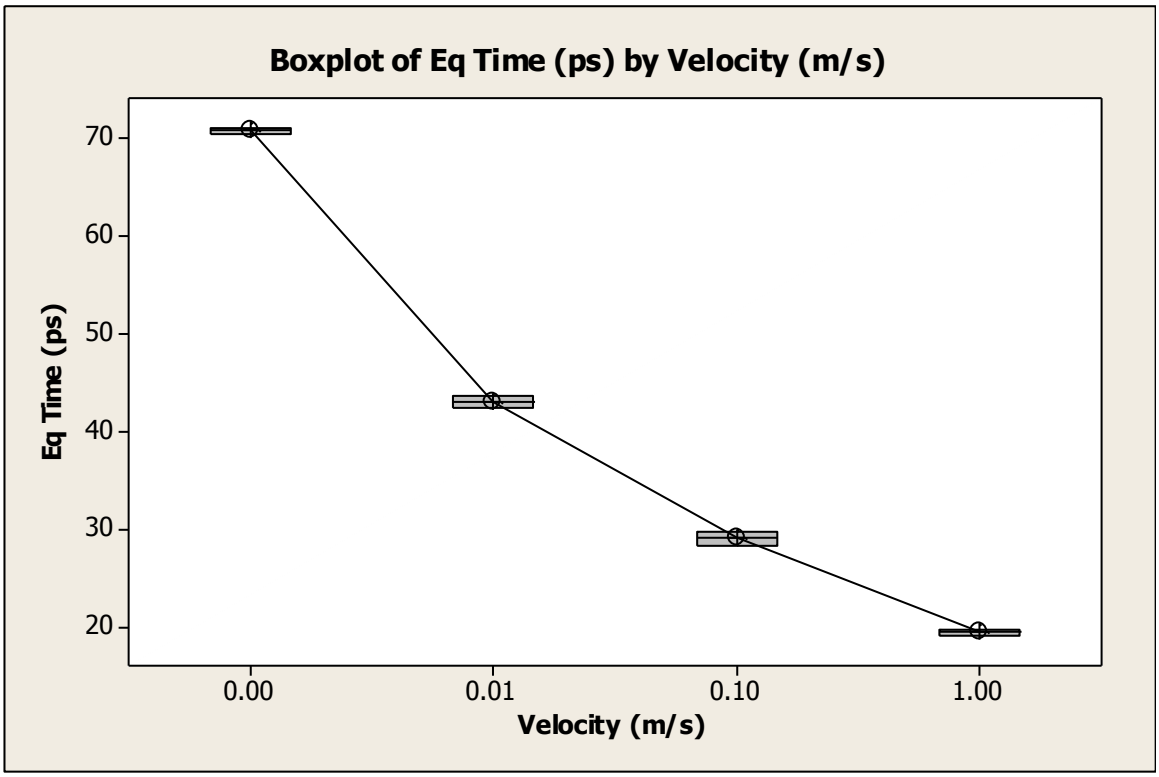

Figure 5.6. Box plot for impingement analysis.

Box plot in Figure 5.6 graphically indicates that the means are different for the various velocity groups. The output of one-way ANOVA is summarized in Table 5.1, which confirms that velocity is statistically significant in affecting equilibrium time with p-value of 0.000 that was less than the desired α level. Moreover, a regression fit for the model yielded a coefficient of determination (R-Square value) of 0.9993. Hence, it confirmed the goodness of fit of the data indicating that approximately 99.93% of the variation in the response variable (i.e. equilibrium time) was attributed to the velocity changes.

To determine specifically which pairs of means are significantly different, Tukey's Multiple Comparison Test was performed. The results of Tukey's Multiple

Comparison Test on equilibrium time data is summarized in following Table 5.2, which suggest that there is a significant difference among all the pairs of means.

Table 5.2. Results of Tukey's multiple comparison test for impingement analysis.

Tukey's Multiple Comparison Test	Mean Diff.	q	Significant? P < 0.05?	Summary	95% CI of diff
1 vs 0.1	-9.59	19.3	Yes	***	-12.5 to -6.74
1 vs 0.01	-23.6	47.6	Yes	***	-26.5 to -20.8
1 vs 0	-51.3	103	Yes	***	-54.2 to -48.4
0.1 vs 0.01	-14	28.3	Yes	***	-16.9 to -11.2
0.1 vs 0	-41.7	84	Yes	***	-44.6 to -38.8
0.01 vs 0	-27.7	55.7	Yes	***	-30.5 to -24.8

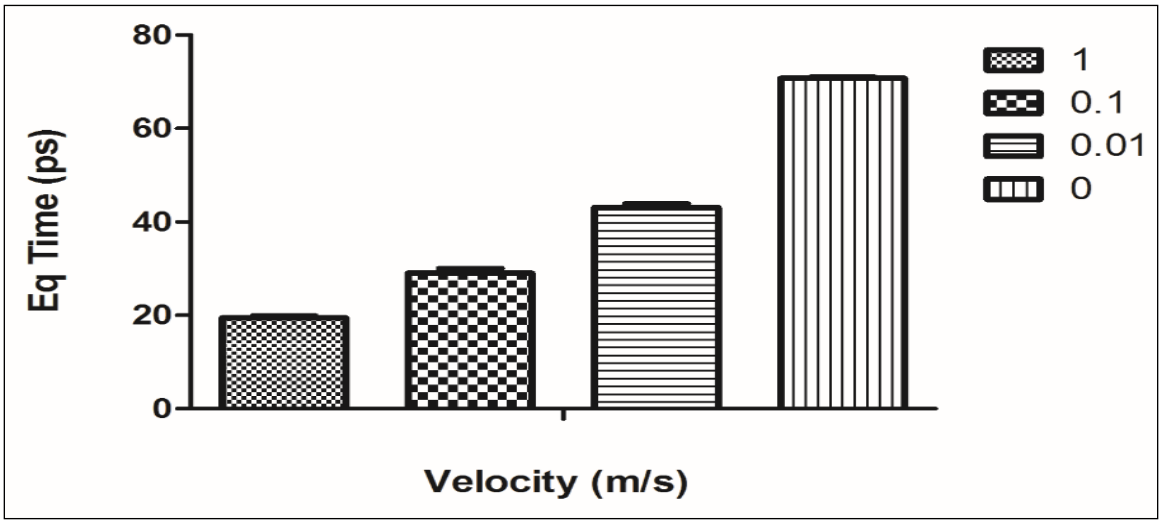

Figure 5.7. Comparison of means for different velocity groups.

Figure 5.7 graphically shows the difference between the means of equilibrium time data for different velocity groups. Thus, the magnitude of impingement velocity is critical in predicting the spreading dynamics of nanodroplet.

5.4 Conclusion of Impingement Study

Results of impingement study established the fact that initial impingement velocity imparted to nanodroplet plays critical role in determining the spreading mechanism of nanodroplet. The significant decline in time to reach equilibrium was observed with rise in impingement velocity. The highest velocity value of 1m/s achieved 73% reduction in equilibrium time of nanodroplet spreading without imparting initial velocity. Impingement with 0.1 m/s and 0.01 m/s velocity to spreading nanodroplet caused 59.51% and 37.64% drop in equilibrium time respectively. This investigation is expected to aid in establishment of relationship between wetting rates and initial impingement velocity. The results are also critical in explaining the role and behavior of water nanodroplet as universal solvent for nanoparticles. Though this study excluded other factors such as temperature and nature of interaction based on substrate material's potential function (hydrophilic or hydrophobic), it confirms inversely proportional relationship between magnitude of impingement velocity and time to reach an equilibrium angle.

CHAPTER 6

NANODROPLET SPREADING ON PATTERNED SUBSTRATES

Wetting phenomenon plays a critical role in a broad range of technological applications. Spreading of liquid droplet on solids surface is a central phenomenon in numerous biological systems and industrial applications [67-68]. The spreading of a droplet on various surfaces is a basic problem and has been researched thoroughly for broad range of applications such as inkjet printing, DNA chip fabrication and cell patterning.

For better accuracy and repeatability, the droplet based inkjet nanomanufacturing method aims at deposition of solvent nanodroplets laden with nanoparticles on pre-patterned substrate. The nanoscale patterns on the substrate are expected to act as positioning channel for the fabrication of required nanofeatures. The nanodroplets are anticipated to be deposited exactly within these channels. Therefore, the study of nanodroplet spreading behavior on pre-patterned surface is pertinent for gaining insight and subsequently exercising adequate control over nanofeatures formation phase.

Broadly, the surface wetting behavior is categorized under two heads; hydrophobic surface (contact angle is above 90^{o}) the hydrophilic surface (water contact angle below 90^{o}). The substrate topology can potentially change the substrate wetting behavior at macroscale. However, it is important to study the role of substrate topology on spreading mechanism at nanoscale for exploring the possibility of tailoring the surface of given substrate to demonstrate hydrophobic or hydrophilic characteristics as required

by applications. For example, making hydrophobic substrate surface rough can improve its nonwetting properties further and convert it into superhydrophobic substrate. Conversely, smoothening of hydrophobic substrate surface may turn it into hydrophilic surface. Moreover, topographic effects can also augment partial wetting by a given liquid droplet into absolute wetting to demonstrate superwetting characteristics. In this chapter, the effect of substrate topology on nanodroplet spreading dynamics is investigated. This investigation is also expected to foresee surface topology as an additional control in droplet based nanomanufacturing; allowing for more flexibility in terms of use of combination of substrate materials and solvents.

In this work, a MD model of spreading water nanodroplet on hydrophilic substrate (SiO_2) is used to investigate the effect of different substrate topologies on overall spreading behavior. Two substrate topologies with different aspect ratios of projected features were used in the study. The MD simulations were performed and dynamic contact angles were measured at certain intervals. The spread was observed at a chosen time intervals and compared for all three substrate topologies. For the evaluation of shift in hydrophilic to hydrophobic nature of plane SiO_2 substrate, the results obtained were also compared with those for SiO_2-water system with flat substrate.

The results of this work are expected to provide the information about behavior of nanodroplet while formation of final nanofeatures on pre-patterned substrate. Furthermore, the possibility of tailoring the surface of given substrate at nanoscale as needed by application is envisioned.

6.1 Methodology

The SiO_2 substrates with two different topologies were modeled using VMD. An identical SiO_2 substrate model with dimensions 20.8 nm X 20.8 nm X 3.37 nm that is used in previous studies was considered as a base model to create two different substrate topologies. Inorganic builder module in VMD was used to model parallelepiped slots on substrate surface. One of the substrate was modeled with a pattern of 0.2 nm wide and 0.6 nm deep (aspect ratio = 3) parallelepiped slots allover on its top surface. The other model was built with a pattern of 0.6 nm wide and 0.2 nm deep (aspect ratio = 1/3) parallelepiped slots on its entire top surface. A water box containing 4 nm diameter water droplet was centrally positioned on the top of both substrate model. The substrate model with a pattern of 0.2 nm wide and 0.6 nm deep parallelepiped slots integrated with water box contained total 39,092 atoms (30,560 for substrate, 3,171 for water droplet and 5,361 for water box). Other substrate-water box model with a pattern of 0.6 nm wide and 0.2nm deep parallelepiped slots was built using altogether 44,612 atoms (36,080 for substrate, 3,171 for water droplet and 5,361 for water box). Expecting similar spreading phenomenon, integration scheme and solver method identical to one discussed in Chapter 4 (section 4.1.2) was used for performing MD simulations. Figure 6.1 and Figure 6.2 show substrate-water box model with a pattern of 0.2 nm wide and 0.6 nm deep parallelepiped slots and substrate-water box model with a pattern of 0.6 nm wide and 0.2 nm deep parallelepiped slots, respectively.

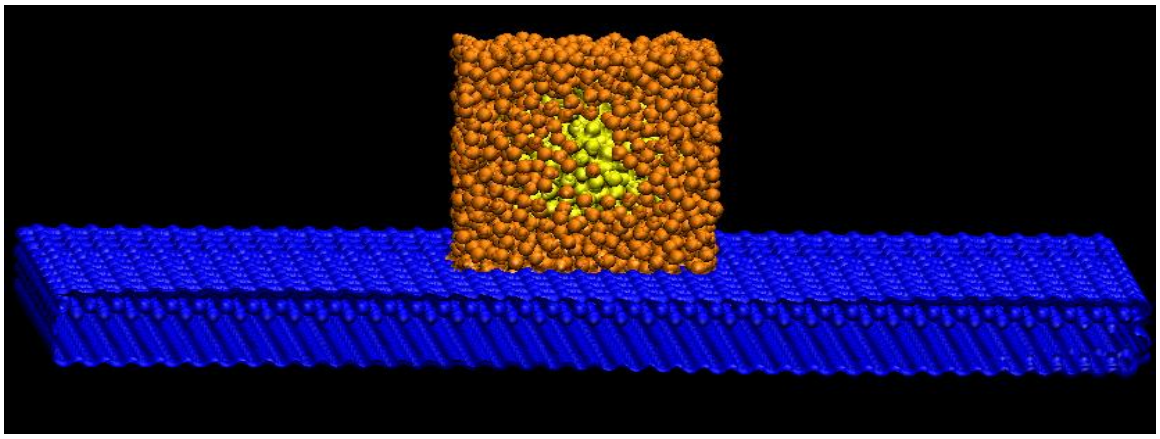

Figure 6.1. Model with pattern of 0.2 nm wide and 0.6 nm deep parallelepiped slots.

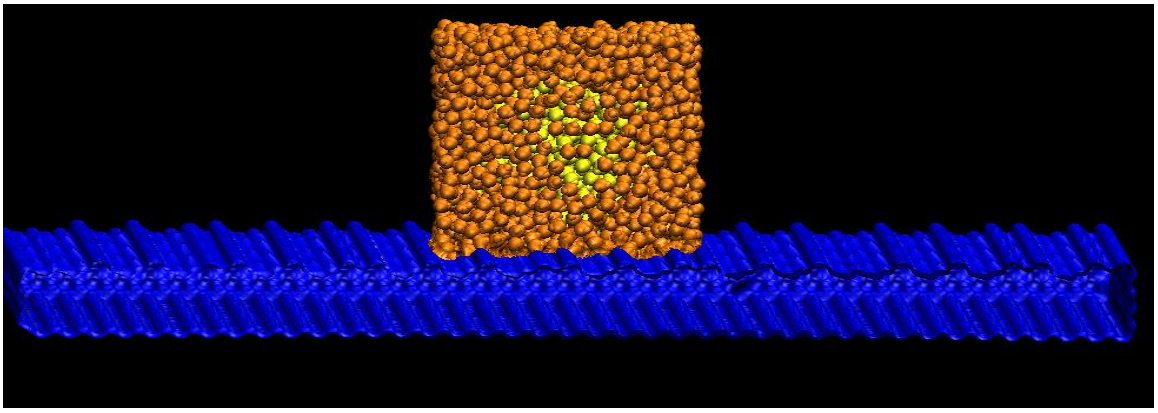

Figure 6.2. Model with pattern of 0.6 nm wide and 0.2 nm deep parallelepiped slots.

6.2 Results and Discussion

Both the models were simulated over a period of 100 picoseconds and observed over the period of 70 picoseconds which is the time required to reach equilibrium contact angle for plane substrate under normal conditions. Distinct spreading patterns were observed parallel and perpendicular to the slots for both the substrate topologies. The higher contact angles were observed for the spread perpendicular to the slots compared to that measured to parallel to slots for both the cases. Droplet is seen spreading more readily along the slots compared to that across the slots. As shown in Figure 6.3 for the

substrate model with aspect ratio of three (0.2 nm wide and 0.6 nm deep), droplet contact angle measured perpendicular to the slots was observed only 47.25^{o} in 70picoseconds against 27.5^{o} (equilibrium contact angle) for plane substrate. However, when measured parallel to the slots, contact angles further dropped to 25.6 ^{o} over an identical period of 70 picoseconds. For the substrate model with aspect ratio of 1/3 (0.6 nm wide and 0.2 nm deep), Figure 6.4 shows that droplet could reach contact angle 32 ^{o} when measured perpendicular to the slots against 28.78 ^{o} measured parallel to the slots over a period of 70 picoseconds. For both the substrate topologies, the droplet spreading is observed to retarded compared to plane substrate indicating shift in hydrophilic behavior of SiO_2-water system towards slightly hydrophobic.

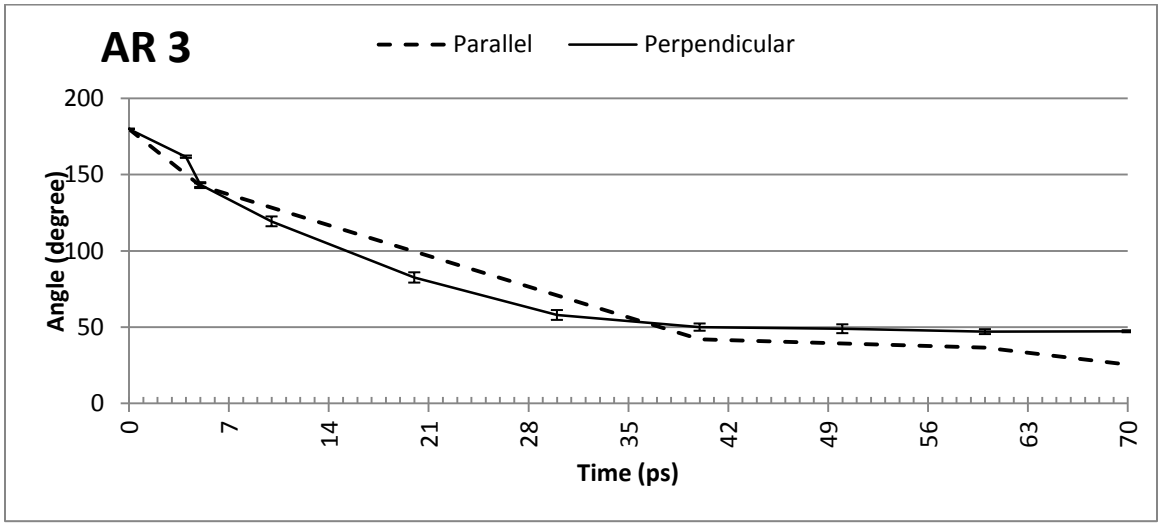

Figure 6.3. Contact angle variations for pattern of 0.2 nm wide and 0.6nm deep slots.

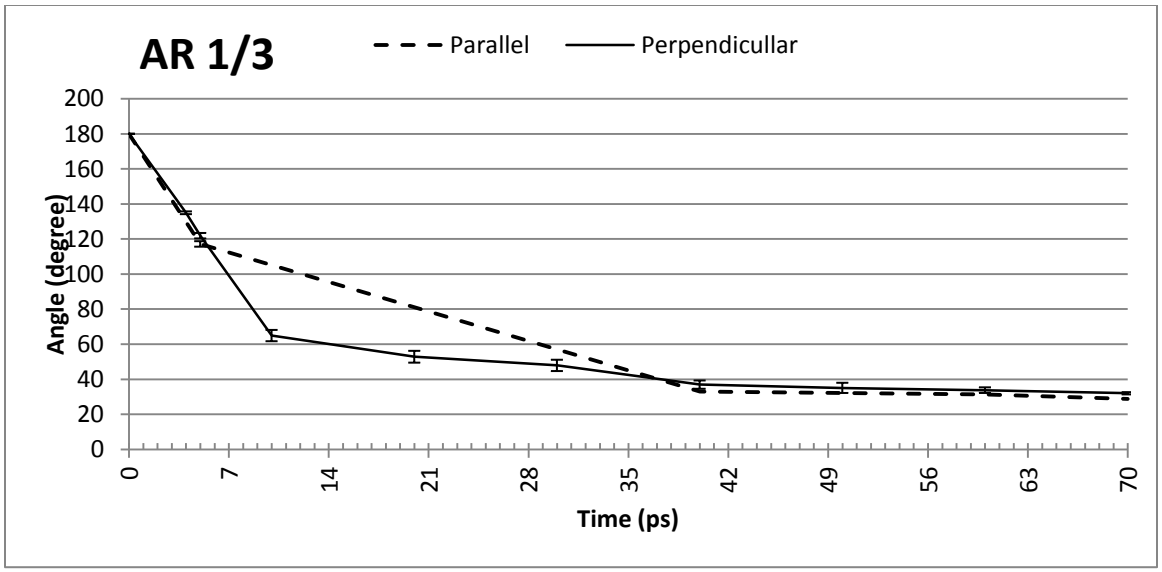

Figure 6.4. Contact angle variations for pattern of 0.6 nm wide and 0.2 nm deep slots.

6.2.1 One-way ANOVA for Contact Angle (θ) Versus Aspect Ratio (H/W)

Figure 6.5 and Figure 6.6 indicate the normality of contact angle data collected for two aspect ratios resulted from perpendicular spread and parallel spread, respectively.

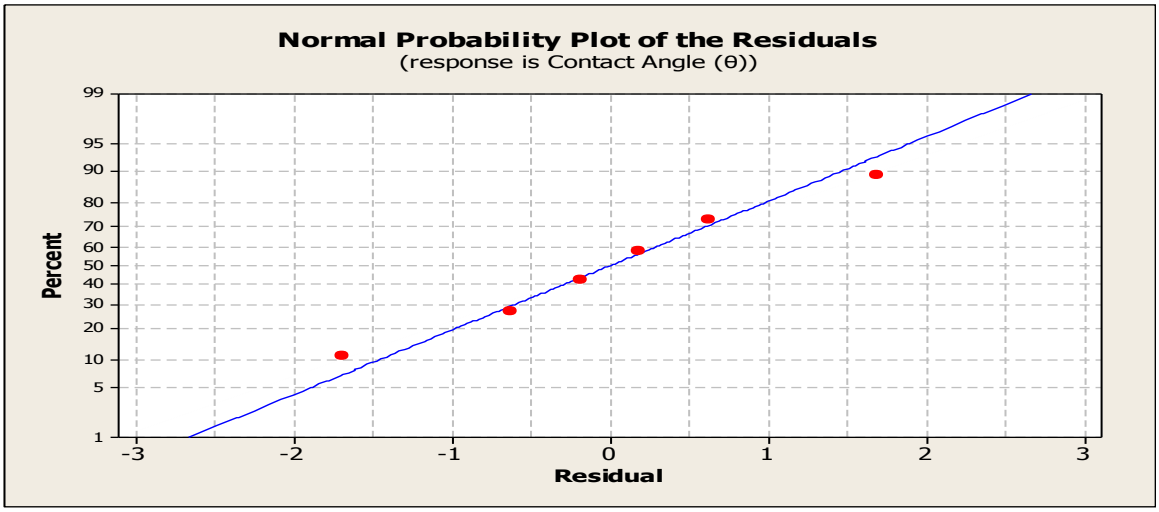

Figure 6.5. Normal probability plot for perpendicular spread.

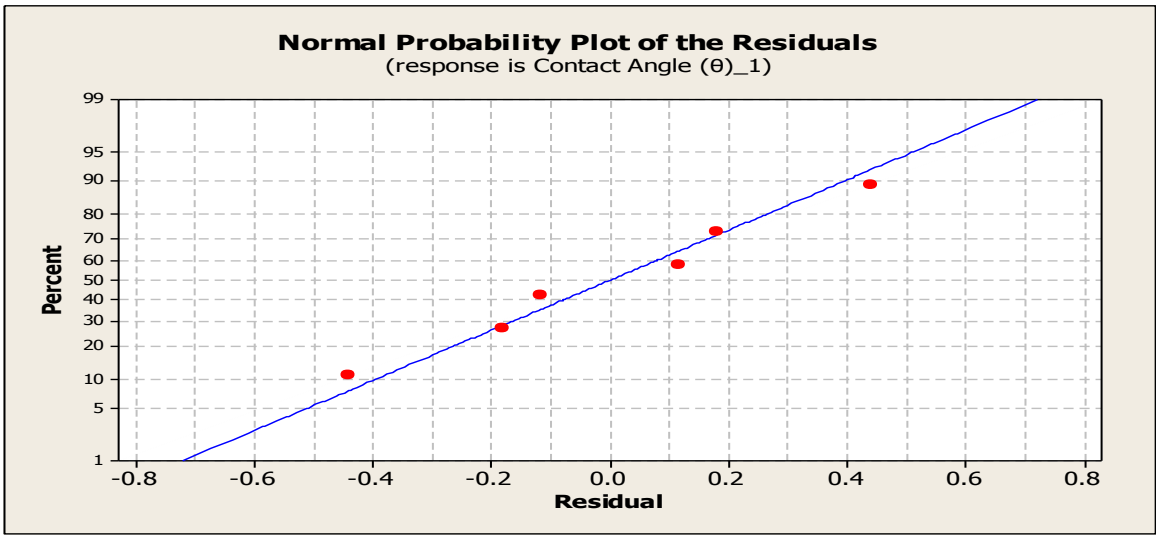

Figure 6.6. Normal probability plot for parallel spread.

Therefore, the one-way ANOVAs were performed to evaluate the difference between contact angles means for two aspect ratios and a flat substrate for both; perpendicular and parallel directions of spread. The outputs of one way ANOVAs are summarized in following sections.

6.2.1.1 One-way ANOVA: Perpendicular Spread

Following is the output of one way ANOVA that was performed on the final contact angle measured perpendicular to the slots for three different topologies; aspect ratio 3, aspect ratio 1/3 and flat surface.

Table 6.1. Results of one-way ANOVA for perpendicular spread.

One-way ANOVA: Contact Angle (θ) versus Aspect Ratio (H/W)s

Source	DF	SS	MS	F	P
Aspect Ratio (H/	2	415.33	207.67	95.19	0.002
Error	3	6.54	2.18		
Total	5	421.88			

S = 1.477 R-Sq = 98.45% R-Sq(adj) = 97.41%

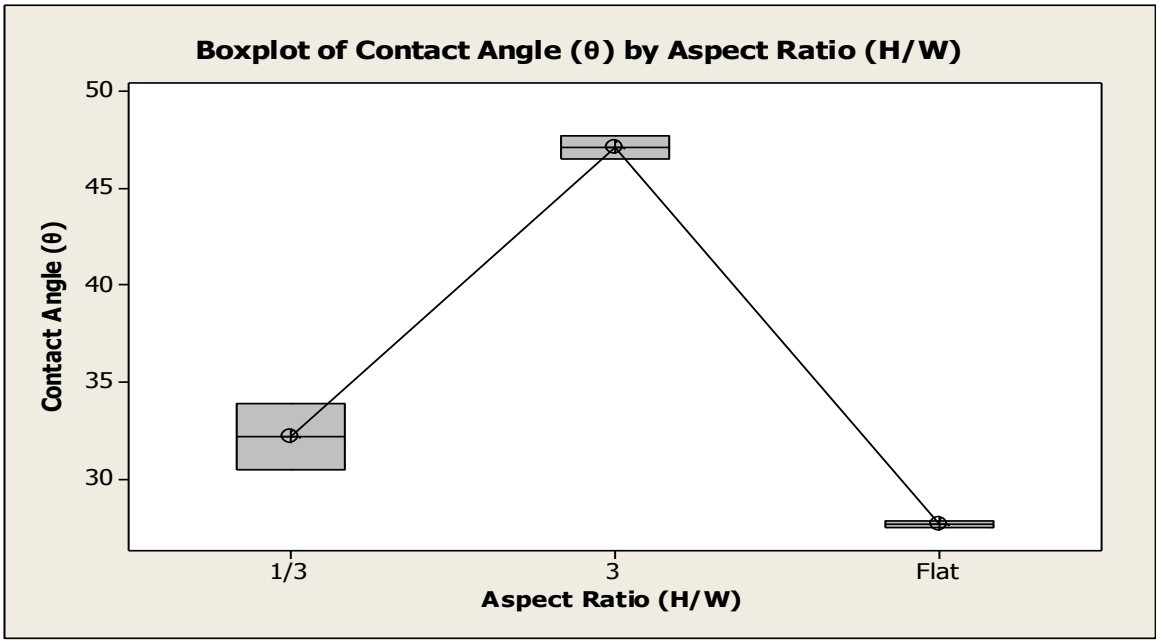

Figure 6.7. Box plot for perpendicular spread.

Box plot in Figure 6.7 graphically points out that the means are different for the three categories; aspect ratio3, aspect ratio 1/3 and flat substrate. Table 6.1 shows results of one-way ANOVA for perpendicular spread. It was observed that aspect ratio is statistically significant in affecting final contact angle with p-value of 0.002 that was less than the desired α level. Moreover, a regression fit for the model yielded a coefficient of determination (R-Square value) of 0.9845. Therefore, it ensured the goodness of fit of the data representing that approximately 98.45% of the variation in the final contact angle was attributed to the change in the aspect ratio.

To find out particularly which pairs of means are considerably different, Tukey's Multiple Comparison Test was performed. The results of Tukey's Multiple Comparison Test on contact angle data are summarized in following Table 6.2, which indicate that there is a significant difference among the means of two pairs of aspect ratios; 3 with 1/3

and 3 with flat substrate. The pair of 1/3 aspect ratio with flat substrate showed no significant difference among their means. This can be attributed to the availability of more flat portion of substrate for spreading in both the categories. Figure 6.8 shows graphical comparison of the means for different topology groups.

Table 6.2 Results of Tukey's multiple comparison test for perpendicular spread

Tukey's Multiple Comparison Test	Mean Diff.	q	Significant? P < 0.05?	Summary	95% CI of diff
3 vs 1/3	15	14.3	Yes	**	8.78 to 21.1
3 vs Flat	19.5	18.6	Yes	**	13.3 to 25.6
1/3 vs Flat	4.52	4.33	No	ns	-1.66 to 10.7

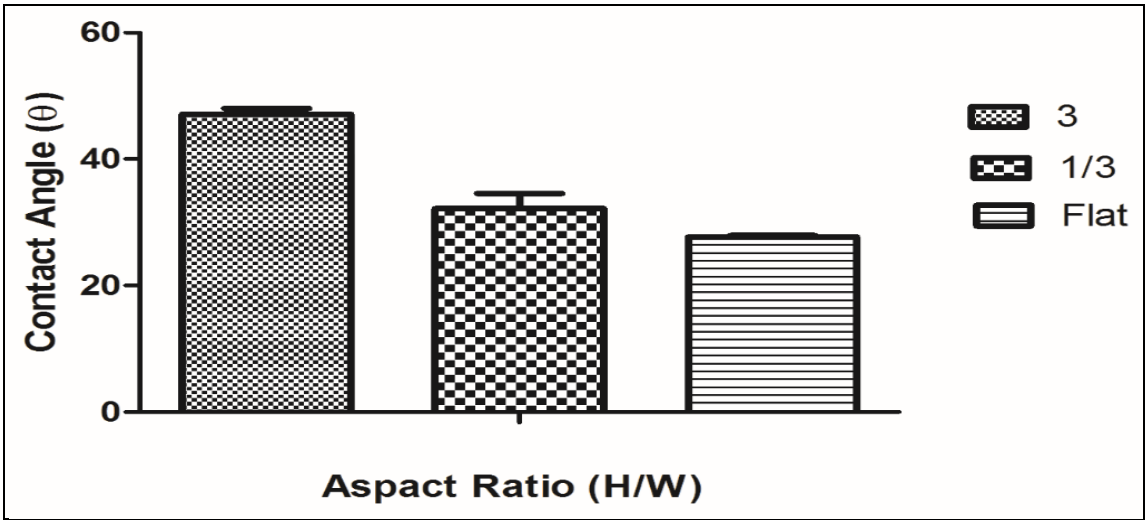

Figure 6.8. Comparison of means for different topology groups (perpendicular spread).

6.2.1.2 One-way ANOVA: Parallel Spread

Following is the output of one way ANOVA that was performed on final contact angle data measured parallel to the slots for three different topologies; aspect ratio 3, aspect ratio 1/3 and flat surface.

Table 6.3. Results of one-way ANOVA for parallel spread.

One-way ANOVA: Contact Angle (θ)_1 versus Aspect Ratio (H/W)_1

Source	DF	SS	MS	F	P
Aspect Ratio (H/	2	18.463	9.231	57.78	0.004
Error	3	0.479	0.160		
Total	5	18.942			

S = 0.3997 R-Sq = 97.47% R-Sq(adj) = 95.78%

Figure 6.9 illustrates disparity between means of three different topology groups. Table 6.3 shows results of one-way ANOVA for parallel spread. The results indicate that aspect ratio is statistically significant in affecting final contact angle with p-value of 0.004 that was less than the desired α level. In addition, a regression fit for the model determined R-Square value of 0.9747. Therefore, it expressed the goodness of fit of the data implying that approximately 97.47% of the variation in the final contact angle was attributed to the change in the aspect ratio.

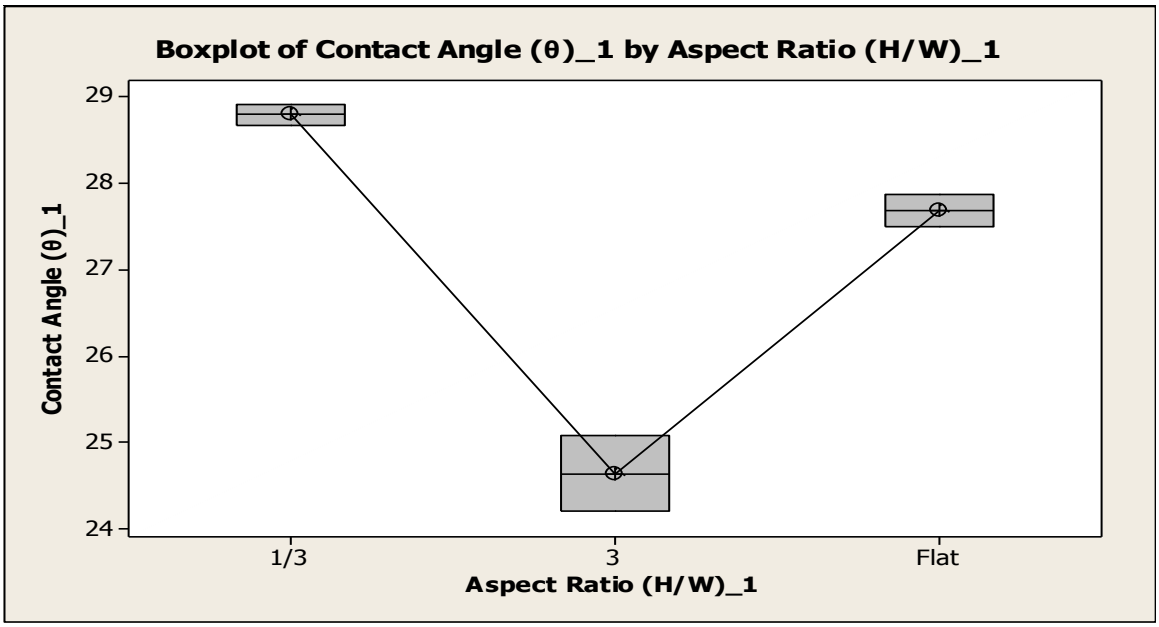

Figure 6.9. Box plot for parallel spread.

The results of Tukey's Multiple Comparison Test on contact angle data measured parallel to slots are summarized in Table 6.4. These results show that, similar to perpendicular measurement results, there is a significant difference among the means of two pairs of aspect ratios; 3 with 1/3 and 3 with flat substrate. Moreover, similar to perpendicular measurement results, the pair of 1/3 aspect ratio with flat substrate showed no significant difference among their means. Figure 6.10 shows graphical assessment of the means for three different topology groups.

Table 6.4. Results of Tukey's multiple comparison test for parallel spread.

Tukey's Multiple Comparison Test	Mean Diff.	q	Significant? P < 0.05?	Summary	95% CI of diff
3 vs 1/3	-4.15	14.7	Yes	**	-5.82 to -2.48
3 vs Flat	-3.04	10.8	Yes	**	-4.71 to -1.37
1/3 vs Flat	1.11	3.91	No	ns	-0.565 to 2.78

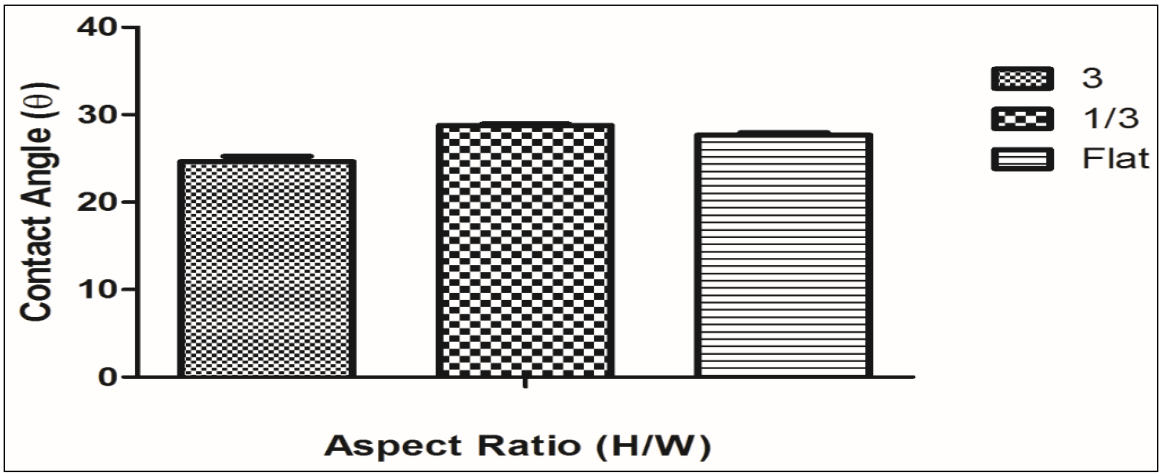

Figure 6.10. Comparison of means for different topology groups (parallel spread).

6.3 Conclusions of Substrate Topology Studies

The results of substrate topology studies clearly show the effect of substrate topology variation on spreading dynamics of nanodroplet. Hydrophilic SiO_2 substrate changed its nature and turned slightly hydrophobic; especially with higher aspect ratio features on the substrate. The droplet on substrate with highest aspect ratio could reach perpendicular contact angle only up to 47.25 ^{o}; 19.75^{o} higher contact angle than equilibrium contact angle observed on flat substrate over 70 picoseconds. However, when measured parallel

to the slots, the contact angle was approximately close to equilibrium angle. For substrate with aspect ratio 1/3, spreading was also retarded to some extent with perpendicular contact angle of 32 ^{o} slightly higher than equilibrium contact angle for flat substrate. However, parallel contact angle (28.78 ^{o}) was observed close to the equilibrium contact angle for flat topology. The results of one-way ANOVA show that there was considerable difference between the means of perpendicular contact angle data for aspect ratio 3 and 1/3. However, the extent of difference was less for the means of parallel contact angle data. In the both cases (parallel and perpendicular measurement), no significant differences were observed between the means of contact angle data for flat substrate and a substrate with 1/3 aspect ratio.

CHAPTER 7

CONCLUSION AND FUTURE WORK

7.1 Conclusions of Nanodroplet Evaporation Modeling

This phase investigated the evaporation mechanism of nanodroplets at different temperatures and time scales. The physical droplet size transformations, RMSD values, and volume slice variation for water and acetone nanodroplets were evaluated. In the case of the water nanodroplet, the distinction between the central dense core and rarified vapor ambience was clearly observed at all the temperatures. In addition, at elevated temperatures, the droplet core region was observed shrinking at a higher rate compared to the lower temperatures. This indicated existence of a differential evaporation phenomenon over the range of temperatures. On the contrary, the acetone droplet evaporation was characterized by molecular scattering and rarification throughout the droplet bulk. The dispersed molecule clusters were observed within the acetone nanodroplet volume at all temperatures on femtosecond time scales. This evaporation pattern can be attributed to the lower specific heat and extremely higher volatility of acetone compared to that of water. This study also confirmed three orders of magnitude difference between functional evaporation timescale of equivalent water and acetone nanodroplets. Moreover, these molecular models provided a better understanding of the effect of heat flux at different time scales and resulting vapor phase progression during nanodroplet evaporation. These results were validated using established *dD/dt* model. Close agreement was observed between MD simulation results and theoretical validation models for evaporation profiles of water and acetone nanodroplets. The results of this

study are significant in estimating process parameters such as temperature, droplet ejection speed and ultimately exposure time of droplet to the heat source towards gaining better control over scalable (micro to nano) droplet-based manufacturing. Moreover, the results of this investigation are also expected to aid in enhanced understanding of difference in heat flux application timescales for highly volatile and less volatile solvents. Furthermore, these results served as a basis for simulating nanodroplet interaction with substrates at different temperatures.

7.2 Conclusions of Nanodroplet and Flat Substrate Interaction Study

This study involved MD modeling and simulation of interaction between water nanodroplet and flat SiO_2 and Si_3N_4 substrates. The results of water nanodroplet-SiO_2 substrate interaction simulation revealed the hydrophilic behavior of SiO_2 substrate with water nanodroplet and yielded an equilibrium contact angle of 27.5^o. The hydrophilic behavior of SiO_2 substrate was also maintained at elevated temperatures. Accelerated nanodroplet spreading rates were witnessed for higher temperatures. This behavior is generally observed at macroscale; mainly due to reduction in surface tension of liquid that maintains fluid in droplet form. In addition, higher kinetic energy of molecules within three phase wetting zone at elevated temperatures aids in rapid spreading of droplet. The results of the study revealed that this behavior was consistent also at nanoscale. Accordingly, rapid wetting rates were also confirmed by higher values of spread diameter ratio to the original diameter (D/D_0) at successively higher temperatures.

The results of water nanodroplet- Si_3N_4 substrate interaction simulation validated hydrophobic behavior at nanoscale (identical with macroscale behavior) at all four temperatures. Hydrophobic nature of interaction was characterized by higher equilibrium contact angle of 42.08^o compared to 27.5^o for hydrophilic SiO_2-water system. Moreover, time to reach equilibrium was the six times the equilibrium time for SiO_2-water system at room temperature. Similar to SiO_2-water system, the hydrophobic behavior of Si_3N_4-water system at nanoscale was consistent at elevated temperatures due to increasing spreading rates at higher temperature. Nanodroplet diameter after spreading up to equilibrium was approximately 50% less than the corresponding spread diameter for SiO_2-water system.

Factorial design results for SiO_2-water and Si_3N_4-water systems confirmed significant role of main and interactions effects based on temperature and substrate factors for reaching the final equilibrium for spreading nanodroplet.

The results of this study are expected to assist in estimating the appropriate temperatures and corresponding time scales required to achieve water nanodroplet equilibrium for SiO_2 and Si_3N_4 substrates. The findings of this investigation are also important for predicting wetting pattern of water based collides for SiO_2 and Si_3N_4 substrates at given ambient conditions. Moreover, the results of this study established a close conformance between nanoscale and macroscale behavior of SiO_2-water system and Si_3N_4-water system. Furthermore, these results formed the basis for modeling droplet impingement phenomenon and substrate topology study.

7.3 Conclusions of Nanodroplet Impingement Study

Results of impingement study confirm that impingement velocity plays an important role in determining the spreading mechanism of nanodroplet. The equilibrium times were drastically reduced with increase in impingement velocity for SiO_2-water system. Impingement with 0.01 m/s and 0.1 m/s velocity reduced normal equilibrium time approximately 1.6 times and 2.5 times, respectively of its original value (70 picoseconds). Finally, imparting initial velocity of 1m/s achieved approximately $1/4^{th}$ of normal equilibrium time.

The results of this investigation confirm proportional relationship between spreading speed and initial impingement velocity. The outcomes of this study are also critical in predicting extent of solvent droplet spread and positioning of suspended nanoparticles in the solvent droplet. In addition, it aids for determining the shape of final feature formed on the substrate; especially under the influence of realistic droplet ejection velocity. Furthermore, the findings of this study may differentiate between natural droplet spreading mechanisms used in other droplet based nanomanufacturing processes and one with impingement velocity in inkjet printing method.

7.4 Conclusions of Nanodroplet-Patterned Substrate Interaction Study

At macroscale, the fact is well established that the substrate wetting behavior can be altered with substrate surface topology changes. The results of substrate topology studies confirmed that a given substrate can be tailored for required spreading mechanism also at nanoscale. At higher the aspect ratios, a more retardation in the spreading is observed resulting in hydrophobic fluid substrate interaction. The flat SiO_2 substrate was more

hydrophilic with equilibrium contact angle of 27.5^{o} reached in 70 picoseconds. However, SiO_2 substrate with 1/3 aspect ratio features was slightly less hydrophilic attaining contact angle of 32^{o} over 70 picoseconds. Further, SiO_2 substrate with an aspect ratio of 3 resulted in a shift towards hydrophobic nature with a contact angle of 47.25^{o}. Therefore, by patterning the surface with successively higher aspect ratios we can migrate the substrate from hydrophilic to hydrophobic disposition. The results of One Way ANOVA on contact angle data further confirmed the fact that higher the difference in aspect ratios, more hydrophilic to hydrophobic shift was observed in nature of nanodroplet-substrate interaction.

Another conclusion form this study was drawn regarding significant difference between spreading dynamics when observed across and along the grooves on substrate surface. Higher contact angles were recorded for both the substrate topologies (with aspect ratio 3 and 1/3) when measured across the groves compared to one measured along the groves. However, this difference was more evident for the substrate with aspect ratio 3 compared to that for aspect ratio 1/3.

Thus this study is expected to widen the functional range of a given substrate-liquid combination for droplet based micro/nanomanufacturing as needed. The results of this investigation emphasized the importance of surface topology as an additional control parameter in droplet based nanomanufacturing. Moreover, the study explored the possibility of offering more flexible combinations of substrate materials and solvents for nanoparticle deposition.

7.5 Limitations and Future Directions

Future directions for this research can be best described using its current limitations in terms of scope and adopted approaches.

7.5.1 Limitations of Research

The following areas have substantial opportunity for further research:

1. Modeling solvent droplet suspended with nanoparticles,
2. Modeling and investigation of larger diameter of nanodroplets,
3. Extending this study to different industrial solvents,
4. Including more substrate materials, and
5. Studying diverse surface topologies and a range of impingement velocities.

7.5.2 Future Directions

As discussed in previous section, there is need for modeling larger size nanodroplet spanning from the range of 4nm to 50 nm diameter for practical applications. An important step is the inclusion of nanoparticulates within solvent nanodroplet. This may aid in comparison of solvent-nanoparticle systems with current standalone solvent systems. Single walled carbon nanotubes are the suitable nanoparticle candidate for thin-film transistor fabrication using inkjet printing method. Further, acetone solvent may be simulated as potential functions and parameters are already compiled and validated for the acetone evaporation modeling. Moreover, other common industrial solvents can be considered for the investigation. In addition, additional substrate materials such as gold, graphite, quartz-alpha, silicon and amorphous silicon dioxide can be simulated.

Furthermore, the effects of more diversified surface topology on interaction of different substrate-solvent combinations may be evaluated. Also, continuum approach may be used to model and simulate some initial micro-to-nano and post deposition nano–to-micro transitions of droplet.

7.5.3 Challenges

The main challenge in the envisioned research discussed in previous section may be building the MD models for given substrate materials and solvents. MD being highly interdisciplinary and nascent field, better physical and chemical insight of the phenomenon, materials and MD concept is of paramount importance for producing reliable results. Selection, compilation and application of suitable force fields, physical bond parameters for various substrate materials and solvents that could be validated may be the critical factors in extending this research. Moreover, robust computational resources required to simulate large systems are essential for avoiding bottlenecks. Furthermore, more sophisticated pre and post processor (molecular modeling and visualization interface) may allow for gaining more insight and flexibility in terms of MD modeling and data analysis. Finally, the selection of appropriate and established physical models describing phenomena at macroscale and their subsequent use for further comparison and validation of nanoscale results is crucial for ensuring accuracy and reliability in predicting nanoscale interactions.

REFERENCES

[1] Chrisey, D.B., *The Power of Direct Writing.* Science, 2000. **289**(5481): p. 879-881.

[2] Pique, A. and D.B. Chrisey, *Direct-write technologies for rapid prototyping applications: sensors, electronics, and integrated power sources*. 2002: Academic Press.

[3] Han, X., et al., *Printable high-speed thin-film transistor on flexible substrate using carbon nanotube solution.* Micro & Nano Letters, IET, 2007. **2**(4): p. 96-98.

[4] Sachlos, E. and J. Czernuszka, *Making tissue engineering scaffolds work. Review: the application of solid freeform fabrication technology to the production of tissue engineering scaffolds.* Eur Cell Mater, 2003. **5**(29): p. 39-40.

[5] Hon, K., L. Li, and I. Hutchings, *Direct writing technology--Advances and developments.* CIRP Annals-Manufacturing Technology, 2008. **57**(2): p. 601-620.

[6] Lewis, J.A. and G.M. Gratson, *Direct writing in three dimensions.* Materials today, 2004. **7**(7): p. 32-39.

[7] Lusk, M.T. and A.E. Mattsson, *High-performance computing for materials design to advance energy science.* MRS Bulletin, 2011. **36**(03): p. 169-174.

[8] Abraham, F.F., et al., *Spanning the length scales in dynamic simulation.* Computers in Physics, 1998. **12**: p. 538-546.

[9] Chelikowsky, J.R. and M.A. Ratner, *Guest Editors' Introduction: Nanoscience, Nanotechnology, and Modeling.* Computing in Science and Engineering, 2001. **3**(4): p. 40-41.

[10] Nakano, A., et al., *Multiscale Simulation of Nanosystems.* Computing in Science and Engg., 2001. **3**(4): p. 56-66.

[11] Salil Desai, Taye Esho, Ravindra Kaware, *Experimental investigation of controlled microdroplet evaporation towards scalable micro/nanomanufacturing.* IIE Transactions, 2012. **44**(2): p. 155-162.

[12] Teller, E., N. Metropolis, and A. Rosenbluth, *Equation of state calculations by fast computing machines.* J. Chem. Phys, 1953. **21**(13): p. 1087-1092.

[13] Rahman, A., *Correlations in the motion of atoms in liquid argon.* phys. Rev, 1964. **136**(2A): p. 405-411.

[14] Verlet, L., *Computer" experiments" on classical fluids. I. Thermodynamical properties of Lennard-Jones molecules.* Physical Review, 1967. **159**(1): p. 98-103.

[15] Harp, G. and B. Berne, *Time-correlation functions, memory functions, and molecular dynamics.* Physical Review A, 1970. **2**(3): p. 975-996.

[16] Rahman, A. and F.H. Stillinger, *Molecular dynamics study of liquid water.* The Journal of Chemical Physics, 1971. **55**: p. 3336-3359.

[17] Stoddard, S.D., *Identifying clusters in computer experiments on systems of particles.* Journal of Computational Physics, 1978. **27**: p. 291-293.

[18] Bunz, H., *Identification of clusters in computer experiments with periodic boundary conditions.* Computer physics communications, 1986. **42**(3): p. 435-439.

[19] Haile, J.M., *Molecular dynamics simulation: elementary methods.* Physical Review Letters, 1992. **104**(19).

[20] Allen, M.P. and D.J. Tildesley, *Computer simulation of liquids*. Vol. 18. 1989: Oxford university press.

[21] Im, W. and Y. Won, *Molecular Dynamics Simulation on thermodynamic and Structural Properties of Liquid Hydrocarbons: Normal Alkanes.* BULLETIN-KOREAN CHEMICAL SOCIETY, 1994. **15**: p. 852-852.

[22] Long, L.N., M.M. Micci, and B.C. Wong, *Molecular dynamics simulations of droplet evaporation.* Computer physics communications, 1996. **96**(2): p. 167-172.

[23] Matsumoto, M., *Molecular dynamics simulation of interphase transport at liquid surfaces.* Fluid phase equilibria, 1996. **125**(1-2): p. 195-203.

[24] Zhakhovskii, V. and S. Anisimov, *Molecular-dynamics simulation of evaporation of a liquid.* Journal of Experimental and Theoretical Physics, 1997. **84**(4): p. 734-745.

[25] Samuelson, S., D. Tobias, and G. Martyna, *Modern computational methodology applied to the simulation of blocked trialanine peptide in vacuo, water clusters, and bulk water.* The Journal of Physical Chemistry B, 1997. **101**(38): p. 7592-7603.

[26] Korlie, M., *Three-dimensional computer simulation of liquid drop evaporation.* Computers & Mathematics with Applications, 2000. **39**(12): p. 43-52.

[27] Walther, J. and P. Koumoutsakos, *Molecular dynamics simulation of nanodroplet evaporation.* Journal of heat transfer, 2001. **123**(4): p. 741-748.

[28] Wu, Y. and C. Pan, *Molecular dynamics simulation of thin film evaporation of Lennard-Jones liquid.* Nanoscale and Microscale Thermophysical Engineering, 2006. **10**(2): p. 157-170.

[29] Yang, T. and C. Pan, *Molecular dynamics simulation of a thin water layer evaporation and evaporation coefficient.* International journal of heat and mass transfer, 2005. **48**(17): p. 3516-3526.

[30] Van den Akker, E., et al., *Thermodynamic analysis of molecular dynamics simulation of evaporation and condensation*, molecules, 2008. **1001**: p. d2ri.

[31] Nagyama, G. and T. Tsuruta, *Transition State Theory and Molecular Dynamics on Condensation/Evaporation Coefficients.* Transactions of the Japan Society of Mechanical Engineers. B, 2001. **67**(656): p. 1041-1048.

[32] Yi, P., et al., *Molecular dynamics simulation of vaporization of an ultra-thin liquid argon layer on a surface.* International journal of heat and mass transfer, 2002. **45**(10): p. 2087-2100.

[33] Kirkman, N., T. Stirner, and W. Hagston, *A new method for investigating the surface tension from molecular dynamics simulations applied to liquid droplets.* Computational materials science, 2004. **30**(1): p. 126-130.

[34] Martin, M.G. and M.J. Biddy, *Monte Carlo molecular simulation predictions for the heat of vaporization of acetone and butyramide.* Fluid phase equilibria, 2005. **236**(1): p. 53-57.

[35] Phillips, J.C., et al., *Scalable molecular dynamics with NAMD.* Journal of computational chemistry, 2005. **26**(16): p. 1781-1802.

[36] Hong, S.D., M.Y. Ha, and S. Balachandar, *Static and dynamic contact angles of water droplet on a solid surface using molecular dynamics simulation.* Journal of colloid and interface science, 2009. **339**(1): p. 187-195.

[37] Bayer, I.S. and C.M. Megaridis, *Contact angle dynamics in droplets impacting on flat surfaces with different wetting characteristics.* Journal of Fluid Mechanics, 2006. **558**: p. 415-450.

[38] Pugliano, N. and R. Saykally, *Measurement of quantum tunneling between chiral isomers of the cyclic water trimer.* Science, 1992. **257**(5078): p. 1937-1940.

[39] Narten, A., W. Thiessen, and L. Blum, *Atom pair distribution functions of liquid water at 25 C from neutron diffraction.* Science, 1982. **217**(4564): p. 1033-1034.

[40] Kropman, M. and H. Bakker, *Dynamics of water molecules in aqueous solvation shells.* Science, 2001. **291**(5511): p. 2118-2120.

[41] Tseng, F.G., et al., *Size effect on surface tension and contact angle between protein solution and silicon compound, PC, and PMMA substrates.* Microscale thermophysical engineering, 2002. **6**(1): p. 31-53.

[42] Werder, T., et al., *On the water-carbon interaction for use in molecular dynamics simulations of graphite and carbon nanotubes.* The Journal of Physical Chemistry B, 2003. **107**(6): p. 1345-1352.

[43] Hirvi, J.T. and T.A. Pakkanen, *Molecular dynamics simulations of water droplets on polymer surfaces.* The Journal of Chemical Physics, 2006. **125**: p. 144712-144726.

[44] Watanabe, Y., Y. Shibuta, and T. Suzuki, *A Molecular Dynamics Study of Thermodynamic and Kinetic Properties of Solid–Liquid Interface for Bcc Iron.* ISIJ international, 2010. **50**(8): p. 1158-1164.

[45] Park, S.H., et al., *Hydrophobic-induced surface reorganization: molecular dynamics simulations of water nanodroplets on perfluorocarbon self-assembled monolayers.* Soft matter, 2010. **6**(8): p. 1644-1654.

[46] Sedighi, N., S. Murad, and S.K. Aggarwal, *Molecular dynamics simulations of spontaneous spreading of a nanodroplet on solid surfaces.* Fluid Dynamics Research, 2011. **43**: p. 015507.

[47] Park, J.Y., et al., *A study on the contact angles of a water droplet on smooth and rough solid surfaces.* Journal of Mechanical Science and Technology, 2011. **25**(2): p. 323-332.

[48] Ohler, B. and W. Langel, *Molecular dynamics simulations on the interface between titanium dioxide and water droplets: a new model for the contact angle.* The Journal of Physical Chemistry C, 2009. **113**(23): p. 10189-10197.

[49] Wu, C.D., et al., *Effects of temperature, size of water droplets, and surface roughness on nanowetting properties investigated using molecular dynamics simulation.* Computational materials science, 2012. **53**(1): p. 25-30.

[50] Taura, G. and M. Matsumoto, *Molecular Dynamics Simulation of Microdroplet Impingement on Solid Surface.* Journal of Fluid Science and Technology, 2010. **5**: p. 207-218.

[51] Desai, S. and R. Kaware, *Computational modeling of nanodroplet evaporation for scalable micro-/nano-manufacturing.* IIE Transactions, 2012. **44**(7): p. 568-579.

[52] Nelson, M.T., et al., *NAMD: a parallel, object-oriented molecular dynamics program.* International Journal of High Performance Computing Applications, 1996. **10**(4): p. 251-268.

[53] Humphrey, W., A. Dalke, and K. Schulten, *VMD: visual molecular dynamics.* Journal of molecular graphics, 1996. **14**(1): p. 33-38.

[54] Foloppe, N. and A.D. MacKerell Jr, *All-atom empirical force field for nucleic acids: I. Parameter optimization based on small molecule and condensed phase macromolecular target data.* Journal of computational chemistry, 2000. **21**(2): p. 86-104.

[55] Wang, J., et al., *Development and testing of a general amber force field.* Journal of computational chemistry, 2004. **25**(9): p. 1157-1174.

[56] Goering, C., L. Bode, and M. Gebhardt, *Mathematical modeling of spray droplet deceleration and evaporation.* Transactions of the ASAE, 1972. **15**(2): p. 220-225.

[57] Kincaid, D. and T. Longley, *A water droplet evaporation and temperature model.* Transaction of the ASAE, 1989. **32**(2): p. 457-463.

[58] Institution, S. and R.J. List, *Smithsonian meteorological tables*. 1951: The Institution.

[59] Frossling, N., *The evaporation of falling drops.* Gerlands Beitr. Geophys, 1938. **52**: p. 170.

[60] Beck, F., A. Polman, and K. Catchpole, *Tunable light trapping for solar cells using localized surface plasmons.* Journal of Applied Physics, 2009. **105**(11): p. 114310-114310-7.

[61] Pierson, H.O., *Handbook of carbon, graphite, diamond, and fullerenes: properties, processing, and applications*. 1993: William Andrew.

[62] de Gennes, P.G., *Wetting: statics and dynamics.* Reviews of modern physics, 1985. **57**(3): p. 827.

[63] Street, R.A., et al., *Jet printing flexible displays.* Materials today, 2006. **9**(4): p. 32-37.

[64] Blake, T., et al., *Contact angle relaxation during droplet spreading: Comparison between molecular kinetic theory and molecular dynamics.* Langmuir, 1997. **13**(7): p. 2164-2166.

[65] Frenkel, J., *Kinetic theory of liquids*. Vol. 488. 1955: Dover New York.

[66] Glasstone, S., K.J. Laidler, and H. Eyring, *The theory of rate processes: the kinetics of chemical reactions, viscosity, diffusion and electrochemical phenomena*. 1941: McGraw-Hill Book Company.

[67] Hu, H. and R.G. Larson, *Evaporation of a sessile droplet on a substrate.* The Journal of Physical Chemistry B, 2002. **106**(6): p. 1334-1344.

[68] Deegan, R.D., *Pattern formation in drying drops.* Physical Review E, 2000. **61**(1): p. 475-485.